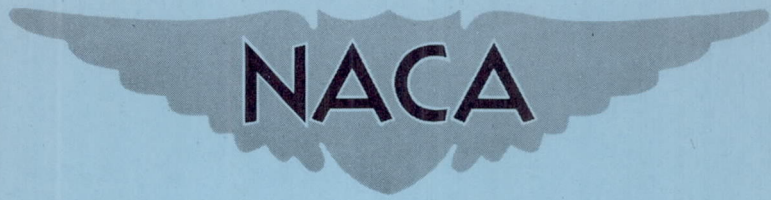


**CONFIDENTIAL**

NACA RM A53F03



# RESEARCH MEMORANDUM

THE LATERAL CONTROL CHARACTERISTICS OF CONSTANT-PERCENT-  
CHORD TRAILING-EDGE ELEVONS ON A POINTED WING OF  
ASPECT RATIO 2 AT MACH NUMBERS UP TO 0.95

By Verlin D. Reed and Donald W. Smith

Ames Aeronautical Laboratory  
Moffett Field, Calif.

CLASSIFICATION CHANGED TO UNCLASSIFIED

AUTHORITY: RESEARCH ABSTRACT NO. 102

DATE: JUNE 22, 1956

WHL

CLASSIFIED DOCUMENT

This material contains information affecting the National Defense of the United States within the meaning of the espionage laws, Title 18, U.S.C., Secs. 793 and 794, the transmission or revelation of which in any manner to an unauthorized person is prohibited by law.

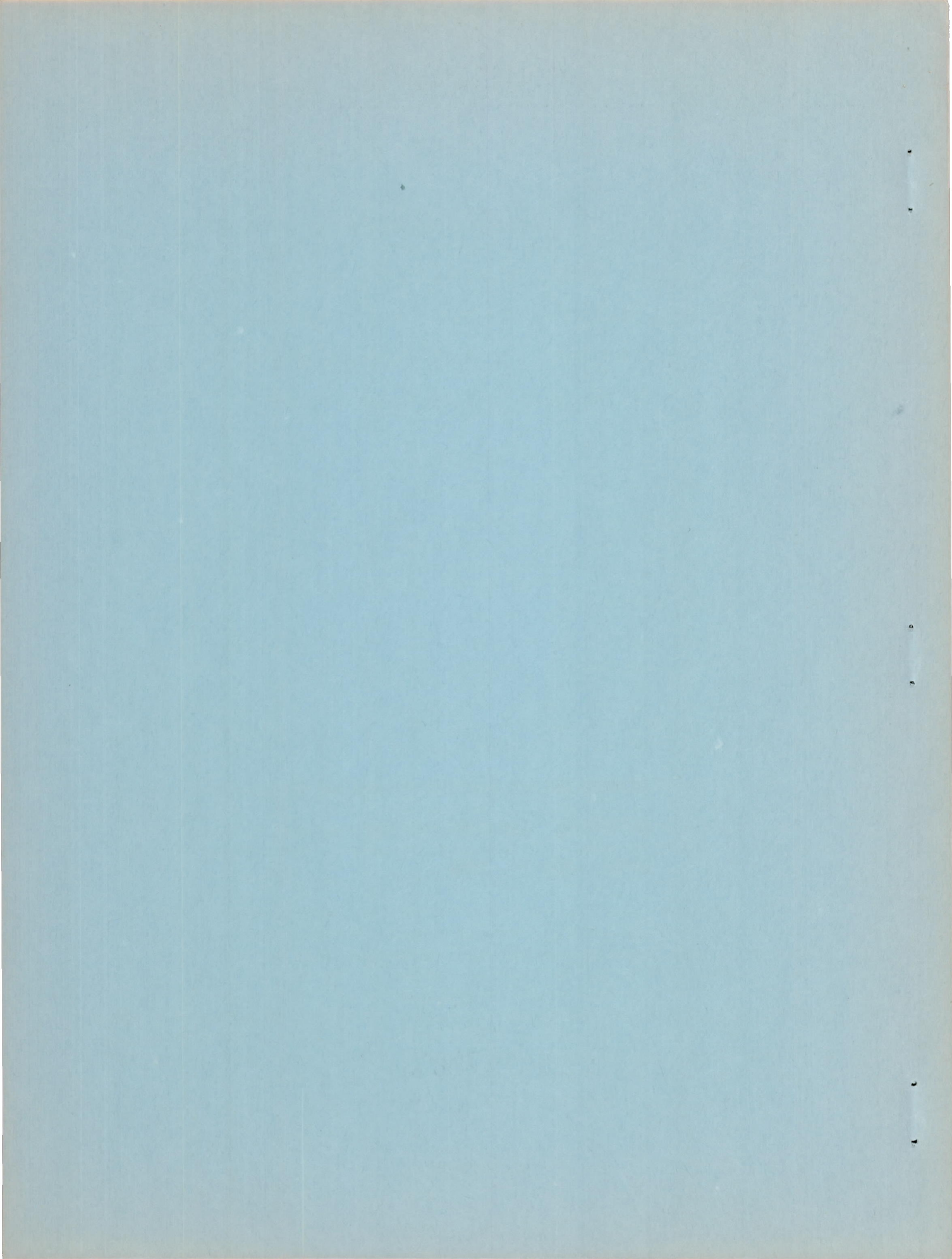
## NATIONAL ADVISORY COMMITTEE FOR AERONAUTICS

WASHINGTON

August 14, 1953

**CONFIDENTIAL**







## NATIONAL ADVISORY COMMITTEE FOR AERONAUTICS

RESEARCH MEMORANDUMTHE LATERAL CONTROL CHARACTERISTICS OF CONSTANT-PERCENT-  
CHORD TRAILING-EDGE ELEVONS ON A POINTED WING OF  
ASPECT RATIO 2 AT MACH NUMBERS UP TO 0.95

By Verlin D. Reed and Donald W. Smith

## SUMMARY

An investigation has been made to determine the lateral control characteristics of constant-percent-chord trailing-edge elevons on a tailless wing-body combination having a pointed wing with an aspect ratio of 2. The effectiveness of inset tabs in reducing the elevon hinge moment was also determined.

Data presented include the lift, drag, pitching moment, rolling moment, elevon hinge moment, tab hinge moment, elevon load, and center of pressure of elevon load. The data are presented for a range of angles of attack, elevon deflection, and tab deflection at a Reynolds number of 3.0 million and at Mach numbers up to 0.95. At a Mach number of 0.24, data were also obtained at Reynolds numbers up to 15.0 million.

The lift and pitching-moment effectiveness of the elevons decreased with an increase in differential elevon deflection. The effectiveness of the elevons in producing rolling moment increased with increasing Mach number but decreased with a change in mean elevon deflection from  $0^\circ$  to  $-10^\circ$ .

The data were used to estimate the lateral control characteristics of an assumed airplane, geometrically similar to the model. Two different types of lateral control systems were considered for the analysis: a direct elevon control and a servotab control. The elevons were found to be capable of producing a wing-tip helix angle of 0.09 radian for the assumed airplane at all Mach numbers with a differential elevon deflection of about  $9^\circ$  or less. The stick forces calculated from experimental data required to maintain a steady roll in level flight were greatly reduced by using the servotab control instead of the plain-elevon control.



## INTRODUCTION

Research is in progress at various NACA facilities to determine the aerodynamic characteristics of flap-type trailing-edge elevons on low-aspect-ratio wings at both subsonic and supersonic speeds. The effects of elevon plan form and of trailing-edge profile on the aerodynamic characteristics of elevons on a thin triangular wing having an aspect ratio of 2 have been investigated at high subsonic and low supersonic speeds and have been reported in reference 1. The results of an investigation to determine the static longitudinal stability and control characteristics of constant-percent-chord, flap-type, trailing-edge elevons on a pointed wing having an aspect ratio of 2 have been presented in reference 2.

With the model which was used for the tests reported in reference 2, an investigation has been conducted in the Ames 12-foot pressure wind tunnel at Mach numbers up to 0.95 to determine the lateral control characteristics of the elevons and the effectiveness of inset tabs in reducing the elevon hinge moment. The results of these tests are reported herein.

## NOTATION

b	wing span, ft
c	local wing chord, ft
$\bar{c}$	wing mean aerodynamic chord, $\frac{\int_0^{b/2} c^2 dy}{\int_0^{b/2} c dy}$ , ft
$c_e$	elevon chord, ft
$c_a$	elevon chord through centroid of elevon area, ft
$c_r$	elevon reference chord, $c_a \cos \delta_e$ , ft
$c_t$	tab chord, ft
l	length of body including portion removed to accommodate sting, ft
M	Mach number
$M_{A_e}$	first moment of area of exposed elevon behind elevon hinge line, ft <sup>3</sup>
$M_{A_t}$	first moment of area of exposed tab behind tab hinge line, ft <sup>3</sup>



p	rolling velocity, radians/sec
q	free-stream dynamic pressure, lb/sq ft
R	Reynolds number based on wing mean aerodynamic chord
r	radius of body, ft
r <sub>0</sub>	maximum body radius, ft
S	total wing area including the area formed by extending the leading and trailing edges to the plane of symmetry, sq ft
S <sub>e</sub>	exposed area of elevon behind elevon hinge line, sq ft
V	free-stream velocity, ft/sec
W	weight of assumed airplane, lb
x	longitudinal distance from elevon hinge line measured in the chord plane of the wing (negative to rear of hinge line), ft
x'	longitudinal distance from nose of body, ft
y	lateral distance normal to plane of symmetry, ft
α	angle of attack of the body axis, deg
δ <sub>e<sub>l</sub></sub>	left elevon deflection, with respect to wing-chord plane, measured in planes perpendicular to the elevon hinge line (positive downward), deg
δ <sub>e<sub>r</sub></sub>	right elevon deflection, with respect to wing-chord plane, measured in planes perpendicular to the elevon hinge line (positive downward), deg
δ <sub>e<sub>a</sub></sub>	differential elevon deflection, δ <sub>e<sub>l</sub></sub> - δ <sub>e<sub>r</sub></sub> , deg
δ <sub>e</sub>	mean elevon deflection, $\frac{\delta_{e_l} + \delta_{e_r}}{2}$ , deg
δ <sub>t</sub>	tab deflection, with respect to elevon-chord plane, measured in planes perpendicular to the tab hinge line (positive downward), deg
δ <sub>t<sub>l</sub></sub>	left tab deflection, deg



$\delta_{t_r}$	right tab deflection, deg
$\delta_{t_a}$	differential tab deflection, $\delta_{t_l} - \delta_{t_r}$ , deg
$\Delta\delta_e$	elevon deflection correction due to applied hinge moment (additive), deg
$\Delta\delta_t$	tab-deflection correction due to applied hinge moment (additive), deg
$\frac{pb}{2V}$	wing-tip helix angle, radians
$C_D$	drag coefficient, $\frac{\text{drag}}{qS}$
$C_F$	elevon load coefficient based on elevon load normal to wing-chord plane, $\frac{\text{elevon load}}{qS_e}$
$C_{h_e}$	elevon hinge-moment coefficient, $\frac{\text{elevon hinge moment}}{2qMA_e}$
$C_{h_t}$	tab hinge-moment coefficient, $\frac{\text{tab hinge moment}}{2qMA_t}$
$C_L$	lift coefficient, $\frac{\text{lift}}{qS}$
$C_m$	pitching-moment coefficient about the 25-percent point of the wing mean aerodynamic chord, $\frac{\text{pitching moment}}{qS\bar{c}}$
$C_l$	rolling-moment coefficient, $\frac{\text{rolling moment}}{qSb}$
$C_{L\delta_e}$	lift effectiveness parameter, $\frac{(C_L)_{\delta_e = -10^\circ} - (C_L)_{\delta_e = 0^\circ}}{-10^\circ}$ , per deg
$C_{m\delta_e}$	pitching-moment effectiveness parameter, $\frac{(C_m)_{\delta_e = -10^\circ} - (C_m)_{\delta_e = 0^\circ}}{-10^\circ}$ , per deg
$C_{l\delta_{ea}}$	rolling-moment effectiveness parameter, $\frac{\partial C_l}{\partial \delta_{ea}}$ , measured at $\delta_{ea} = 0$ , per deg

## MODEL

The model used in this investigation was the one used in the tests reported in reference 2. Figure 1 is a photograph of the model mounted in the wind tunnel, and figure 2 is a drawing of the plan and front views of the model showing some of the model dimensions. For a more detailed description of the model, see table I.

## TESTS

Tests of the model were made to determine the effectiveness of the constant-percent-chord trailing-edge elevons as a lateral control device and to determine the effectiveness of constant-percent-chord inset tabs in reducing the elevon hinge moment. The majority of the tests were conducted throughout a range of Mach numbers from 0.24 to 0.95 at a constant Reynolds number of 3.0 million. The test data were obtained for a differential elevon deflection of  $10^\circ$  with mean elevon deflections of  $0^\circ$  and  $-10^\circ$  in combination with tab deflections of  $0^\circ$  and  $5^\circ$ ; some additional data were obtained for differential elevon deflections of  $20^\circ$ . Data for Reynolds numbers up to 15.0 million for differential elevon deflections of  $20^\circ$  were obtained at a Mach number of 0.24.

## CORRECTIONS TO DATA

By the method of reference 3, the data presented herein have been corrected for the induced effects of the wind-tunnel walls resulting from lift on the model. The magnitudes of the corrections which were added to the measured values are

$$\Delta\alpha = 0.26 C_L$$

$$\Delta C_D = 0.0046 C_L^2$$

The induced effects of the tunnel walls on the pitching moment, hinge moment, and rolling moment were calculated and found to be negligible.

Corrections for the effects of constriction due to the wind-tunnel walls were calculated by the method of reference 4. These corrections were calculated for the model at  $0^\circ$  angle of attack and were applied to the data throughout the range of angles of attack. At a Mach number of 0.90, the correction amounted to an increase of about 2 percent in the dynamic pressure.



The effect of the interference between the model and the sting support on the aerodynamic characteristics is not known. It is believed, however, that the main effect of the sting was to alter the pressure at the base of the model body; consequently, the pressure at the base of the model was measured, and the drag data were adjusted to correspond to a base pressure equal to free-stream static pressure.

The basic data have not been corrected for the change in elevon and tab angles due to the deflection under load of the hinge-moment strain gages; however, the summary plots have been adjusted to account for these angle changes. In order to facilitate correction of the data, there is given in figure 3 a summary of the deflection of the elevons and tabs due to applied hinge moment at various values of Mach number and Reynolds number.

## RESULTS

The basic data are presented graphically in figures 4 through 17 and show the variation of the angle of attack, drag coefficient, pitching-moment coefficient, and rolling-moment coefficient with lift coefficient; the variation of elevon and tab hinge moments with angle of attack; and the variation of elevon load coefficient and the center of pressure of elevon load with angle of attack. All basic data are given for uncorrected values of elevon and tab deflection. Pitching-moment data are presented about a moment center at the 25-percent point of the wing mean aerodynamic chord. Table II lists the figures presenting the basic data and shows the range of variables covered by the tests at each Mach number and Reynolds number.

A summary of the effects of compressibility on the lift, pitching-moment, and rolling-moment effectiveness parameters and on the wing-tip helix angle is presented in figures 18 through 20. Results of application of the data to estimate the lateral control characteristics of an assumed airplane geometrically similar to the model are presented in figure 21. The data of reference 2, for equal deflection of the two elevons, were utilized in obtaining some of the aerodynamic characteristics presented in figures 18 through 21.

## DISCUSSION

### Lift and Pitching Moment

The effect of differential elevon deflection on the lift and pitching-moment effectiveness of the elevons for Mach numbers up to 0.95

is summarized in figure 18. An increase of differential elevon deflection resulted in a decrease in effectiveness, except at the lower Mach numbers, with the greatest decrease occurring at a Mach number of about 0.80.

#### Rolling Moment

The effectiveness of the elevons in producing rolling moment is summarized in figure 19. The rolling-moment effectiveness for a mean elevon deflection of  $0^\circ$  increased with increasing Mach number up to 0.90. A further increase of Mach number to 0.95 resulted in a slight increase in effectiveness for an angle of attack of  $0^\circ$  and a decrease for an angle of attack of  $6^\circ$ . A change of mean elevon deflection to  $-10^\circ$  resulted in a decrease in effectiveness at Mach numbers above 0.50; the greatest decrease occurred at a Mach number of about 0.90. An increase in angle of attack from  $0^\circ$  to  $6^\circ$  reduced the rolling-moment effectiveness at the higher Mach numbers but had little effect below a Mach number of 0.60. The rolling moment was little affected by an increase of Reynolds number from 3.0 million to 15.0 million at a Mach number of 0.24 (figs. 16 and 17).

#### Wing-Tip Helix Angle

Theoretical values of the damping-in-roll (rate of change of rolling-moment coefficient with wing-tip helix angle) calculated by the method of reference 5 and experimental values of rolling-moment coefficient corrected for the effect of rolling velocity by the method of reference 6 were used to calculate the helix angle generated by the wing tip in a steady equilibrium roll for differential elevon deflections of  $10^\circ$  and  $20^\circ$ .

As shown in figure 20 for a differential elevon deflection of  $10^\circ$  there was little effect of compressibility on  $pb/2V$  for a mean elevon deflection of  $0^\circ$ ; however, for a change in mean elevon deflection to  $-10^\circ$ ,  $pb/2V$  decreased with increasing Mach number at all but the lowest Mach numbers. An increase in differential elevon deflection from  $10^\circ$  to  $20^\circ$  approximately doubled the calculated  $pb/2V$ . At all test Mach numbers, the calculations indicate that the elevons were capable of producing a  $pb/2V$  in excess of that specified in reference 7 for fighter-type aircraft.



## APPLICATION OF DATA

In order to assess the merits of this particular wing plan form and control, the data have been applied to the prediction of the lateral control characteristics of a hypothetical airplane geometrically similar to the model. The wing span was assumed to be 30 feet; the wing area, 450 square feet; the wing loading, 40 pounds per square foot; the center of gravity at 0.25  $\bar{c}$ ; and the control gearing, 2.0° per inch of stick travel. The assumed airplane was initially trimmed for straight and level flight at an altitude of 30,000 feet.

In the application of the data, two types of lateral control have been considered: first, elevons directly connected to the control stick, second, tabs directly connected to the control stick so that movement of the stick changes the elevon deflection by changing the angle for zero hinge moment (elevon floating angle).

In the estimation of the stick force for steady rolling flight the airplane was assumed to roll about its longitudinal axis with zero yaw, to have a rolling moment equal to the damping moment caused by the wing rolling velocity, and to have a rigid wing. The stick force and the rolling-moment coefficient, which was used to calculate the wing-tip helix angle, were corrected for the effect of rolling velocity by the method of reference 6.

The variation with Mach number of the calculated stick force and control deflection required to give various values of  $pb/2V$  are presented in figure 21(a). A wing-tip helix angle of 0.09 (rolling velocity need not exceed 220° per second) is considered necessary for satisfactory lateral control (ref. 7). The plain elevons were found to be capable of producing a  $pb/2V$  of 0.09 radian throughout the Mach number range with a differential elevon deflection of about 9° or less. With the servotab control the differential elevon deflection required for a given  $pb/2V$  was increased over that for the plain elevons, but the stick force was greatly reduced. For example, at a Mach number of 0.90, the stick force required to maintain a  $pb/2V$  of 0.03 could be reduced from about 415 pounds to about 25 pounds by use of the servotab control. The servotab analysis was limited to the lower values of  $pb/2V$  because of the lack of data for tab deflections greater than 5°.

Figure 21(b) presents the variation with Mach number of the calculated rolling velocity and wing-tip helix angle for a constant stick force of 10 pounds. The servotab analysis was limited to this low value of stick force because of the lack of data for tab deflections greater than 5°. For both the plain-elevon and servotab control systems, the values of  $p$  and  $pb/2V$  decreased with increasing Mach number.

The variation of stick force and wing-tip helix angle with Mach number for a constant rolling velocity of  $15^{\circ}$  per second is presented in figure 21(c). This value of rolling velocity was chosen for the comparison of the control systems because, as specified under the emergency requirements (power control system inoperative) of reference 7, the minimum rolling velocity shall exceed  $15^{\circ}$  per second. The calculated stick force required to maintain the prescribed rolling velocity with the plain-elevon control increased rapidly with an increase of Mach number from 0.60 to 0.95; whereas that for the servotab control was much smaller and increased more gradually with increasing Mach number. A stick force of 50 pounds was required to maintain a rolling velocity of  $15^{\circ}$  per second at a Mach number of 0.85 for the plain elevon; the corresponding stick force for the servotab control was less than 3 pounds.

### CONCLUSIONS

An investigation has been made of the lateral control characteristics of a constant-percent-chord, trailing-edge elevon on a pointed wing having an aspect ratio of 2. The effectiveness of inset tabs in reducing the elevon hinge moment was also investigated. The following conclusions are based on an analysis of the data:

1. Generally, there was a decrease in lift and pitching-moment effectiveness of the elevons with an increase in differential elevon deflection.

2. The rolling-moment effectiveness for a mean elevon deflection of  $0^{\circ}$  increased slightly with increasing Mach number; however, the effectiveness, for a mean elevon deflection of  $-10^{\circ}$ , decreased with increasing Mach number.

Application of the data to an assumed airplane with either a plain elevon control or an elevon with servotab resulted in the following conclusions:

1. The plain elevons were capable of producing a wing-tip helix angle of 0.09 radian at all Mach numbers with a differential elevon deflection of about  $9^{\circ}$  or less.

2. The servotabs were effective in reducing the high stick forces associated with the plain-elevon control.



3. A stick force of 50 pounds was required to maintain a rolling velocity of  $15^{\circ}$  per second at a Mach number of 0.85 for the plain elevon control. With the servotab control, the corresponding stick force was 3 pounds.

Ames Aeronautical Laboratory  
National Advisory Committee for Aeronautics  
Moffett Field, Calif., June 3, 1953

#### REFERENCES

1. Boyd, John W.: Aerodynamic Characteristics of Two 25-Percent-Area Trailing-Edge Flaps on An Aspect Ratio 2 Triangular Wing at Subsonic and Supersonic Speeds. NACA RM A52D01c, 1952.
2. Smith, Donald W., and Reed, Verlin D.: Subsonic Static Longitudinal Stability and Control Characteristics of a Wing-Body Combination Having a Pointed Wing of Aspect Ratio 2 With Constant-Percent-Chord Trailing-Edge Elevons. NACA RM A53C20, 1953.
3. Glauert, H.: The Elements of Aerofoil and Airscrew Theory. Ch. XIV, The University Press, Cambridge, England, 1926.
4. Herriot, John G.: Blockage Corrections for Three-Dimensional-Flow Closed-Throat Wind Tunnels, with Consideration of the Effect of Compressibility. NACA Rep. 995, 1950. (Formerly NACA RM A7B28.)
5. Bird, John D.: Some Theoretical Low-Speed Span Loading Characteristics of Swept Wings in Roll and Sideslip. NACA Rep. 969, 1950.
6. Perkins, Courtland D., and Hage, Robert E.: Airplane Performance Stability and Control. Ch. 9-7, John Wiley & Sons, Inc., New York, 1949.
7. Anon.: Specification of Flying Qualities of Piloted Airplanes. Bureau of Aeronautics Specifications, NAVAER, SR-119B, 1948. (Also Flying Qualities of Piloted Airplanes. U.S. Air Force Specification No. 1815-B, 1948.)

TABLE I.- MODEL DIMENSIONS

Body	
Fineness ratio	
Basic . . . . .	12.5
Modified for installation on sting . . . . .	10.0
Ratio of sting diameter to base diameter of body . . . . .	0.89
Wing	
Area, sq ft . . . . .	4.014
Aspect ratio . . . . .	2.0
Taper ratio . . . . .	0
Sweep, leading edge, deg . . . . .	56.31
Sweep, trailing edge, deg . . . . .	26.57
Incidence, deg . . . . .	0
Dihedral, deg . . . . .	0
Section (streamwise) . . . . .	NACA 0005-63
Elevon	
Sweep, hinge line, deg . . . . .	0
Ratio of elevon chord to wing chord, $c_e/c$ . . . . .	0.25
Ratio of exposed elevon area to exposed wing area . . . . .	0.25
Gap between wing and elevons, measured chordwise	
Right, in. . . . .	0.015
Left, in. . . . .	0.025
Gap between elevons and body, measured spanwise,	
$\delta_e = 0^\circ$ , in. . . . .	0.015
First moment of area of exposed elevon behind	
hinge line, $\text{ft}^3$ . . . . .	0.0699
Tab	
Ratio of tab chord to elevon chord, $c_t/c_e$ . . . . .	0.25
Ratio of exposed tab span to exposed elevon span . . . . .	0.40
Ratio of exposed tab area to exposed wing area . . . . .	0.04
Gap between elevons and tabs, in. . . . .	0.015
First moment of area of exposed tab behind	
hinge line, $\text{ft}^3$ . . . . .	0.00321





TABLE II.- INDEX TO BASIC DATA

(a) Effect of elevon deflection							
Figure number	Mach number	Reynolds number	Mean elevon deflection $\delta_e$ , deg	Differential elevon deflection, $\delta_{e_a}$ , deg	Tab deflection, $\delta_t$ , deg		
4	0.24	$3.0 \times 10^6$	0, - 10	10, 20	0		
5	.60	↓	↓	↓	↓		
6	.80						
7	.85						
8	.90						
9	.92						
10	.95						
11	.24					10	5
12	.60						
13	.80						
14	.90						
15	.95						
(b) Effect of Reynolds number							
16	0.24	3.0, 5.0, 8.0, $15.0 \times 10^6$	0	20	0		
17	↓	↓	-10	↓	↓		



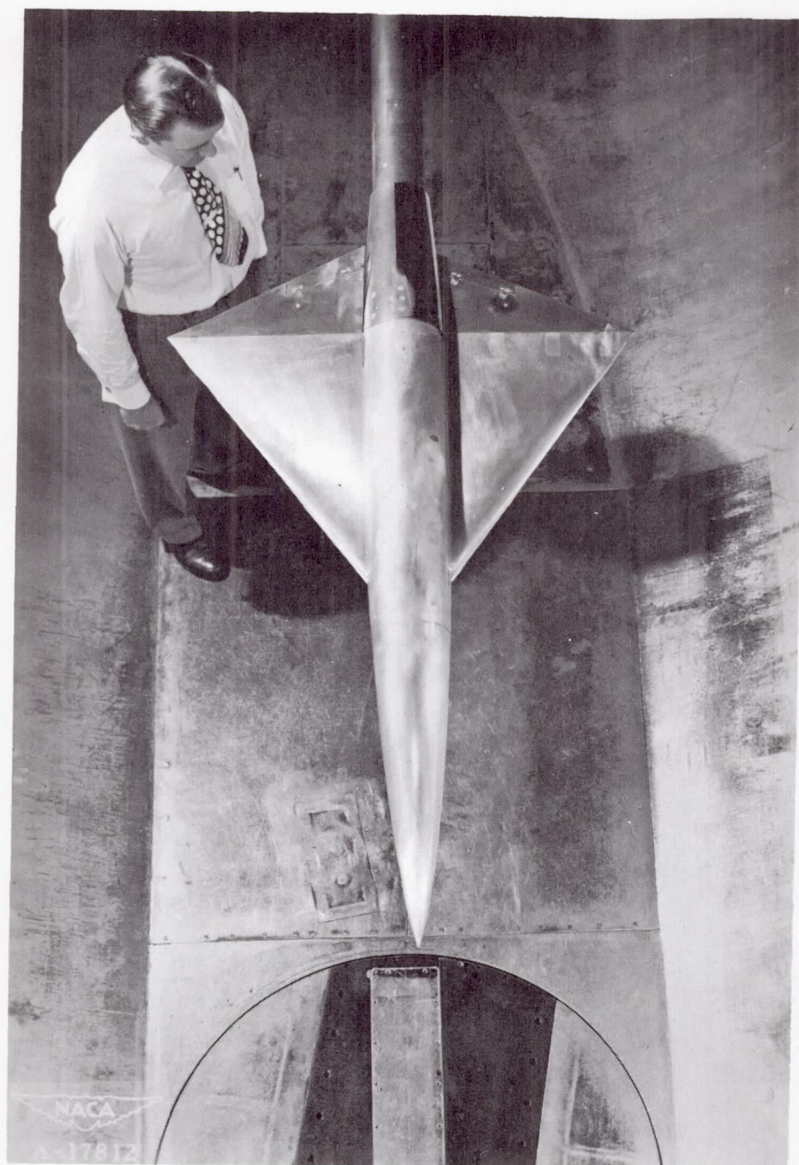


Figure 1.- A photograph of the model in the Ames 12-foot pressure wind tunnel.



Equation of fuselage ordinates:

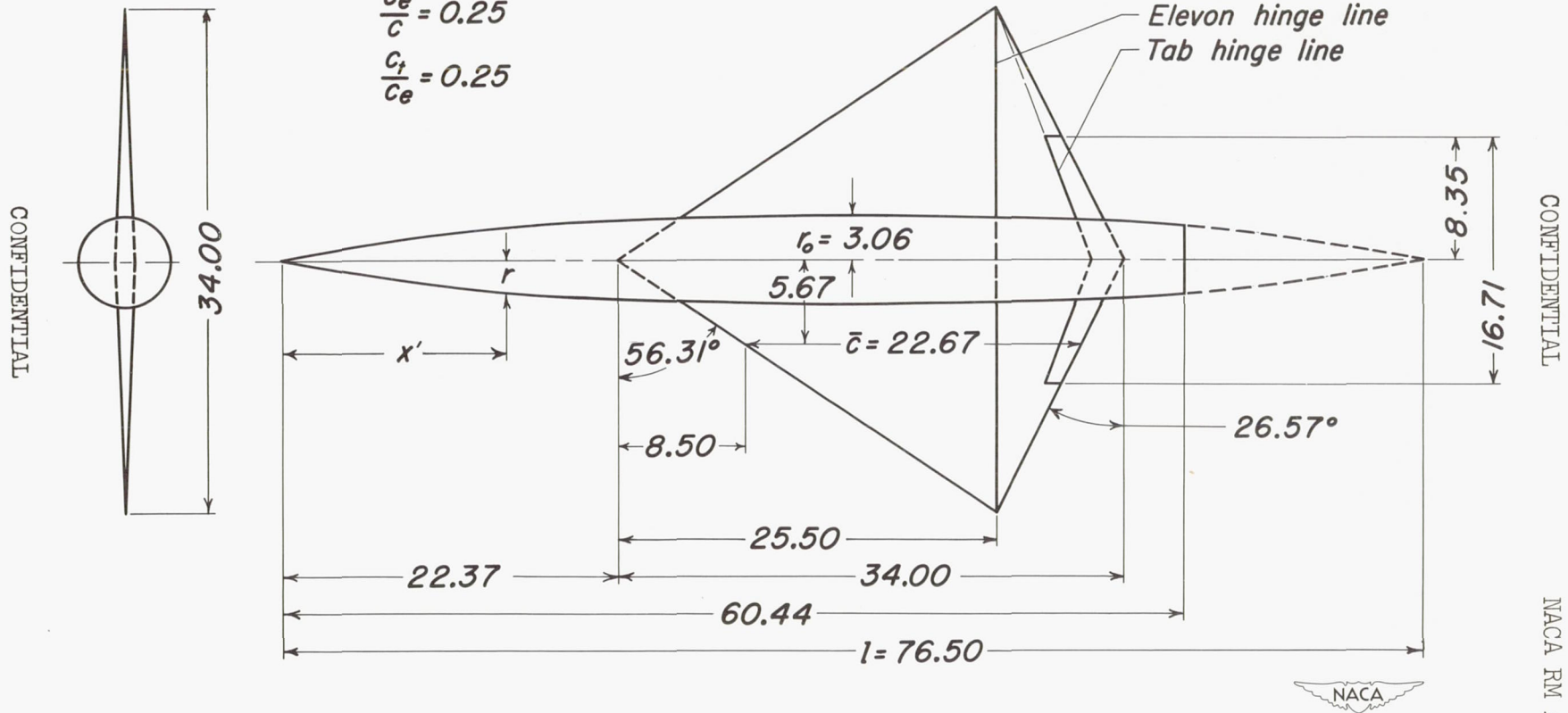
$$\frac{r}{b} = \left[ 1 - \left( 1 - \frac{2x'}{l} \right)^2 \right]^{\frac{3}{4}}$$

All dimensions shown in inches  
unless otherwise noted

Airfoil section, NACA 0005-63

$$\frac{c_e}{c} = 0.25$$

$$\frac{c_t}{c_e} = 0.25$$



CONFIDENTIAL

NACA RM A53F03

Figure 2.- Plan and front views of the model.

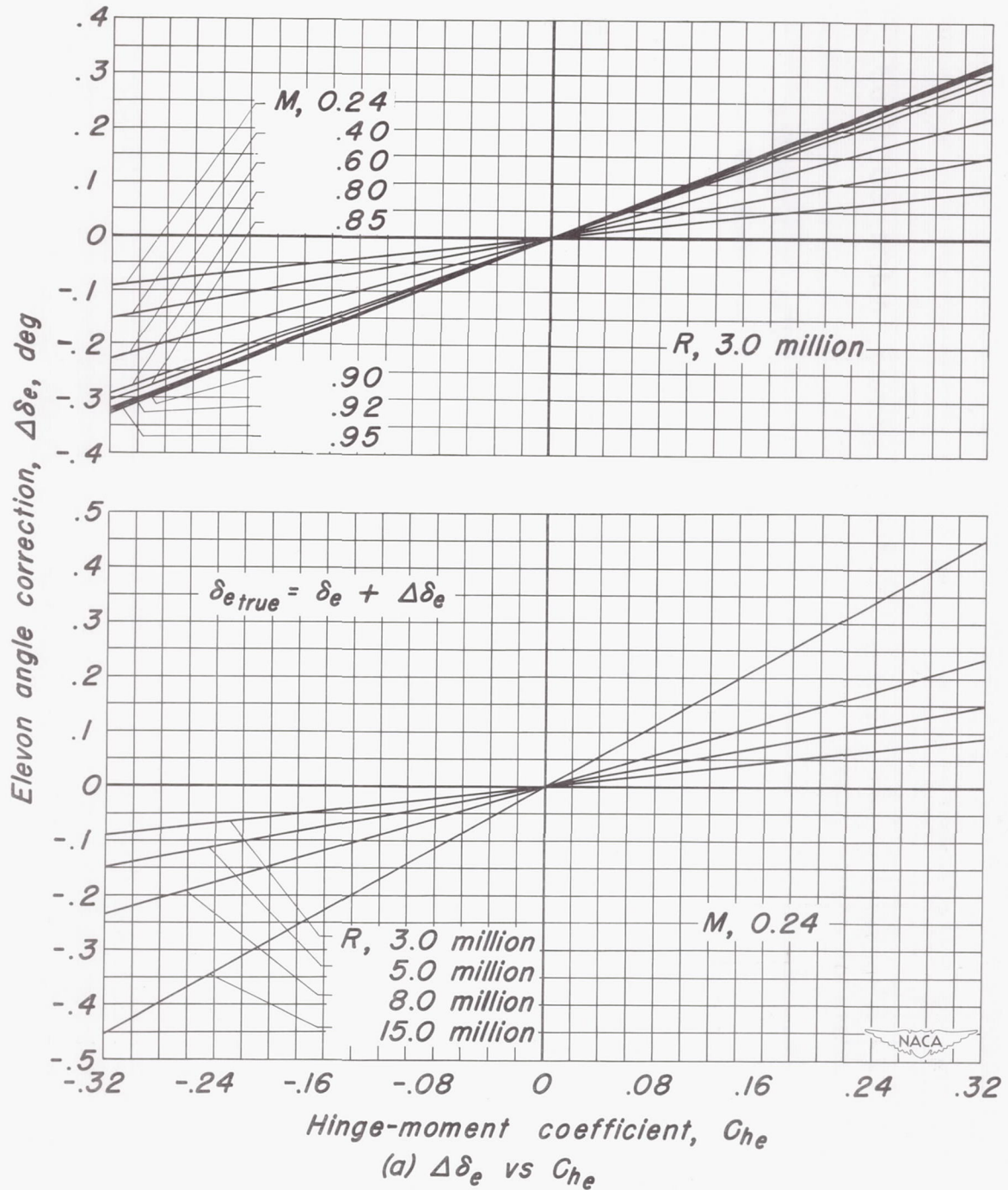
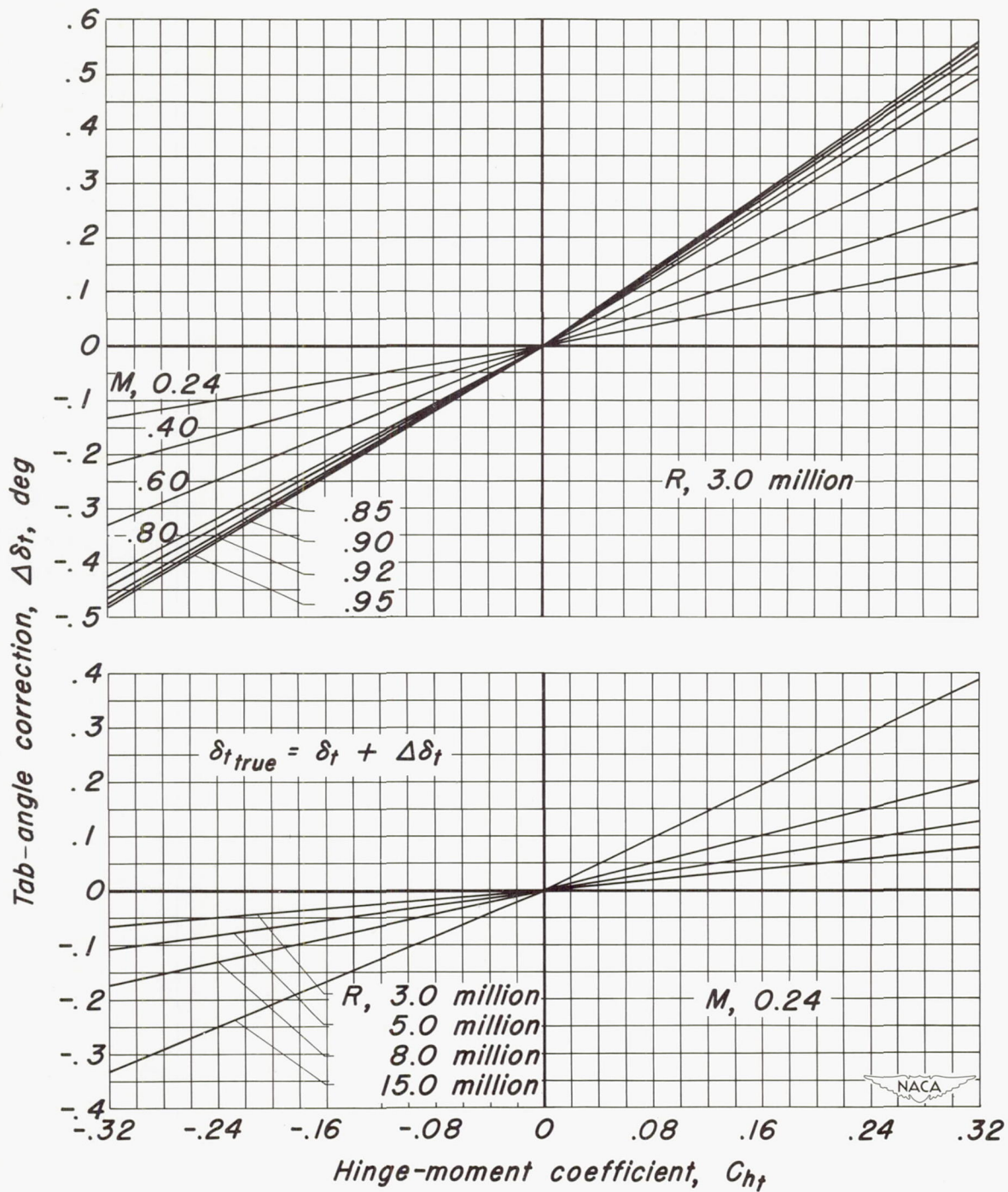


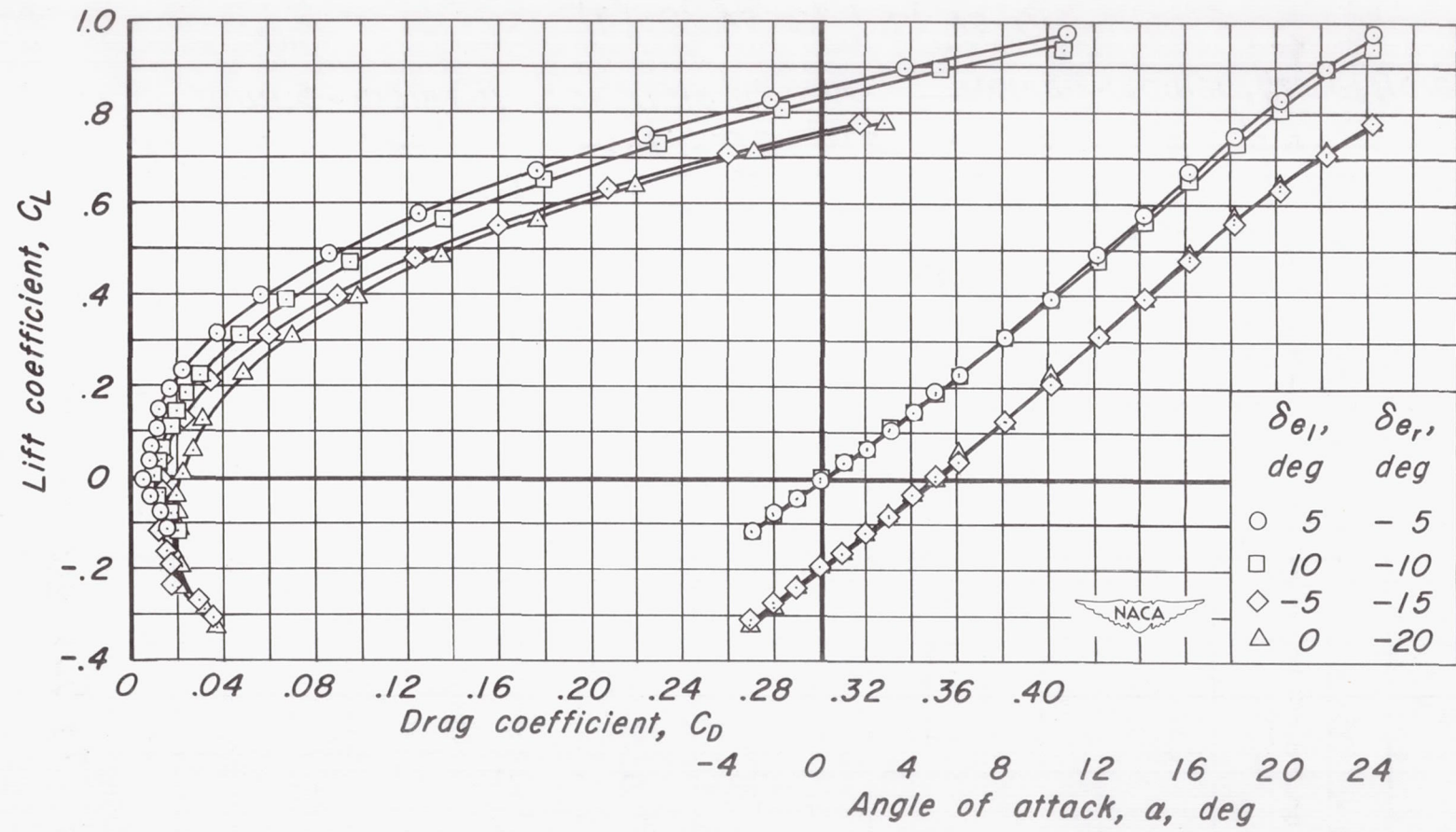
Figure 3.- The variation with hinge-moment coefficient of the elevon and tab-angle corrections,  $\Delta\delta$ , at various Mach numbers and Reynolds numbers.





(b)  $\Delta\delta_t$  vs  $C_{h_t}$

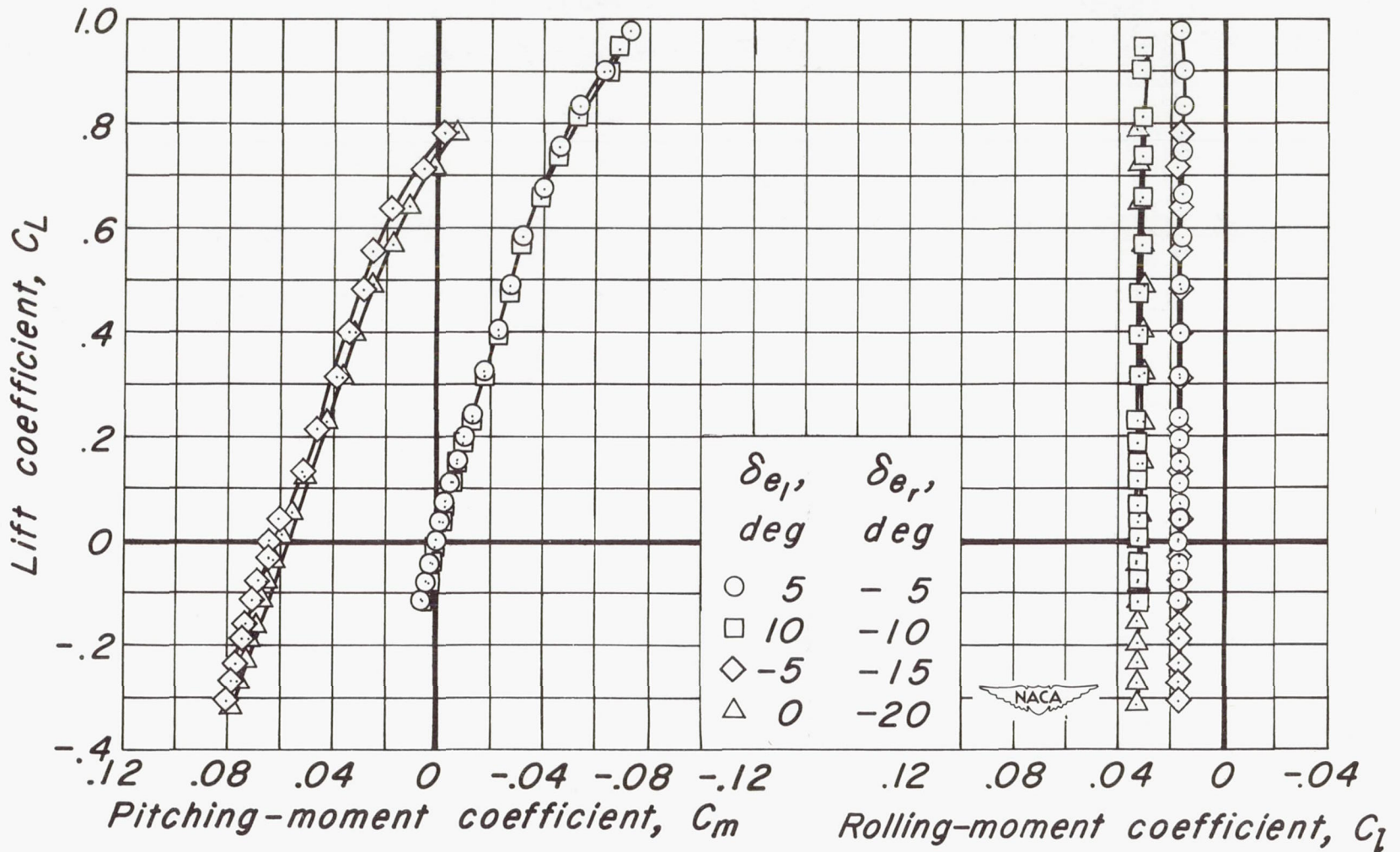
Figure 3.- Concluded.



(a)  $C_L$  vs  $\alpha$ ,  $C_L$  vs  $C_D$

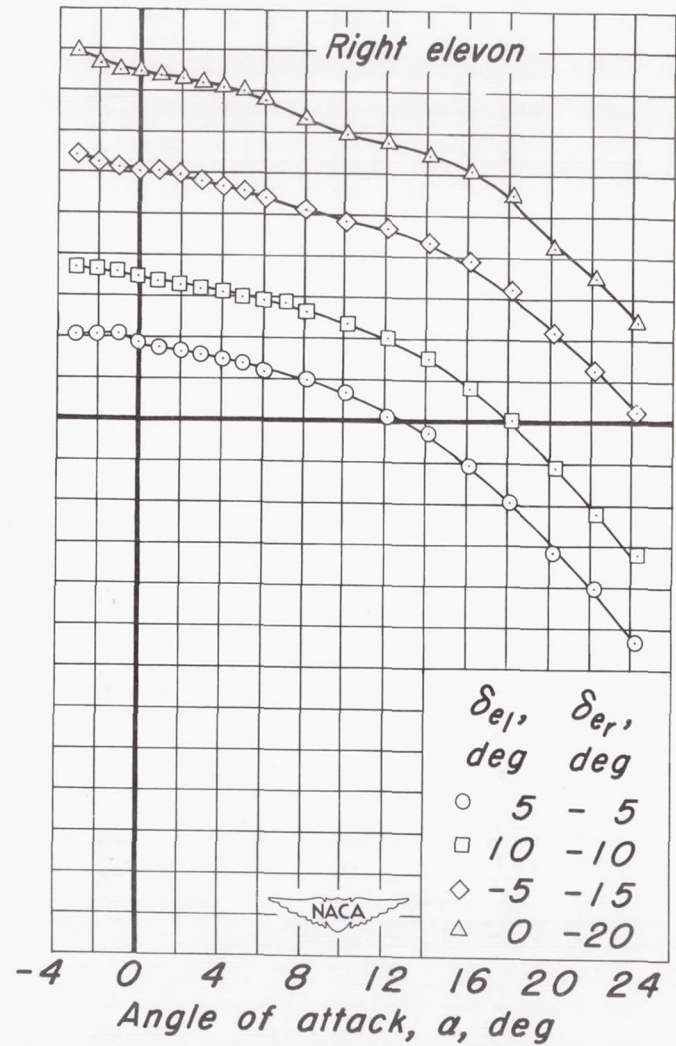
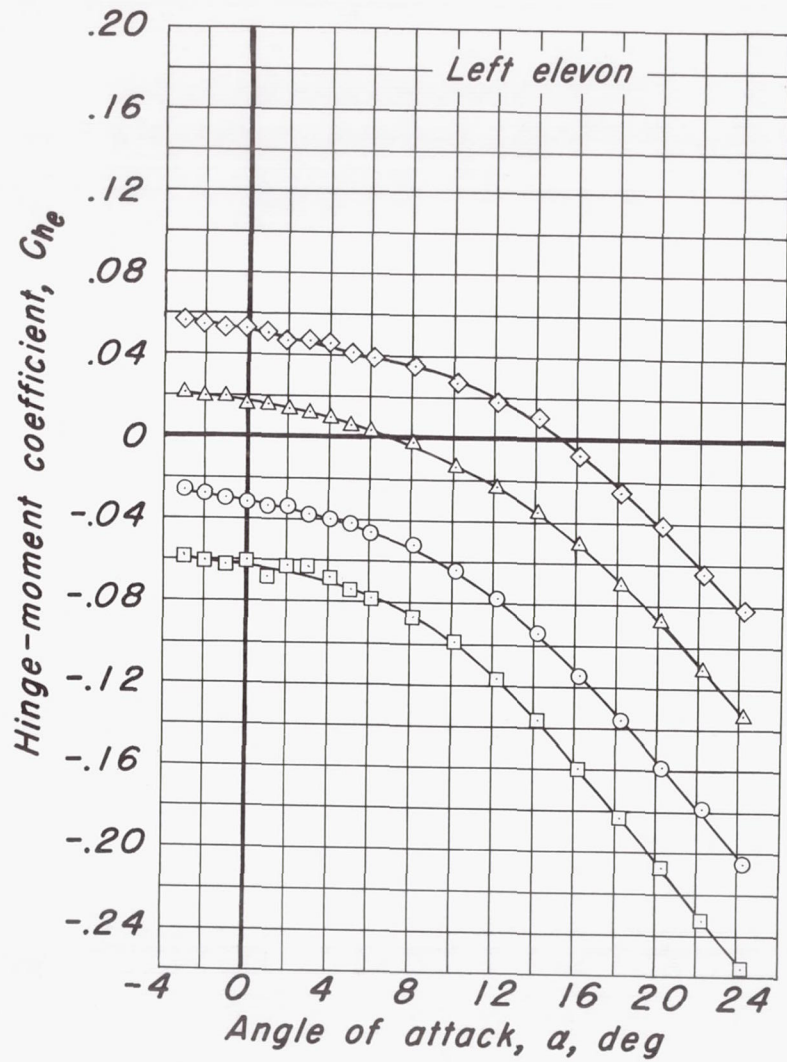
Figure 4.- The effect of differential elevon deflection on the aerodynamic characteristics at a Mach number of 0.24.  $R$ , 3.0 million;  $\delta_t$ ,  $0^\circ$ .





(b)  $C_L$  vs  $C_m$ ,  $C_L$  vs  $C_l$

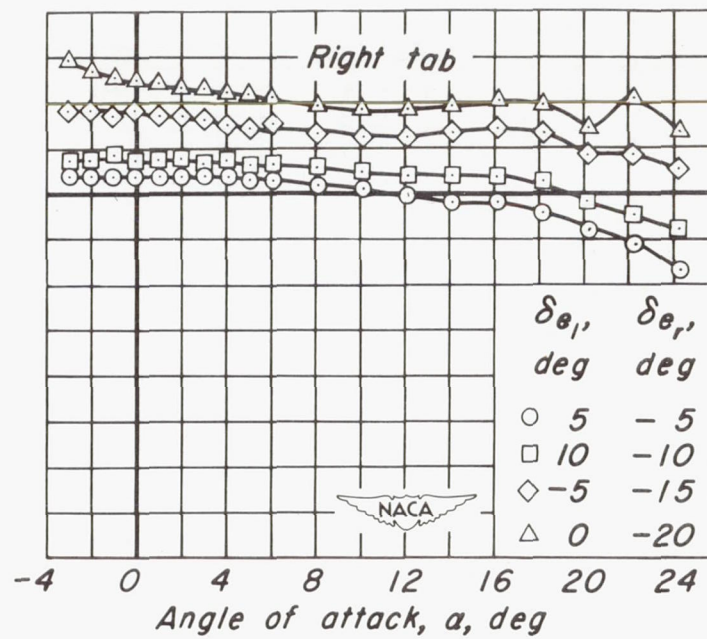
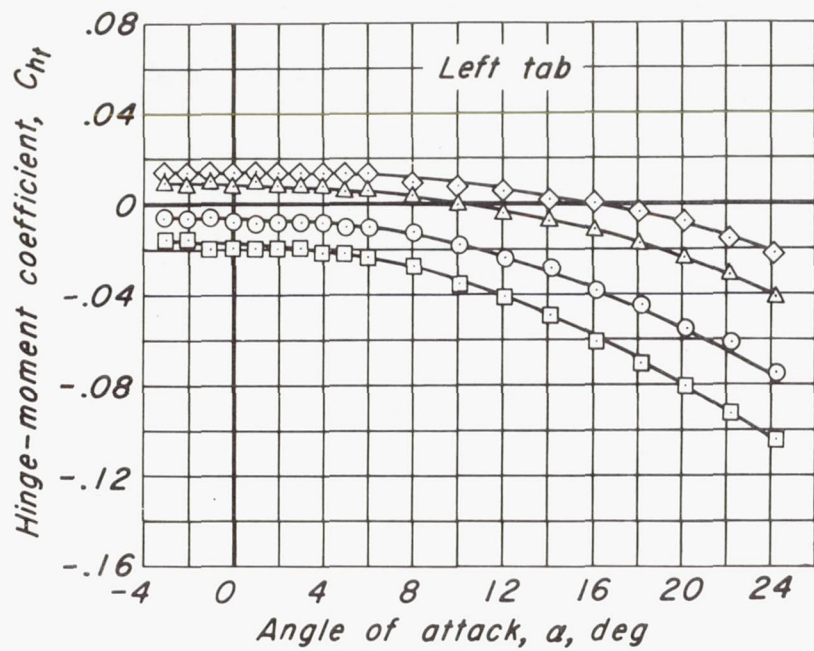
Figure 4.- Continued.



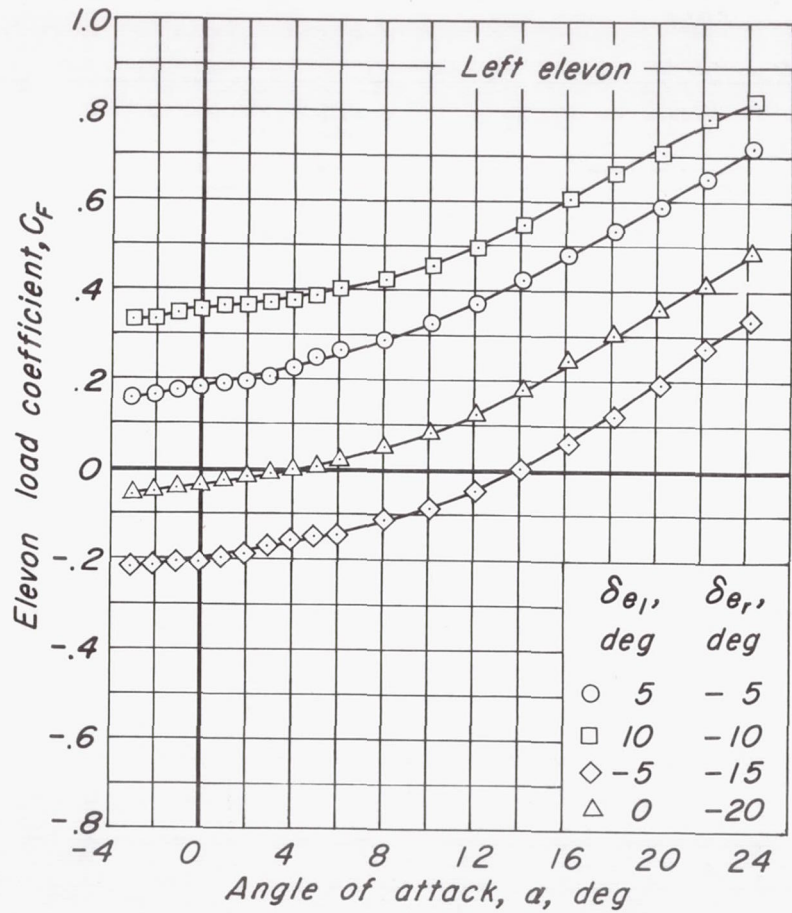
(c)  $C_{he}$  vs  $\alpha$

Figure 4.- Continued.

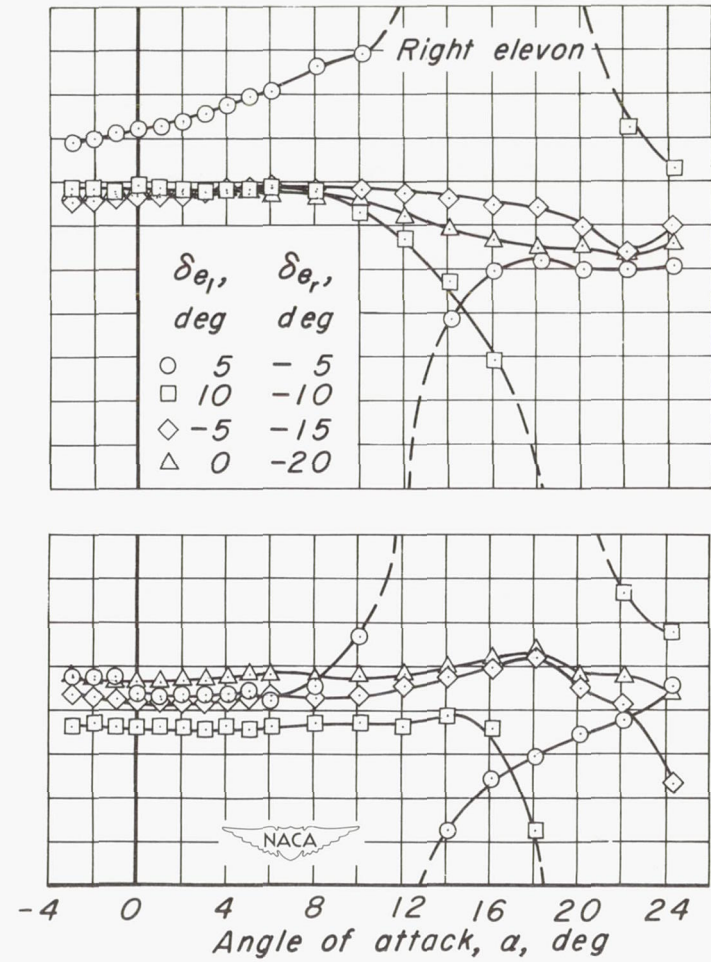
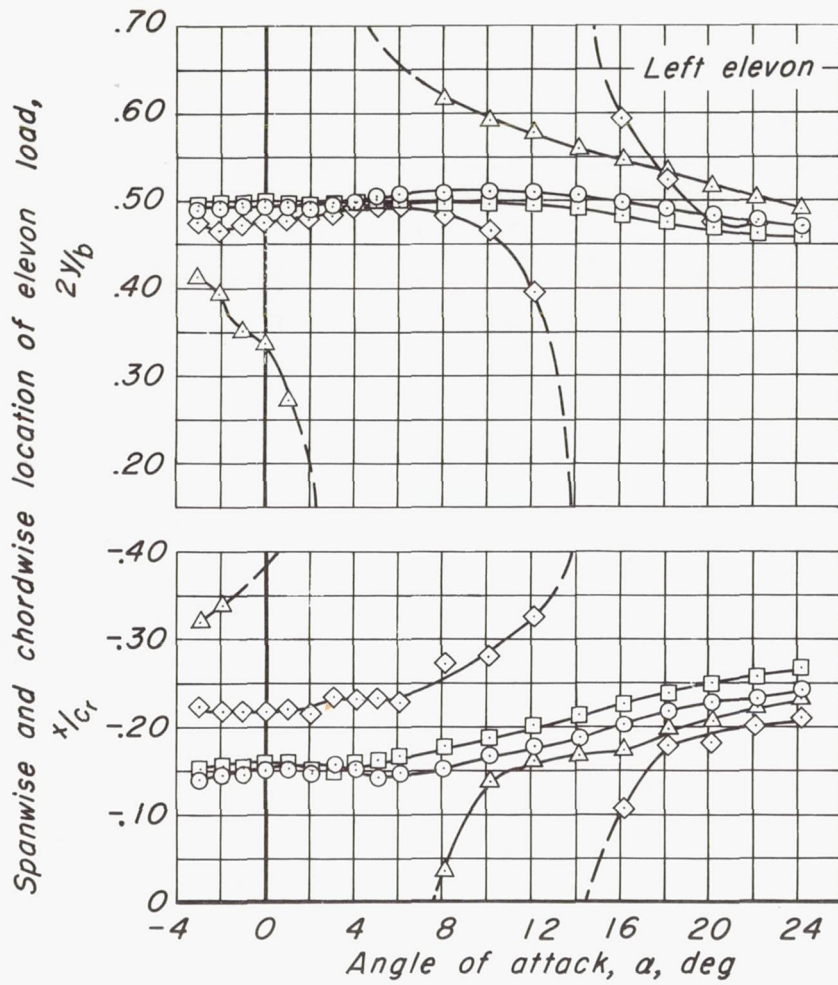




(d)  $C_{h_t}$  vs  $\alpha$   
Figure 4.-Continued.

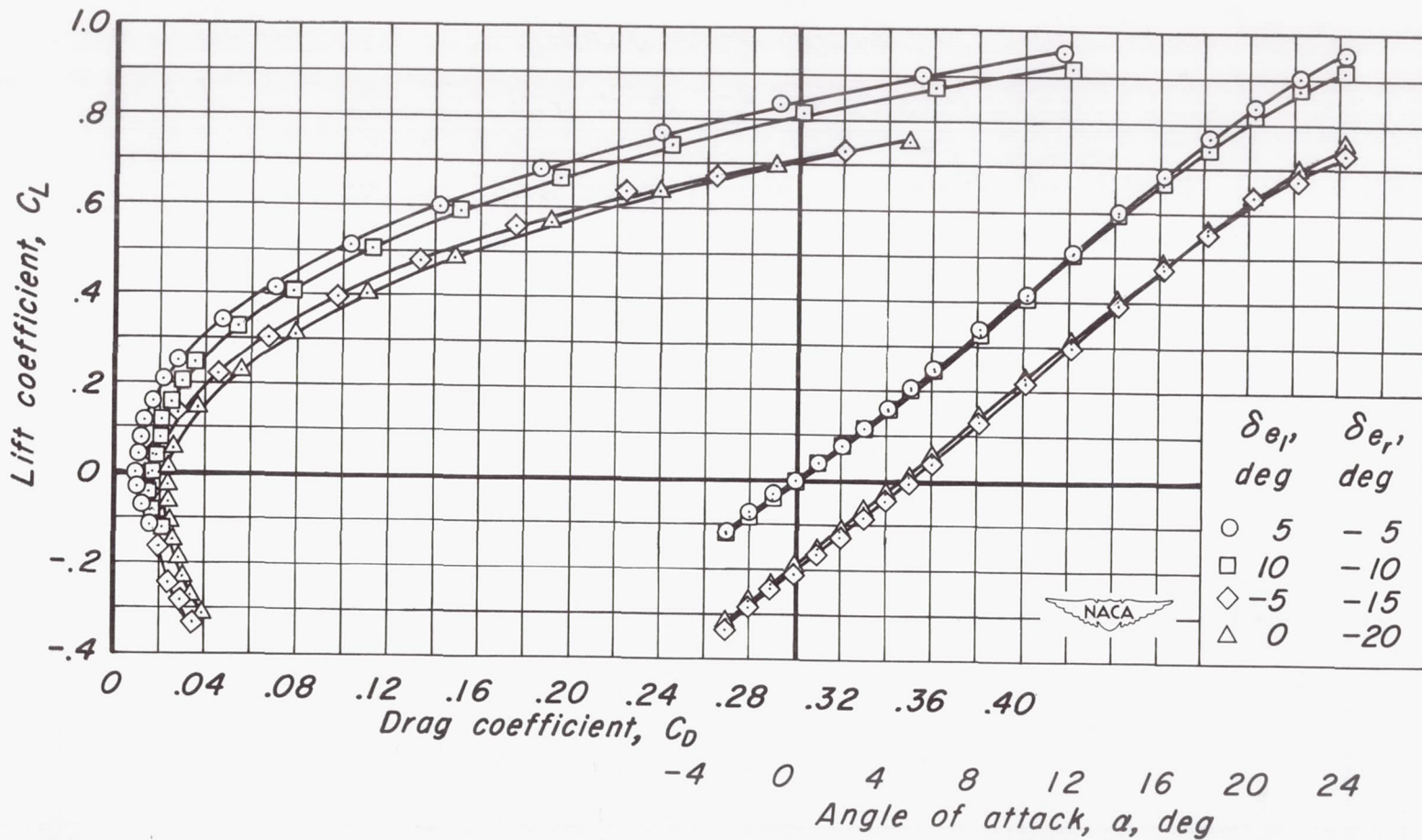


(e)  $C_F$  vs  $\alpha$   
Figure 4.- Continued.



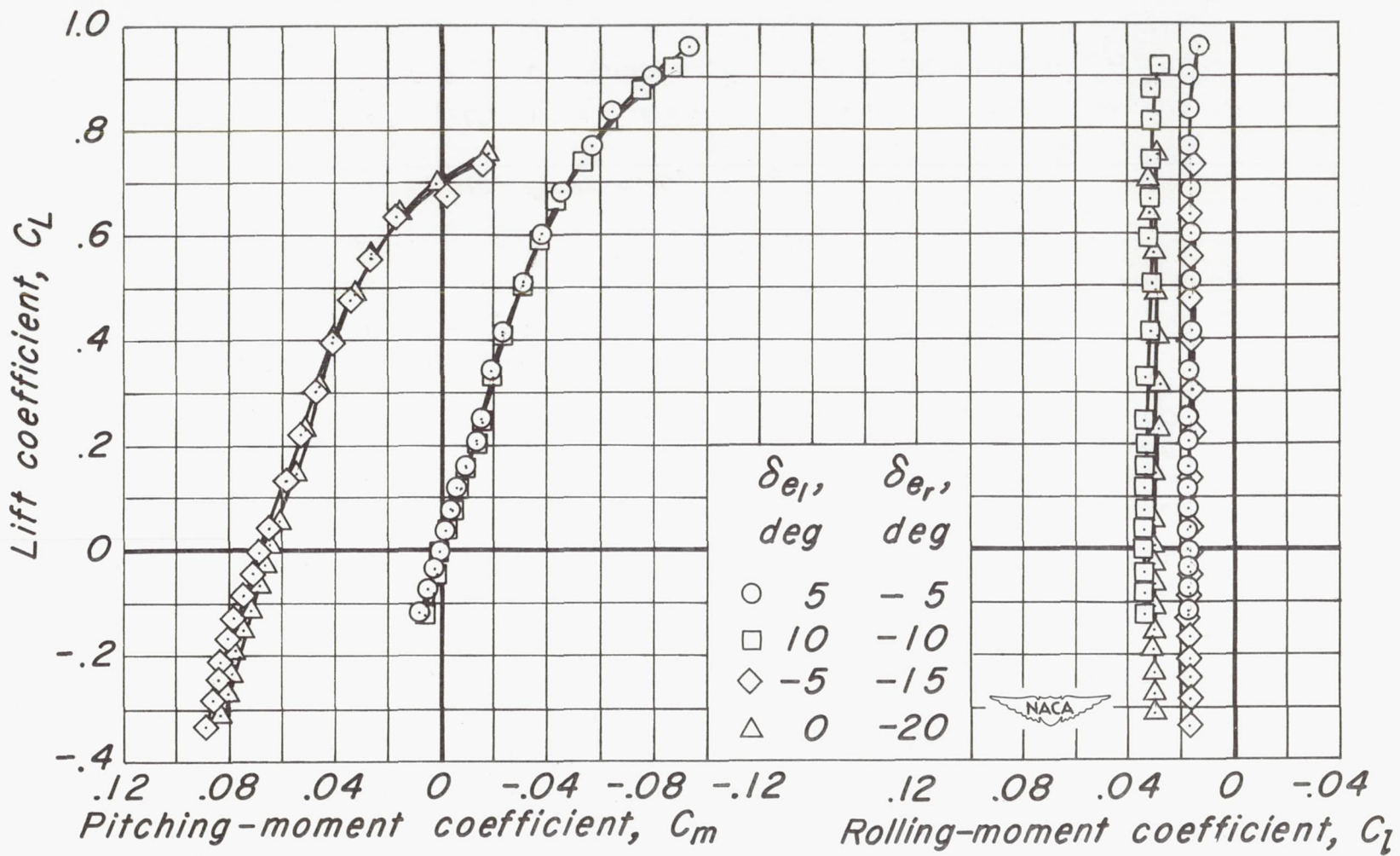
(f)  $2y/b$  vs  $\alpha$ ,  $x/c_r$  vs  $\alpha$   
 Figure 4.- Concluded.



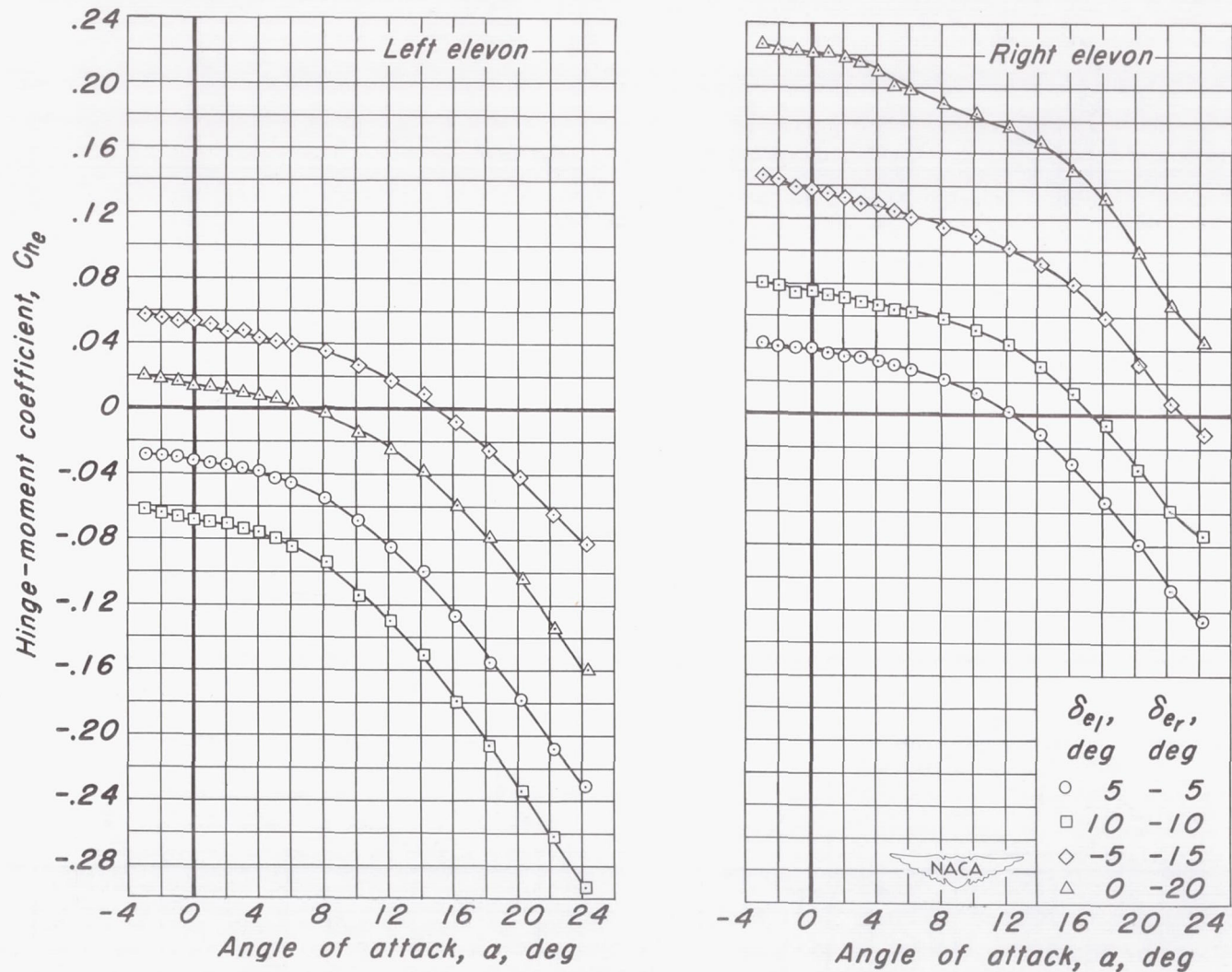


(a)  $C_L$  vs  $\alpha$ ,  $C_L$  vs  $C_D$

Figure 5.- The effect of differential elevon deflection on the aerodynamic characteristics at a Mach number of 0.60.  $R$ , 3.0 million;  $\delta_t$ ,  $0^\circ$ .



(b)  $C_L$  vs  $C_m$ ,  $C_L$  vs  $C_l$   
Figure 5.- Continued.

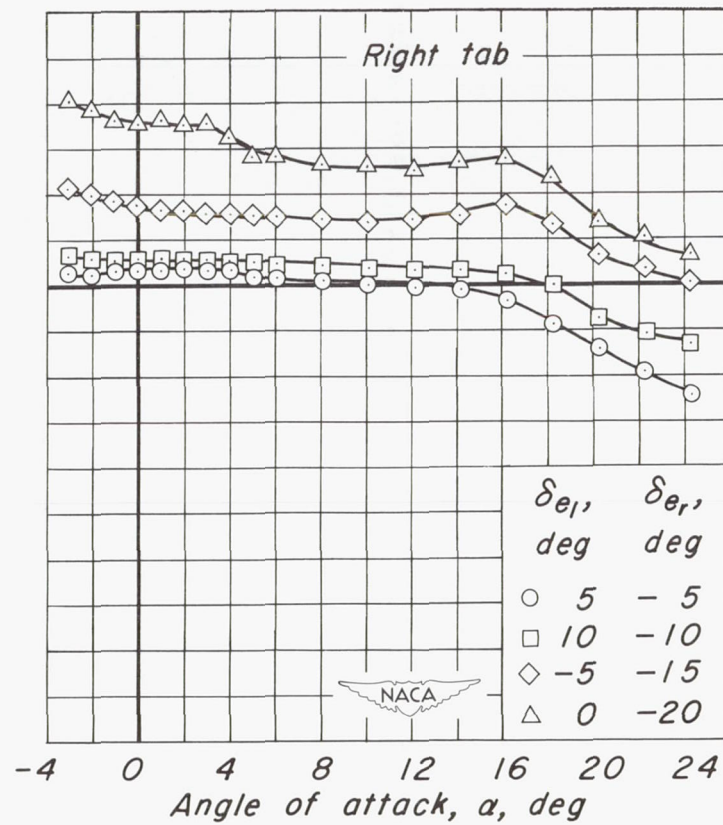
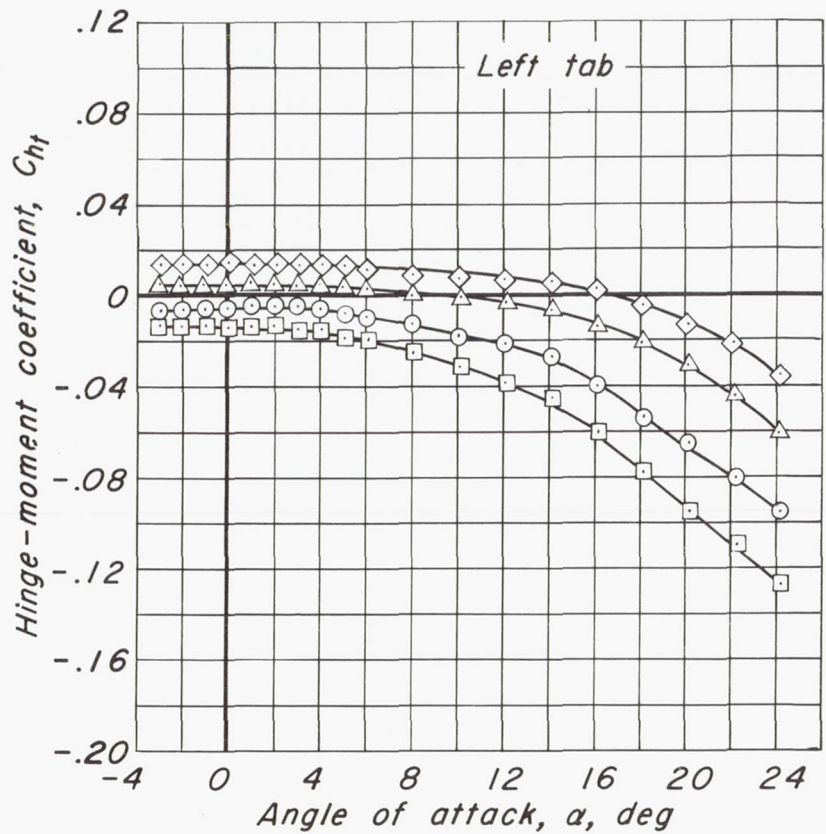


(c)  $C_{he}$  vs  $\alpha$

Figure 5.- Continued.



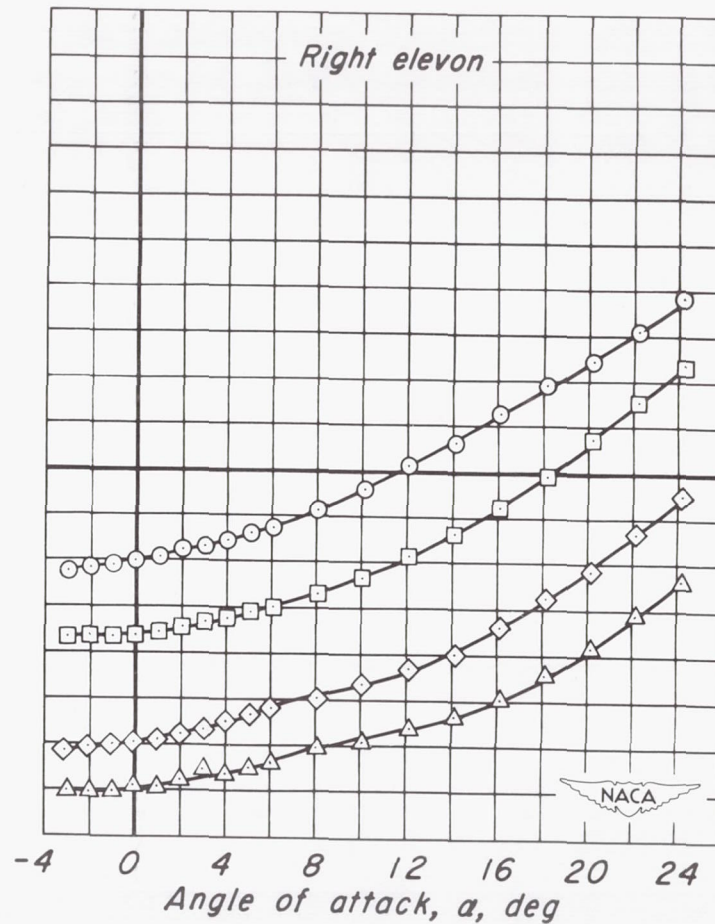
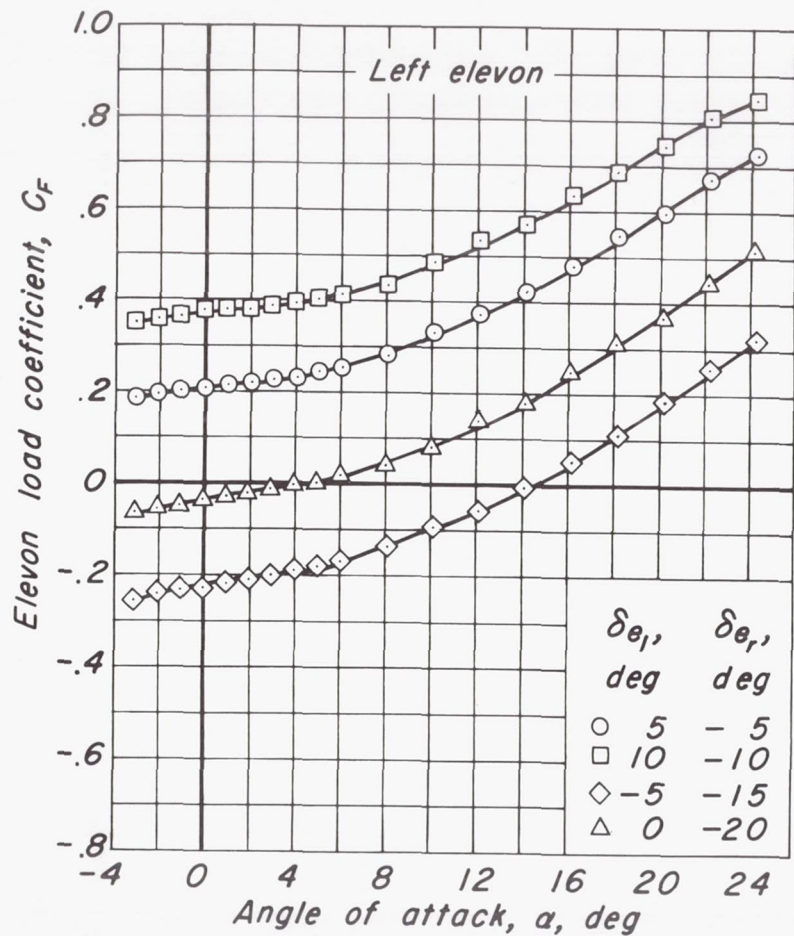
CONFIDENTIAL



(d)  $C_{ht}$  vs  $\alpha$

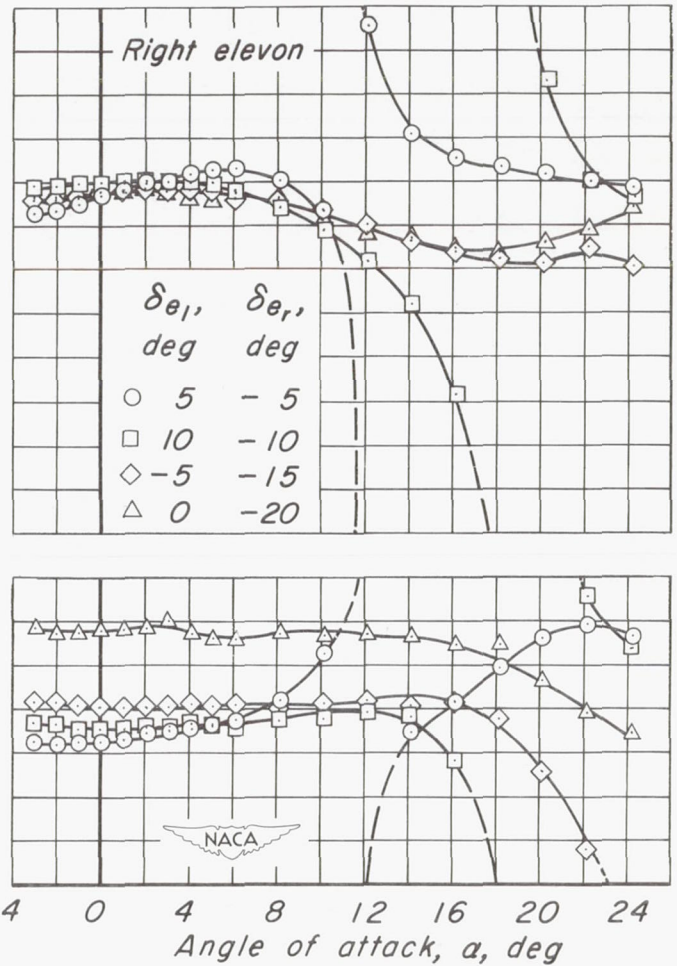
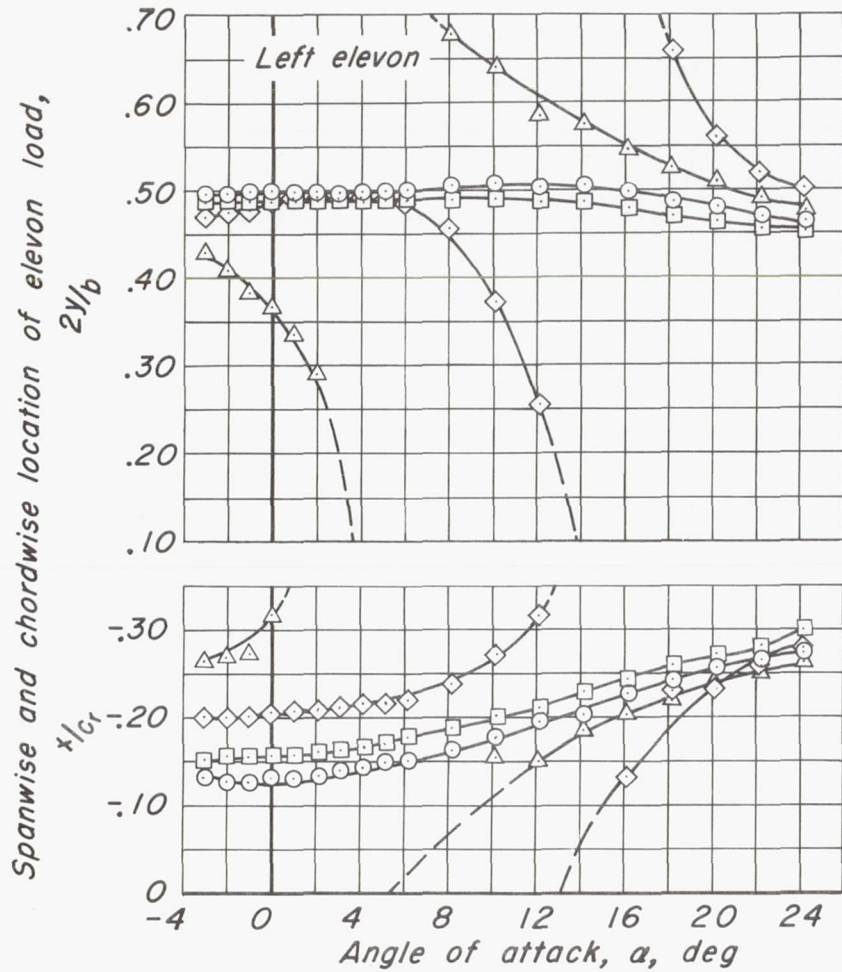
Figure 5.- Continued.

CONFIDENTIAL



(e)  $C_F$  vs  $\alpha$

Figure 5.- Continued.



(f)  $2y/b$  vs  $\alpha$ ,  $x/c_r$  vs  $\alpha$   
 Figure 5.- Concluded.



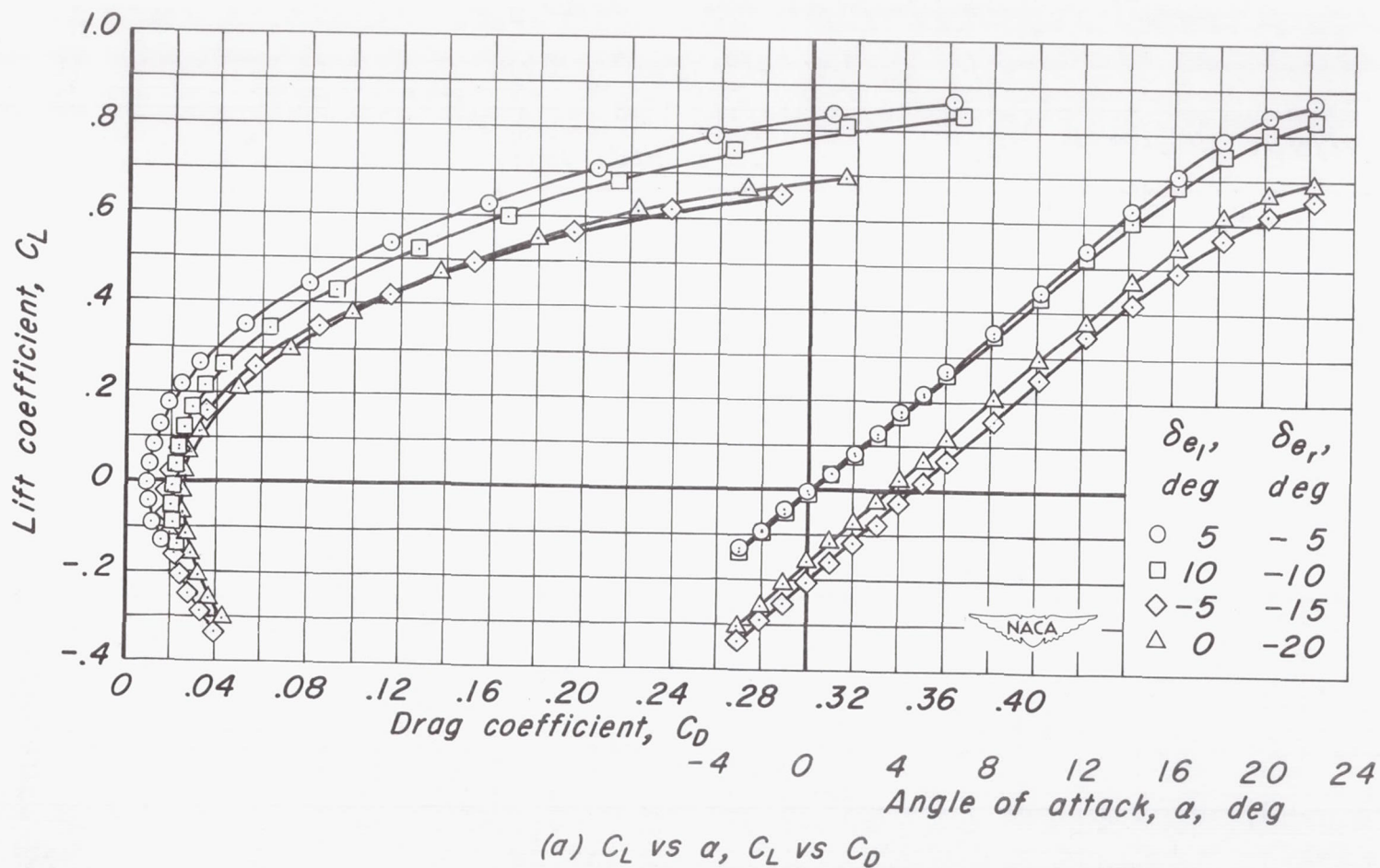
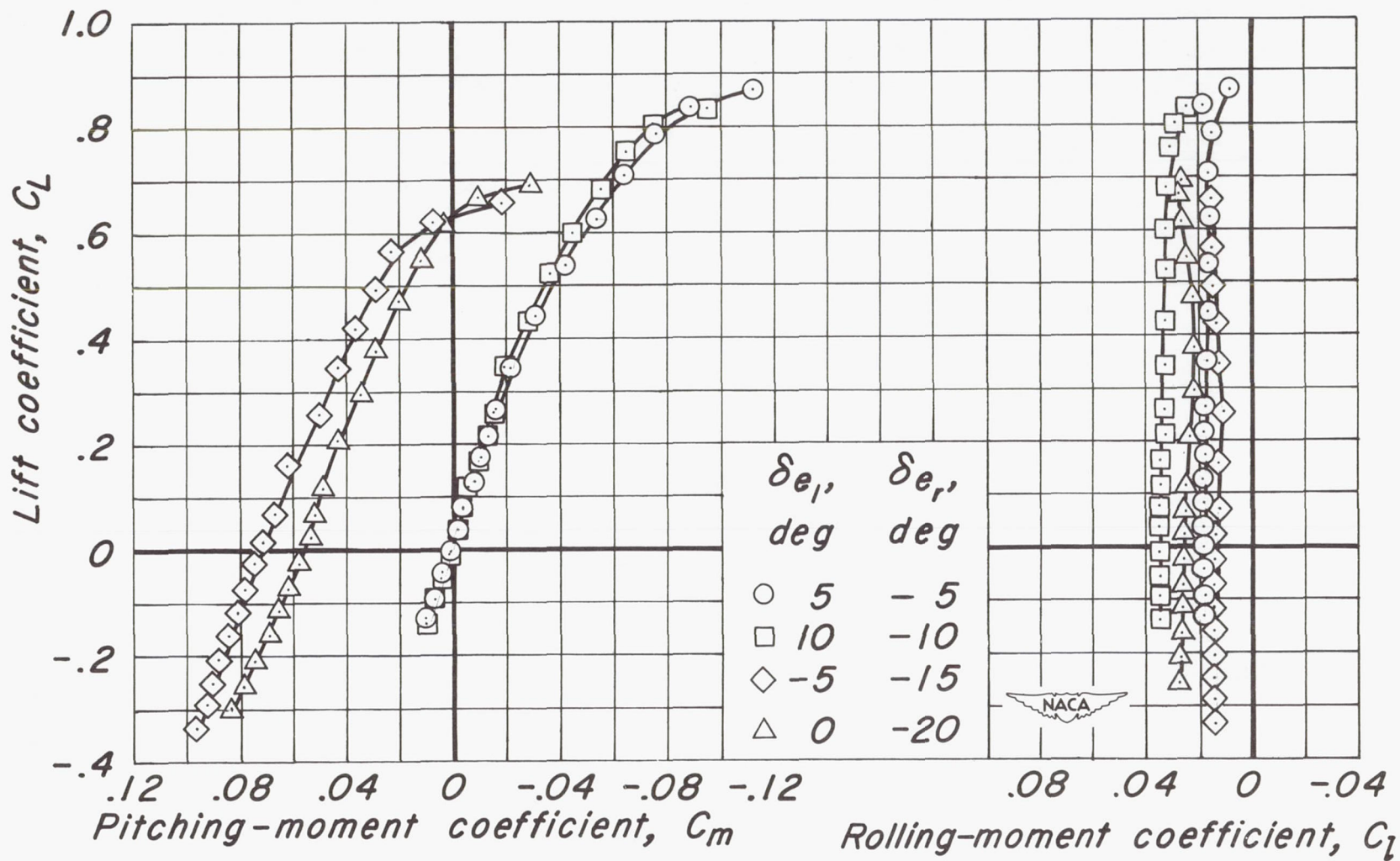
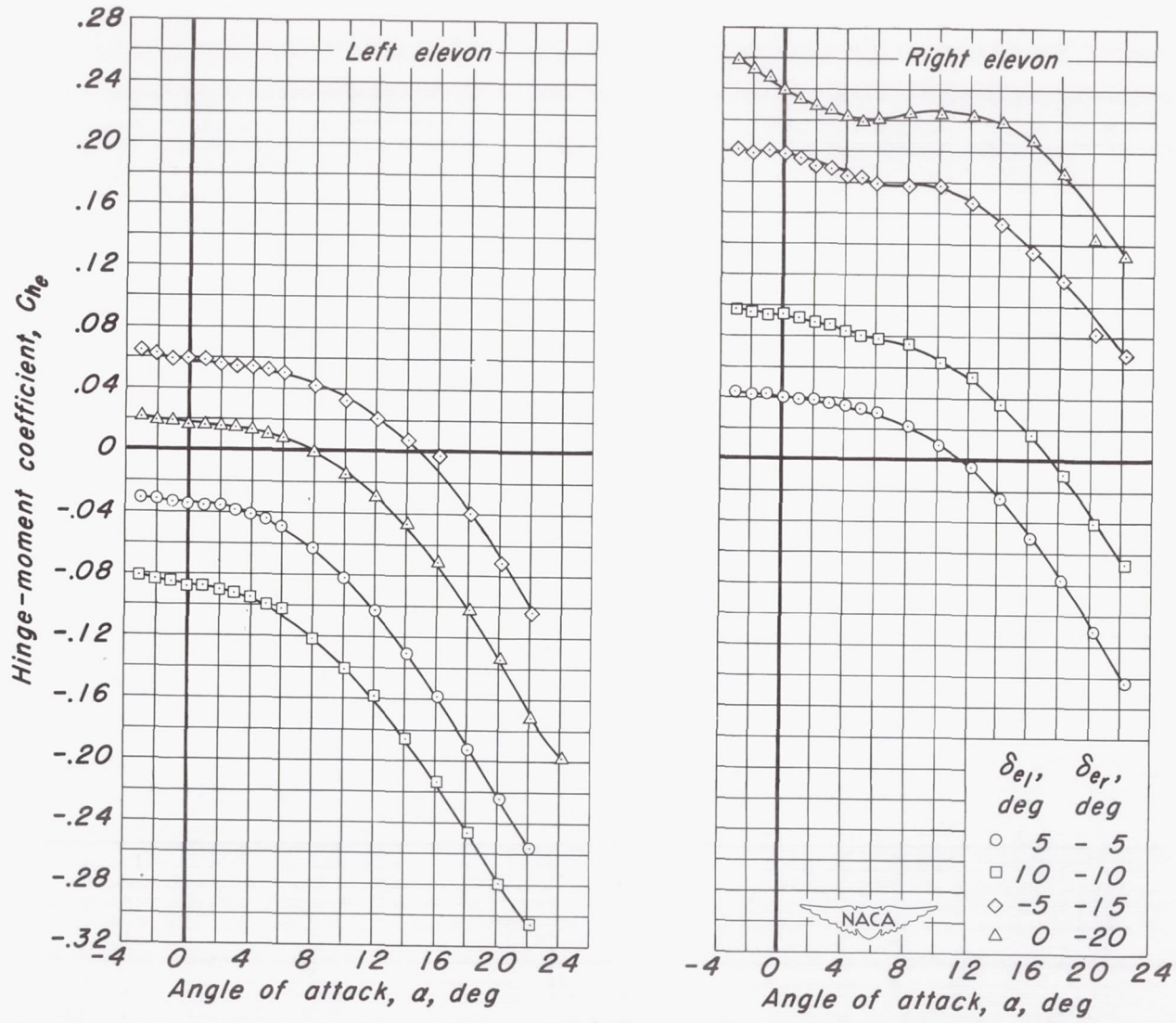


Figure 6.- The effect of differential elevon deflection on the aerodynamic characteristics at a Mach number of 0.80.  $R$ , 3.0 million;  $\delta_t$ ,  $0^\circ$ .



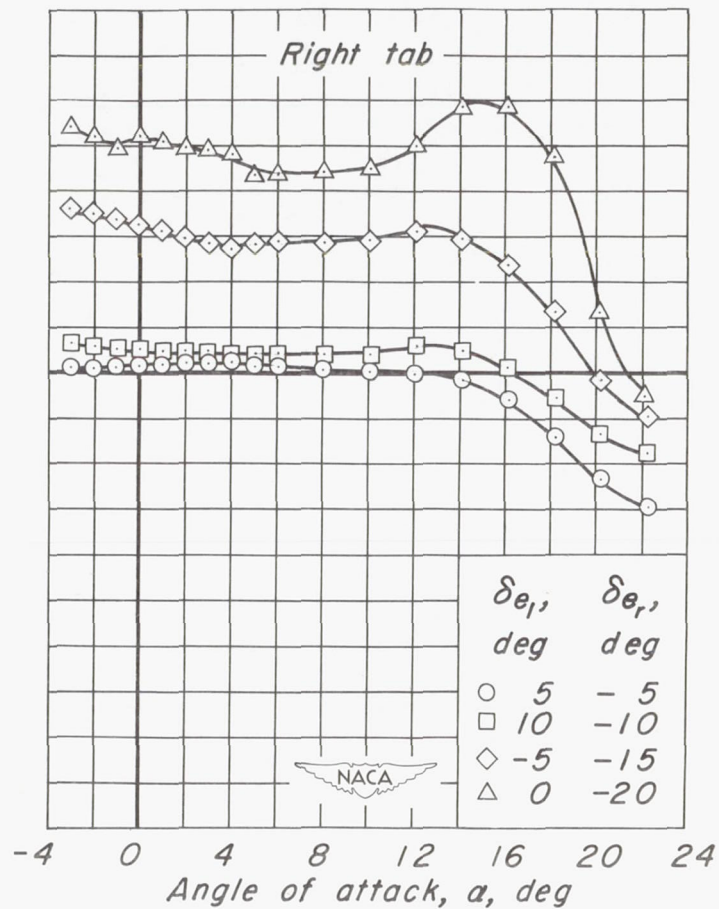
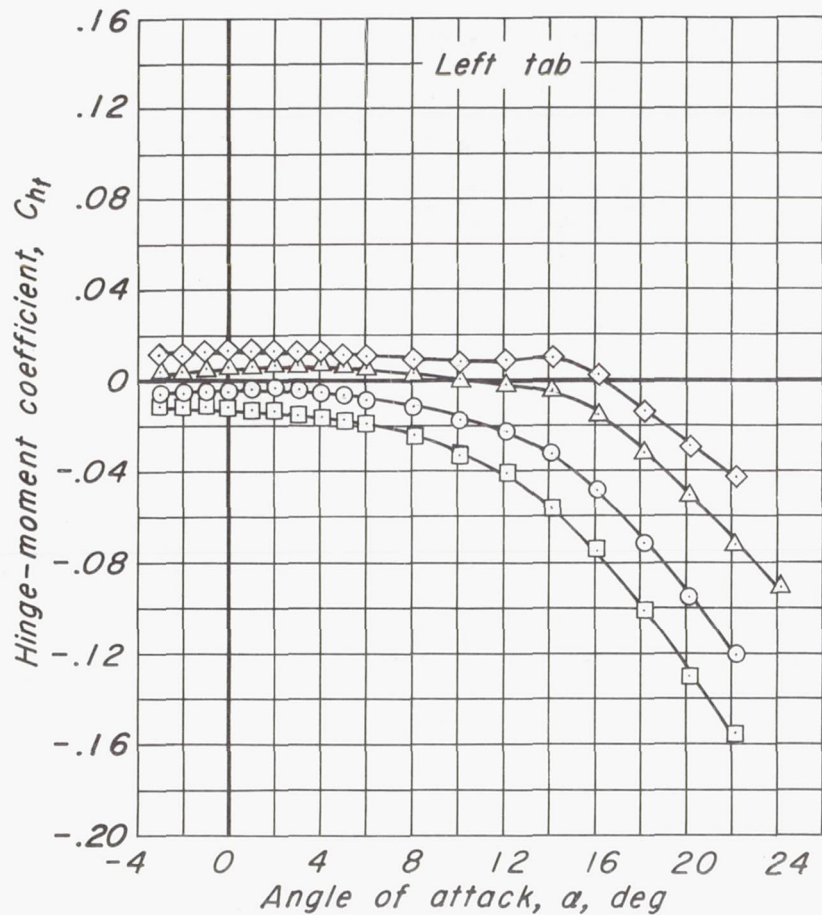
(b)  $C_L$  vs  $C_m$ ,  $C_L$  vs  $C_l$

Figure 6.- Continued.



(c)  $C_{he}$  vs  $\alpha$   
Figure 6.- Continued.





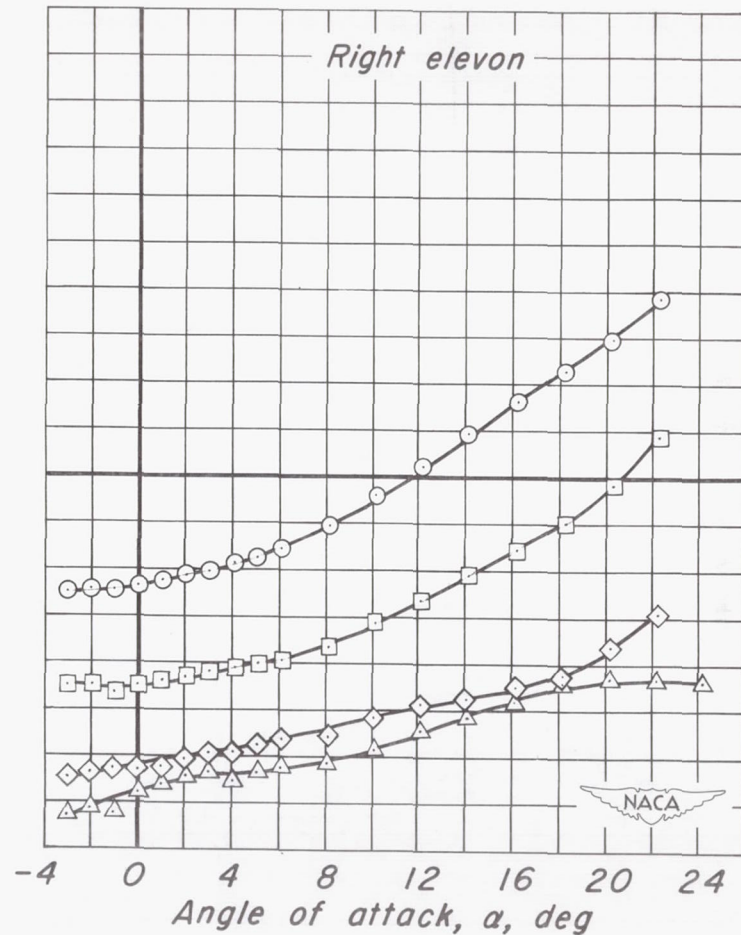
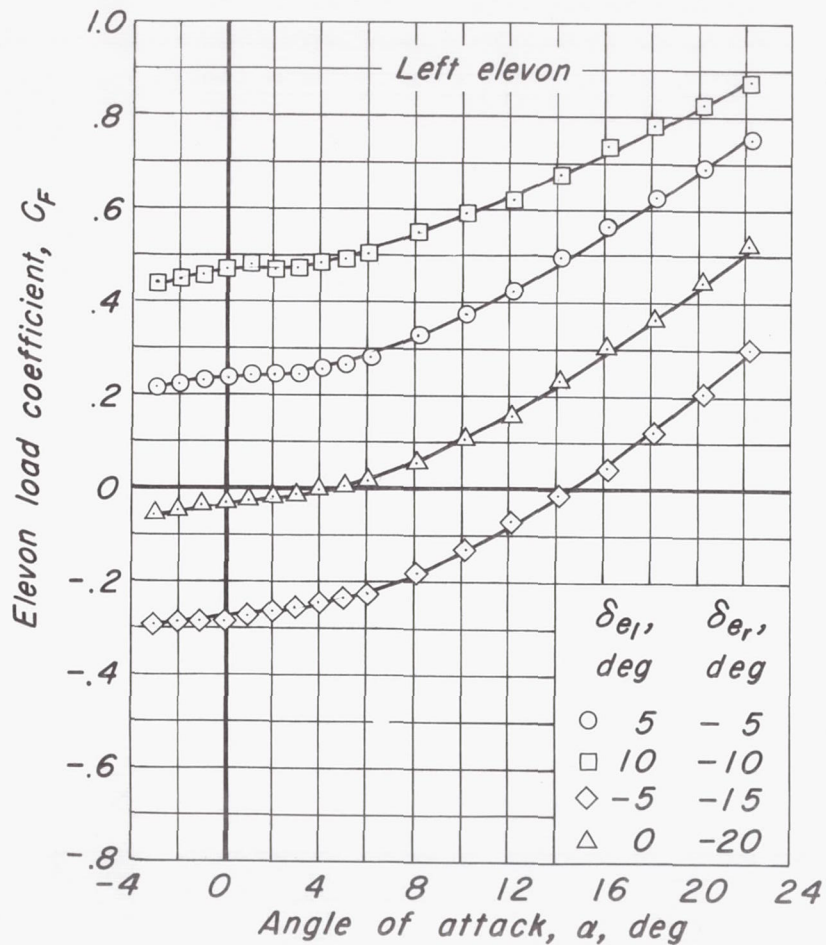
$\delta e_1$ , deg	$\delta e_1$ , deg
○ 5	- 5
□ 10	- 10
◇ -5	- 15
△ 0	- 20



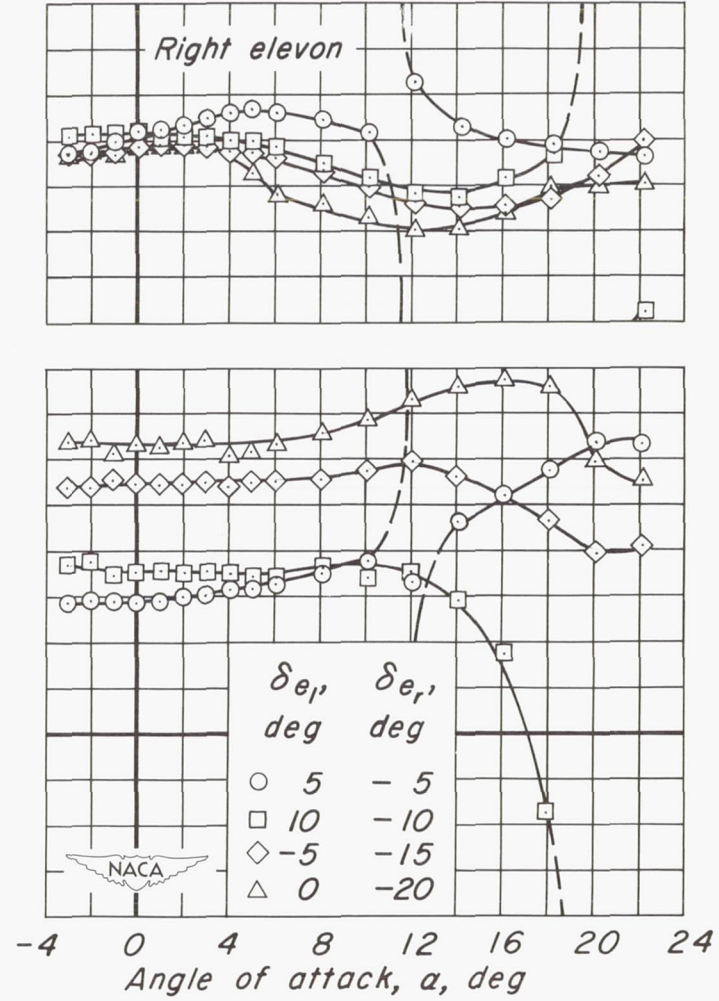
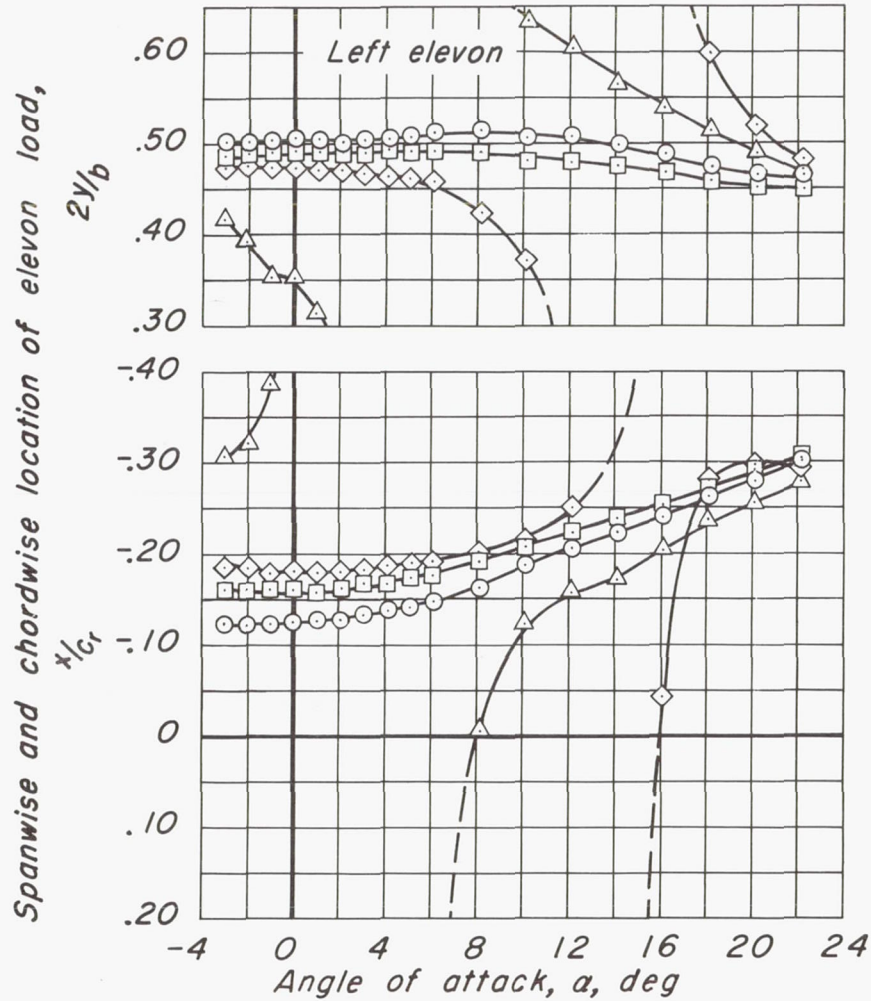
(d)  $C_{ht}$  vs  $\alpha$

Figure 6.- Continued.

CONFIDENTIAL

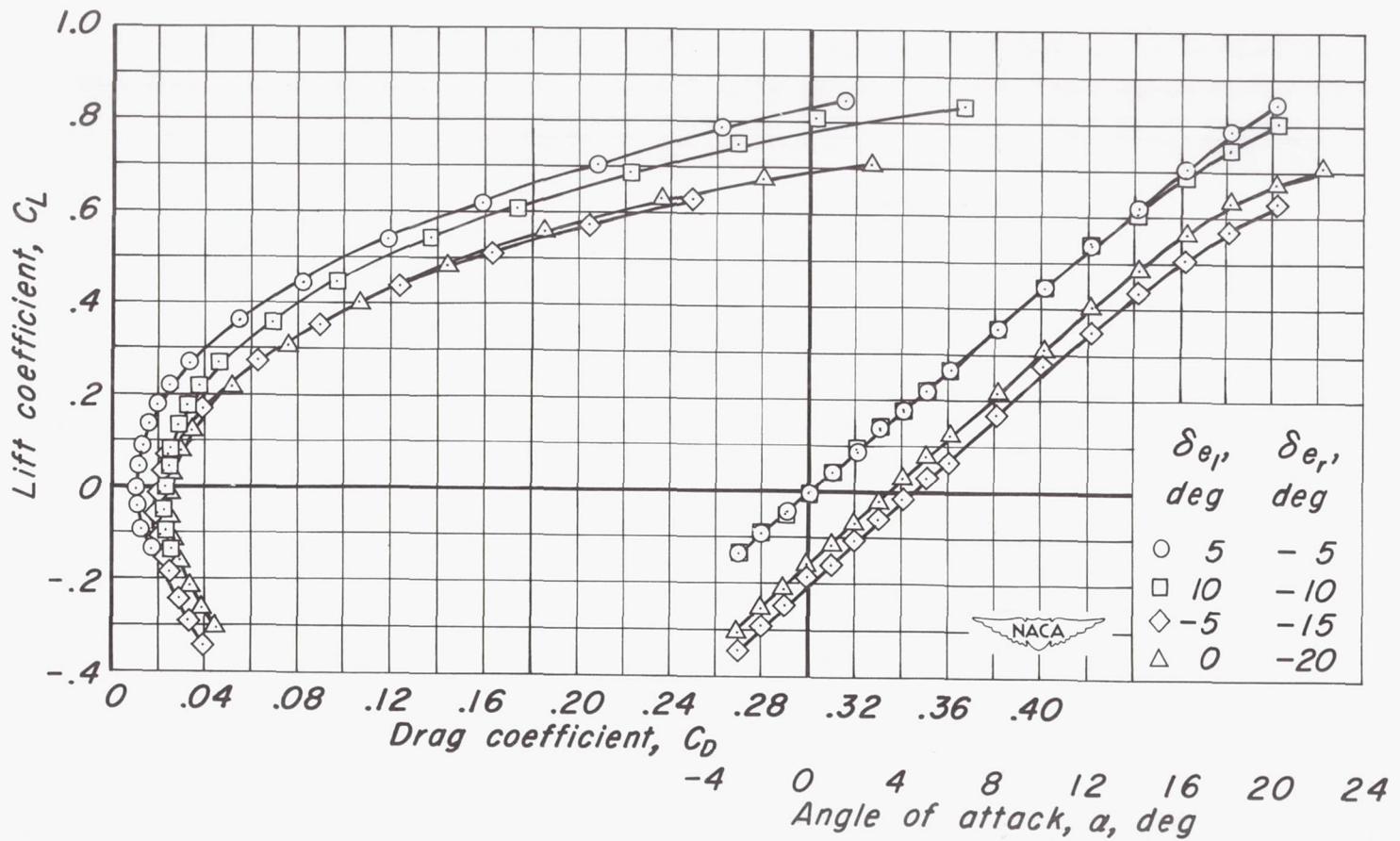


(e)  $C_F$  vs  $\alpha$   
 Figure 6- Continued.



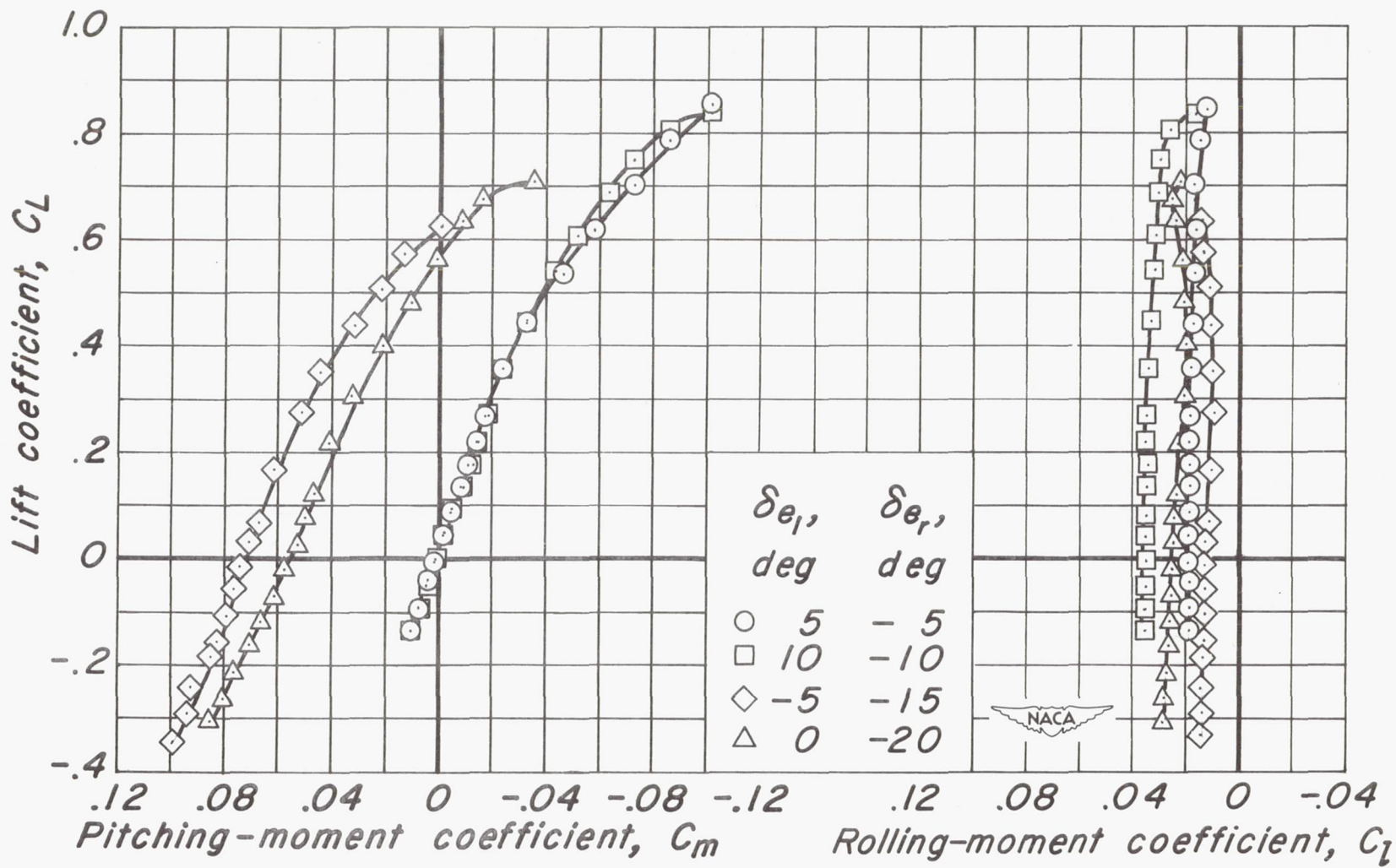
(f)  $2y/b$  vs  $\alpha$ ,  $x/c_r$  vs  $\alpha$   
Figure 6.- Concluded.



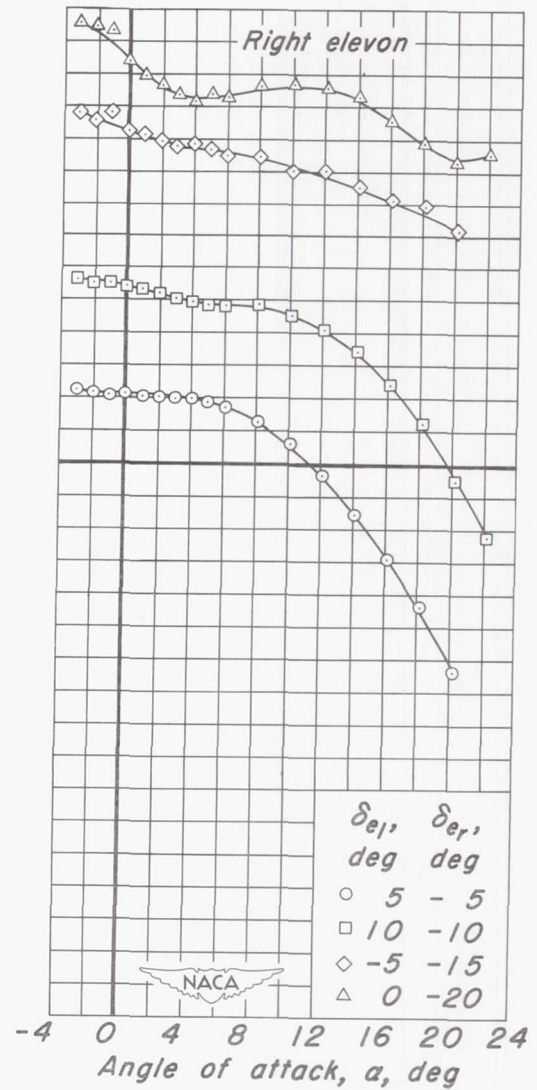
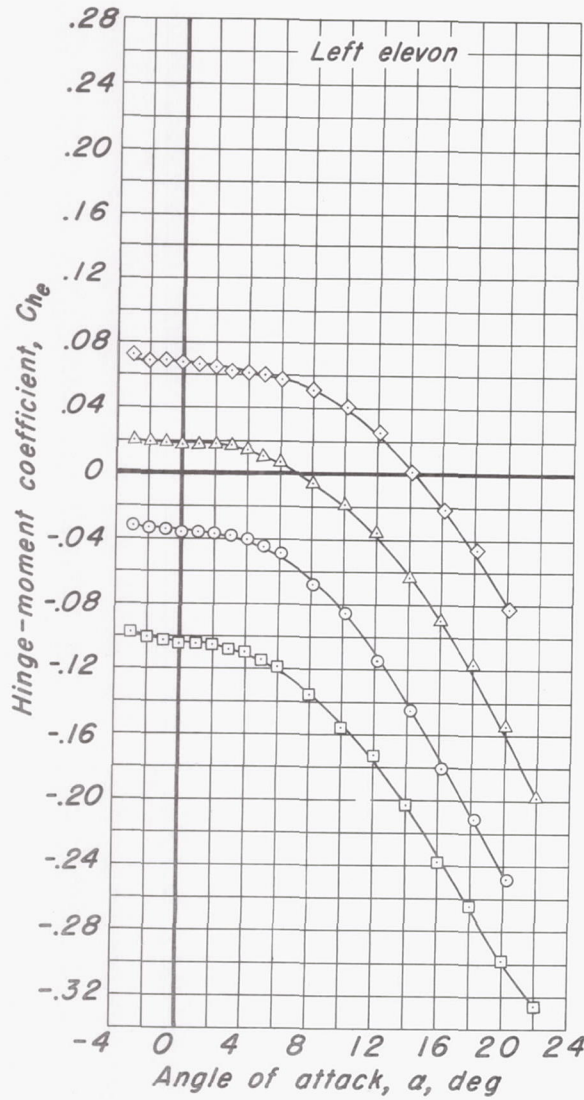


(a)  $C_L$  vs  $\alpha$ ,  $C_L$  vs  $C_D$

Figure 7:- The effect of differential elevon deflection on the aerodynamic characteristics at a Mach number of 0.85.  $R$ , 3.0 million;  $\delta_t$ ,  $0^\circ$ .

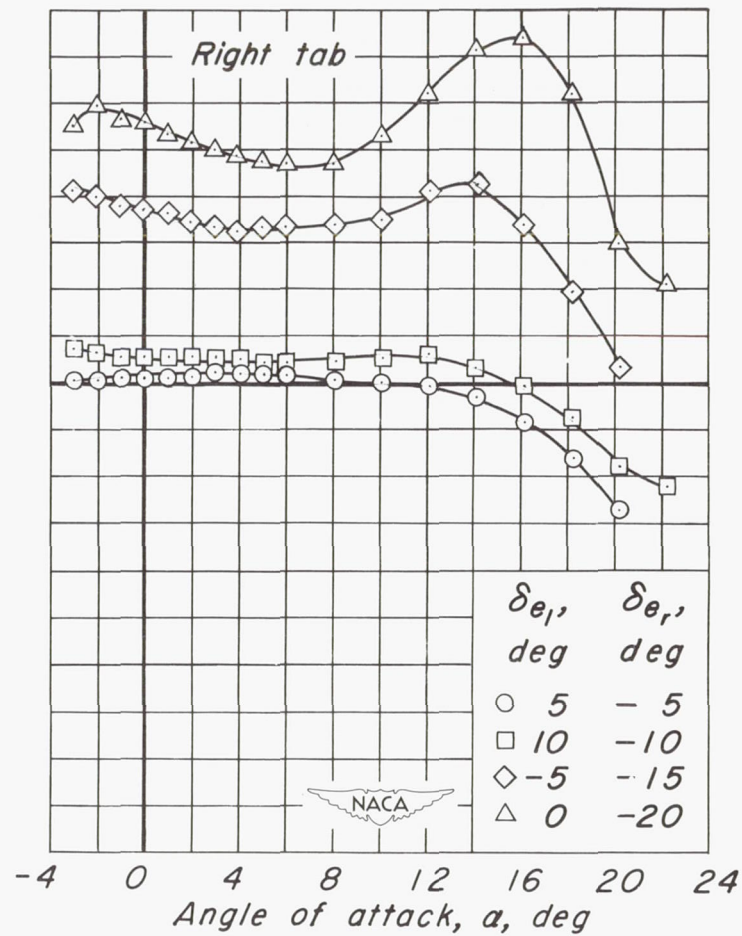
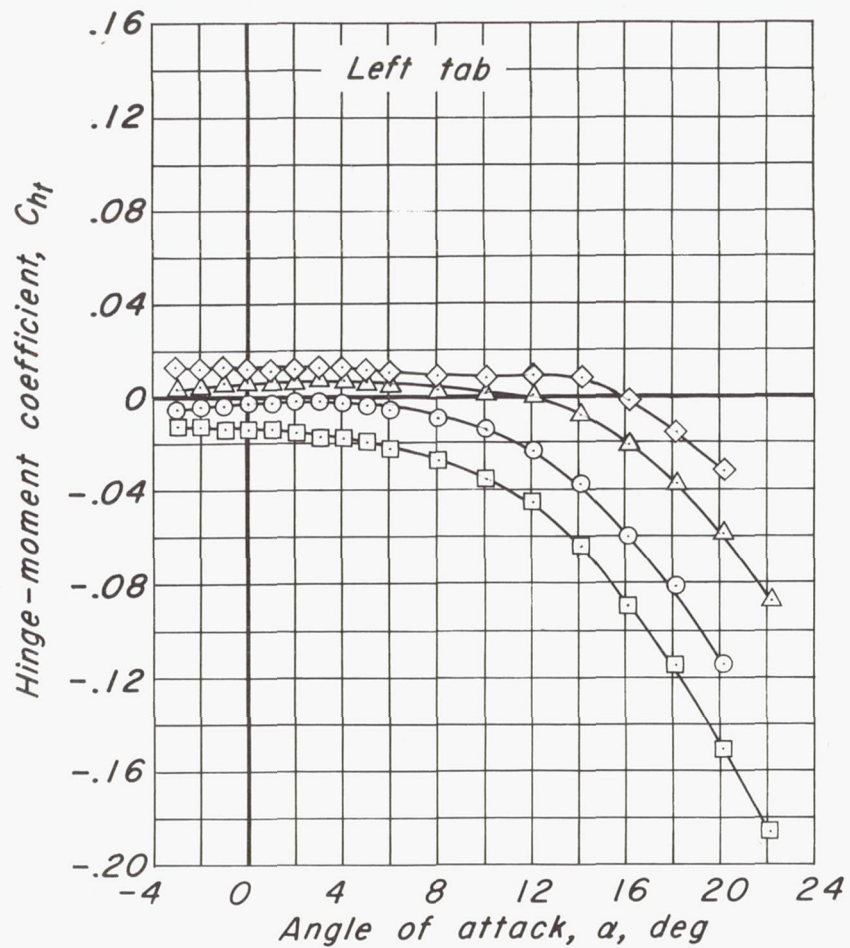


(b)  $C_L$  vs  $C_m$ ,  $C_L$  vs  $C_l$   
 Figure 7.- Continued.



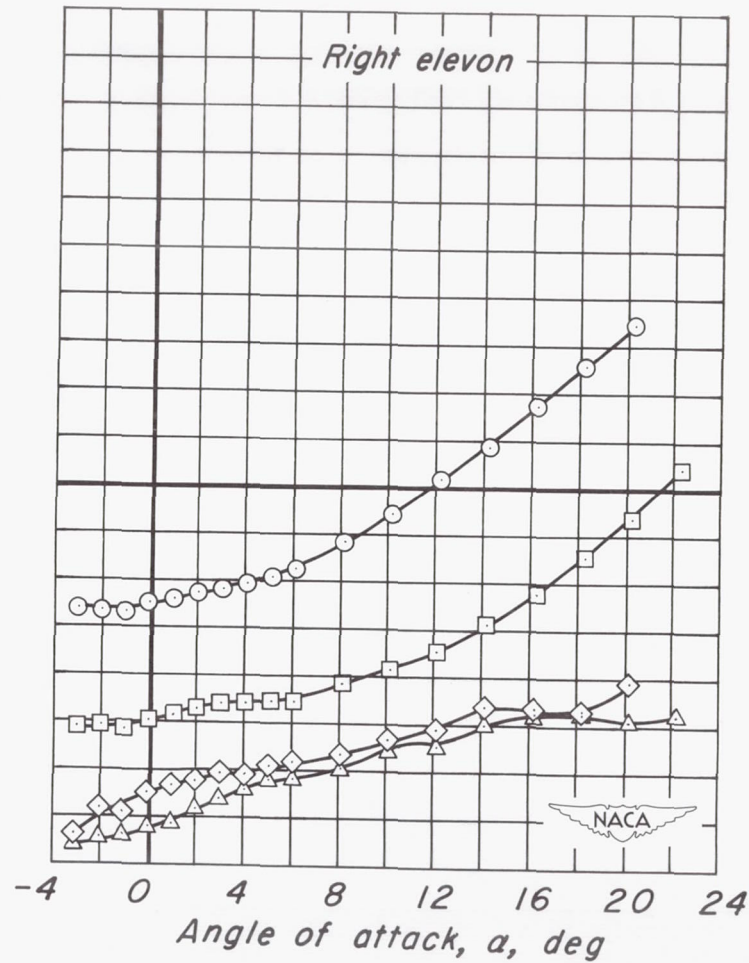
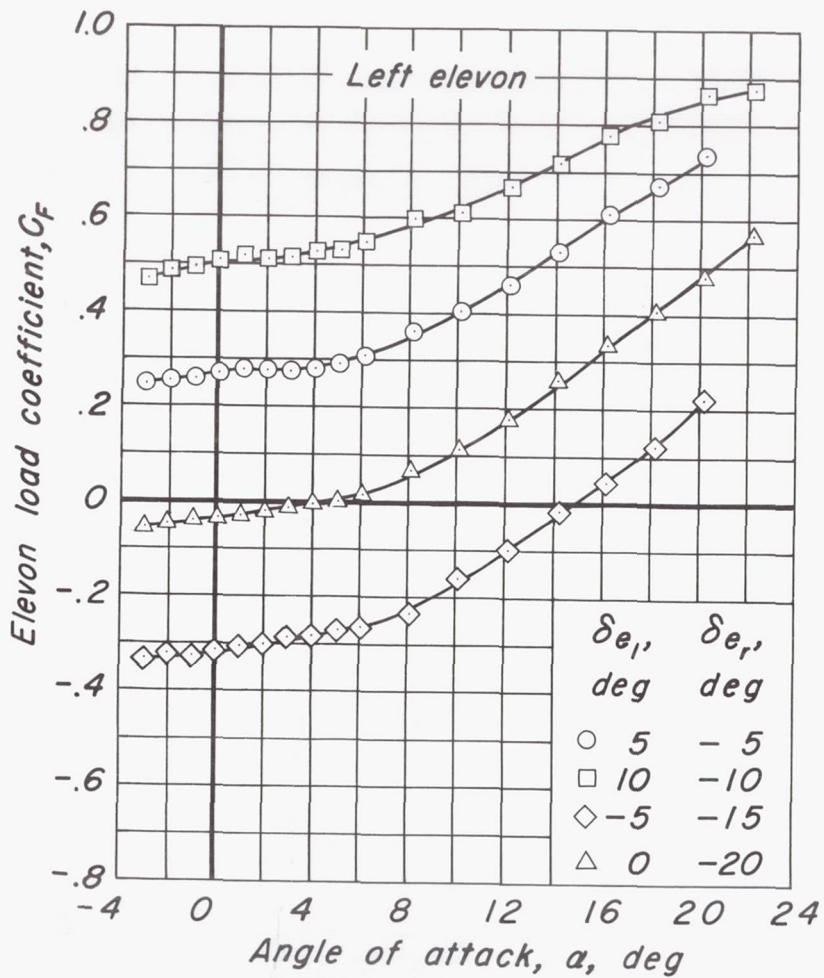
(c)  $C_{he}$  vs  $\alpha$   
 Figure 7.- Continued.



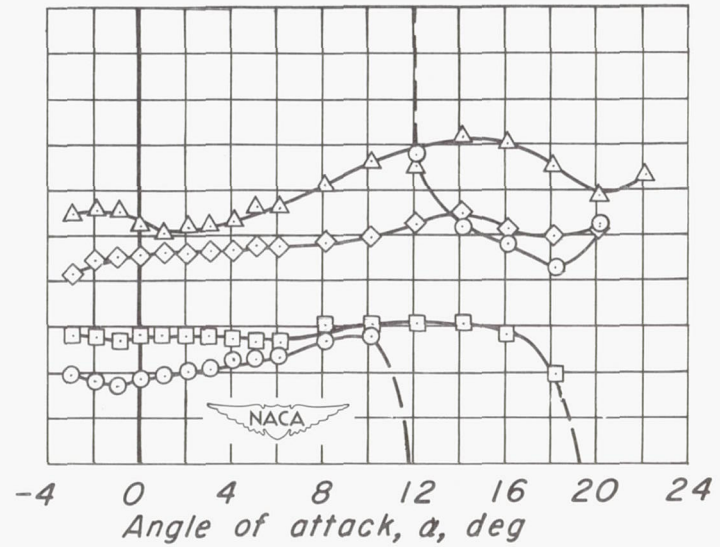
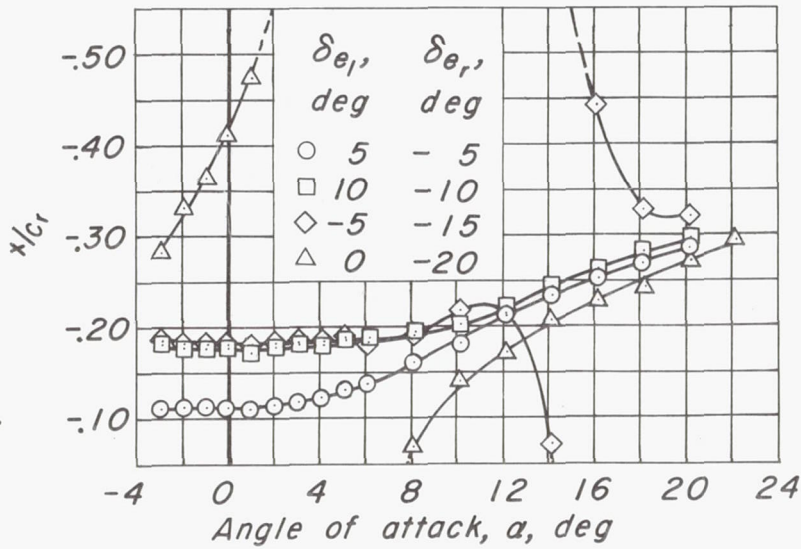
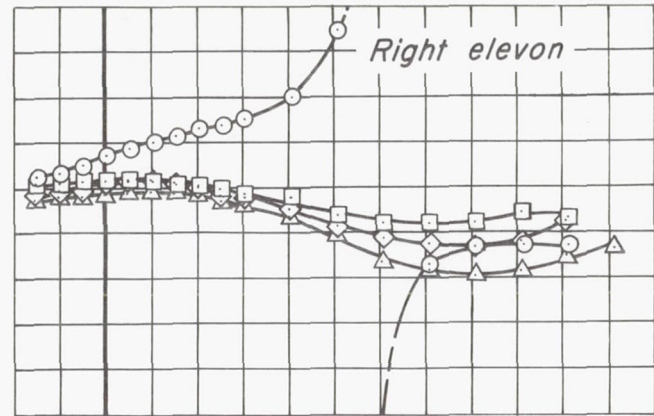
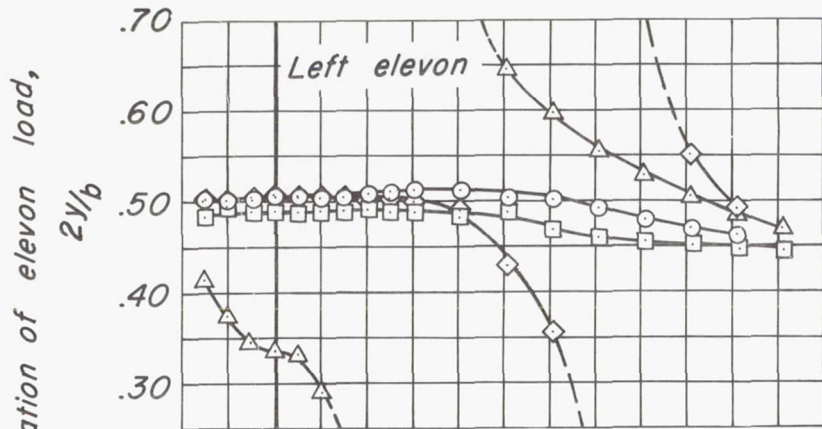


(d)  $C_{ht}$  vs  $\alpha$

Figure 7.- Continued.



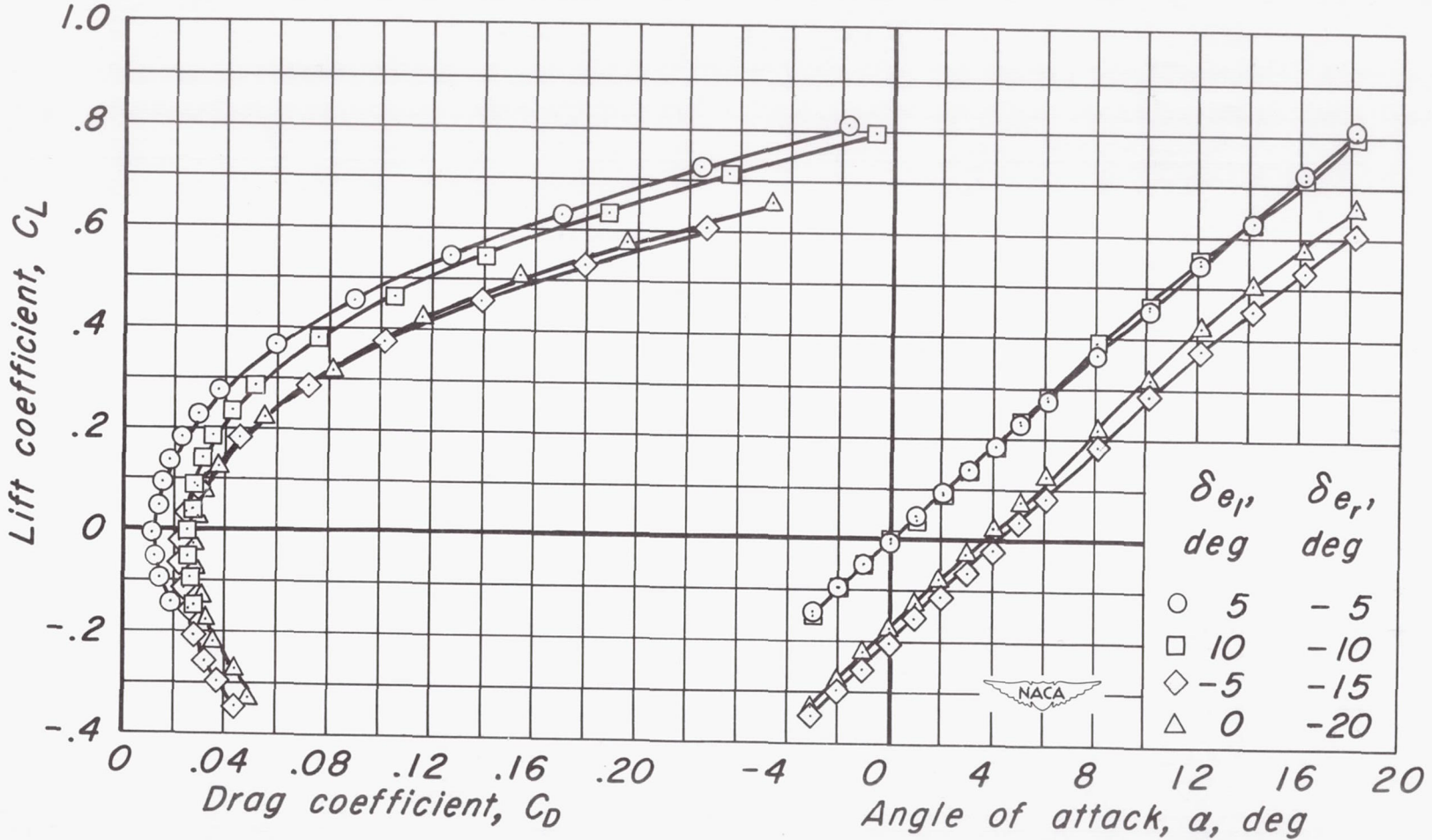
(e)  $C_F$  vs  $a$   
 Figure 7.- Continued.



(f)  $2y/b$  vs  $\alpha$ ,  $x/c_r$  vs  $\alpha$   
Figure 7.- Concluded.

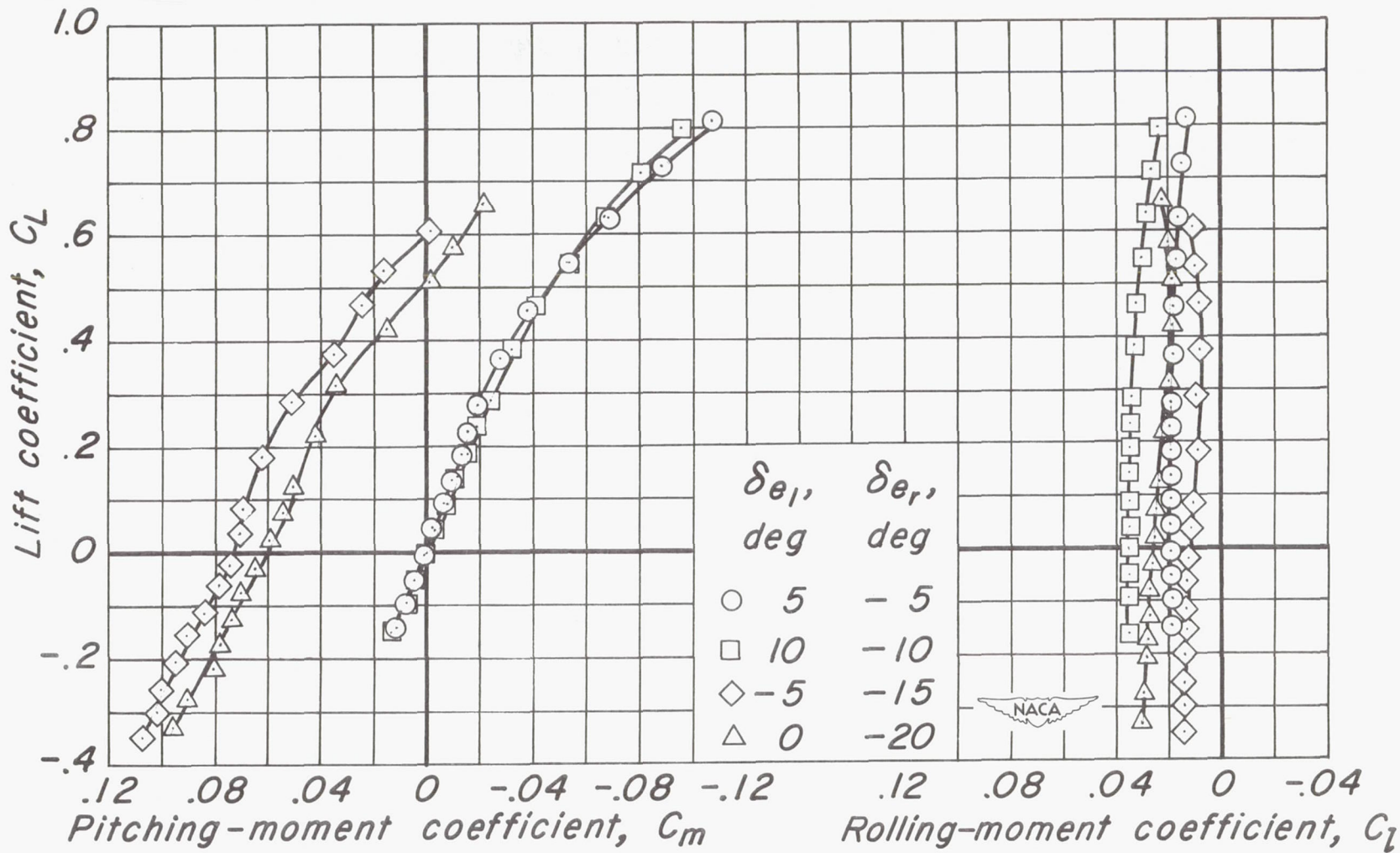


CONFIDENTIAL



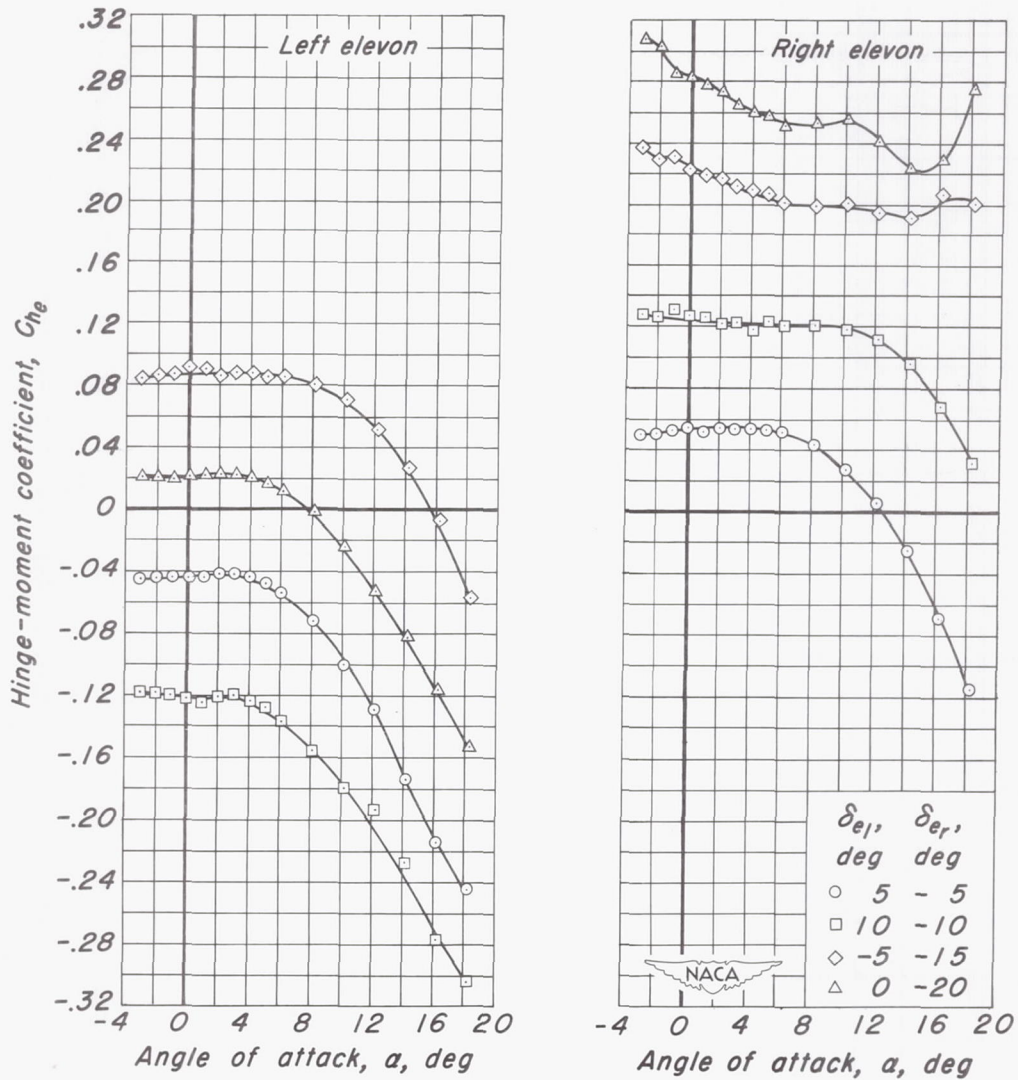
(a)  $C_L$  vs  $\alpha$ ,  $C_L$  vs  $C_D$

Figure 8.- The effect of differential elevon deflection on the aerodynamic characteristics at a Mach number of 0.90.  $R$ , 3.0 million;  $\delta_t$ ,  $0^\circ$ .



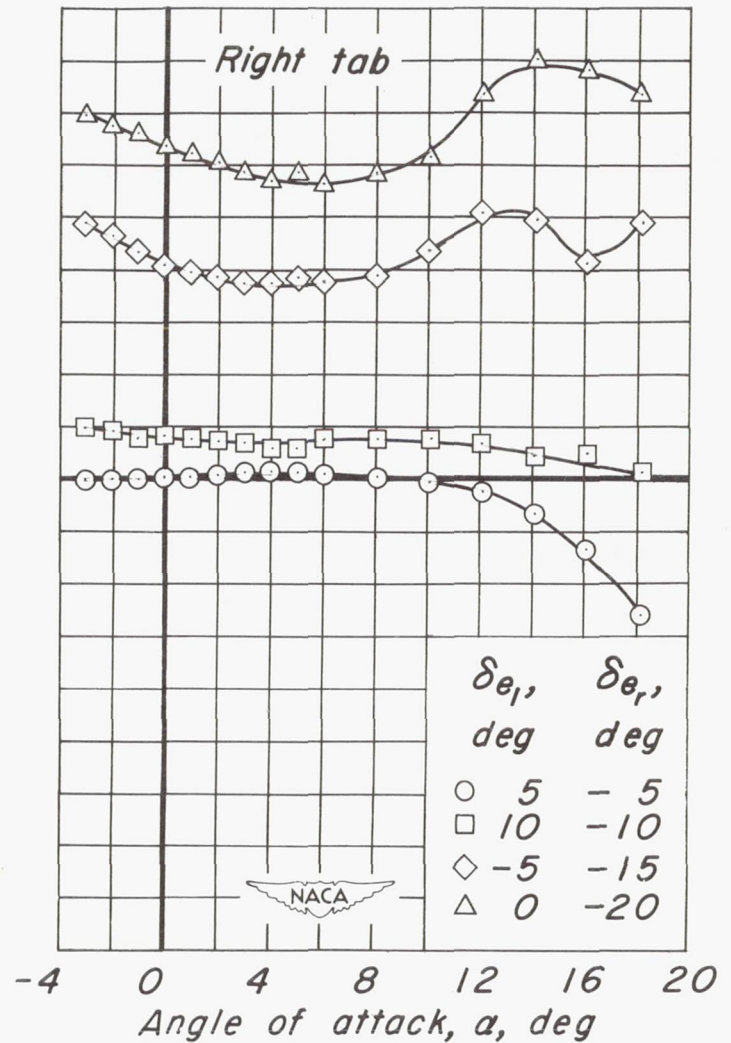
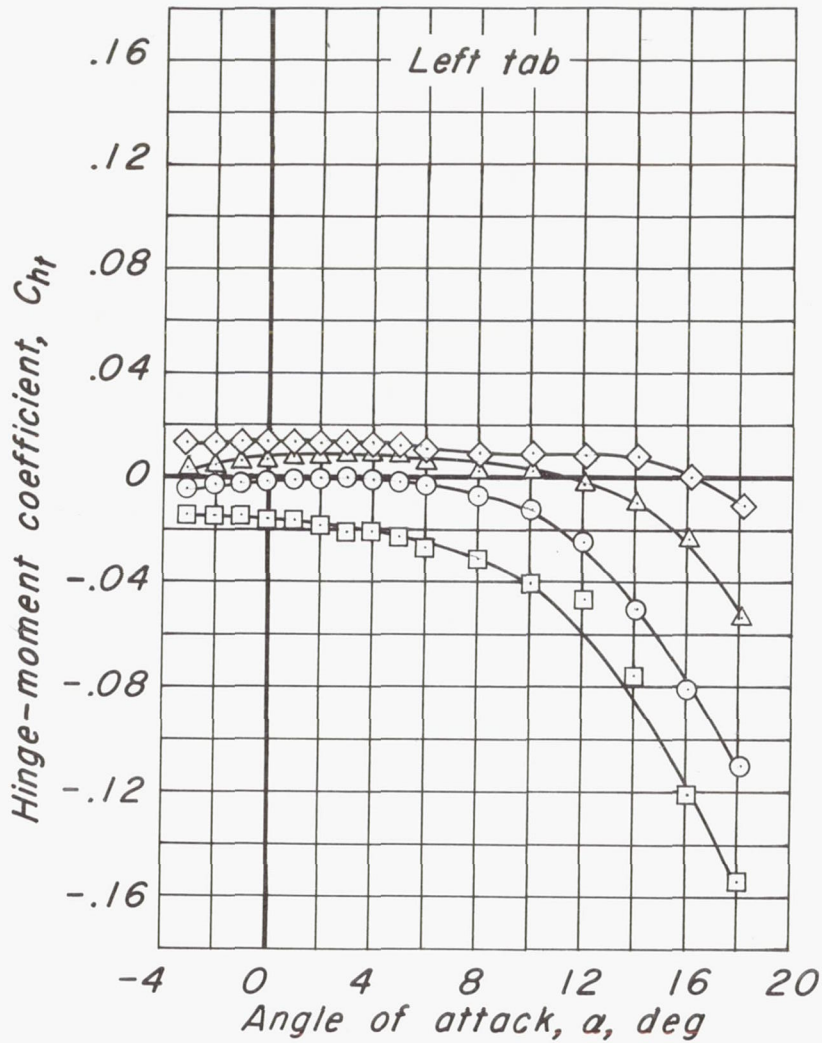
(b)  $C_L$  vs  $C_m$ ,  $C_L$  vs  $C_l$

Figure 8.- Continued.



(c)  $C_{he}$  vs  $\alpha$   
 Figure 8.- Continued.



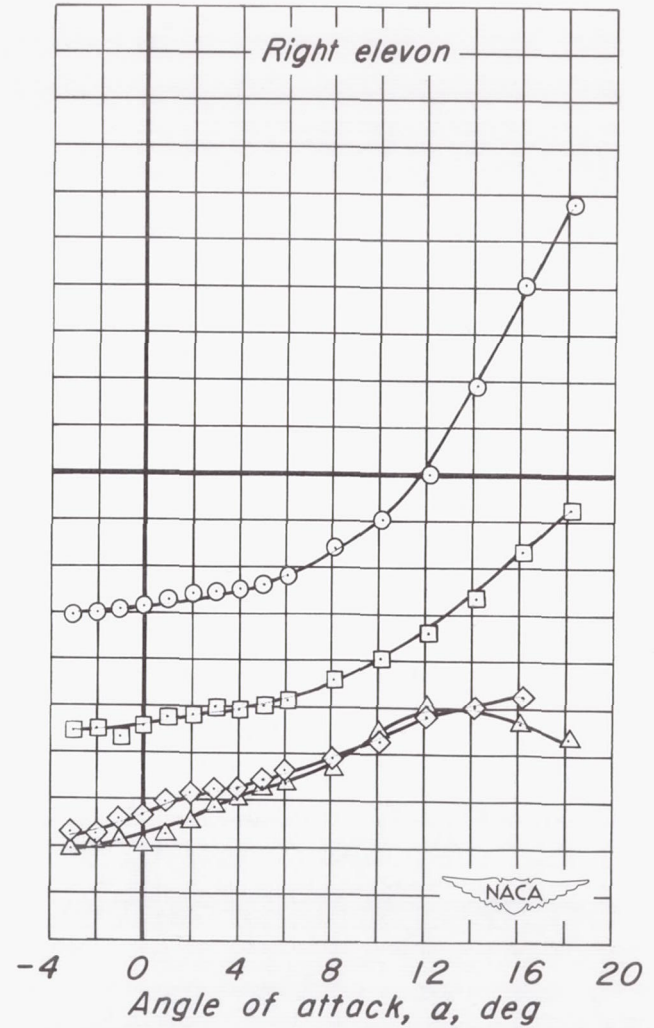
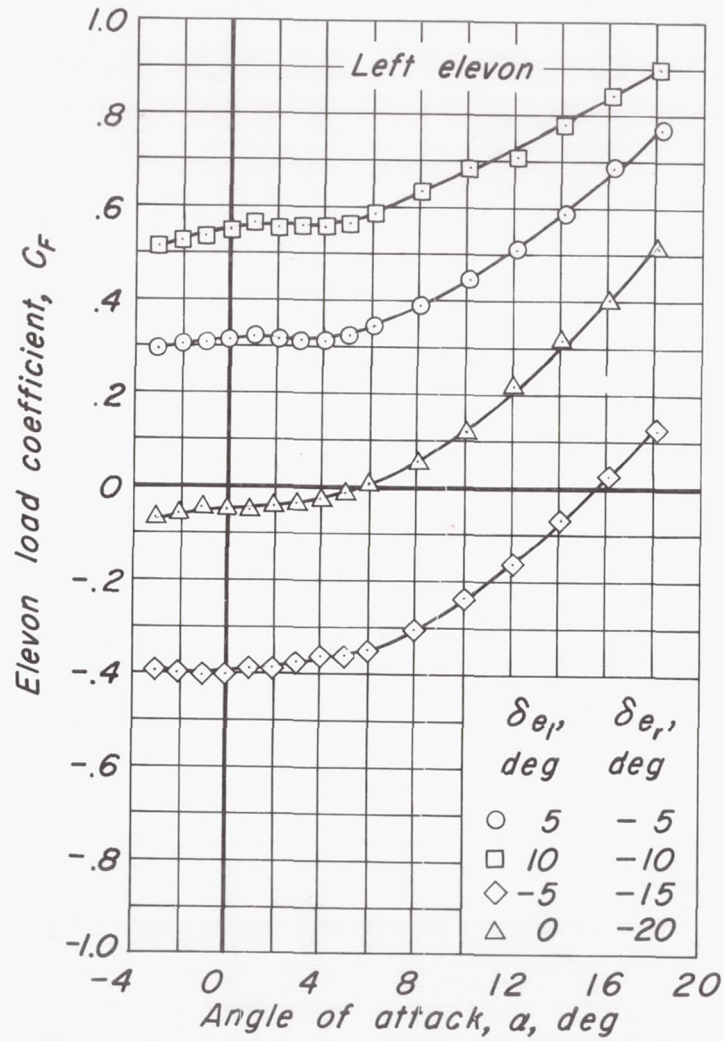


	$\delta e_l$ , deg	$\delta e_r$ , deg
○	5	-5
□	10	-10
◇	-5	-15
△	0	-20



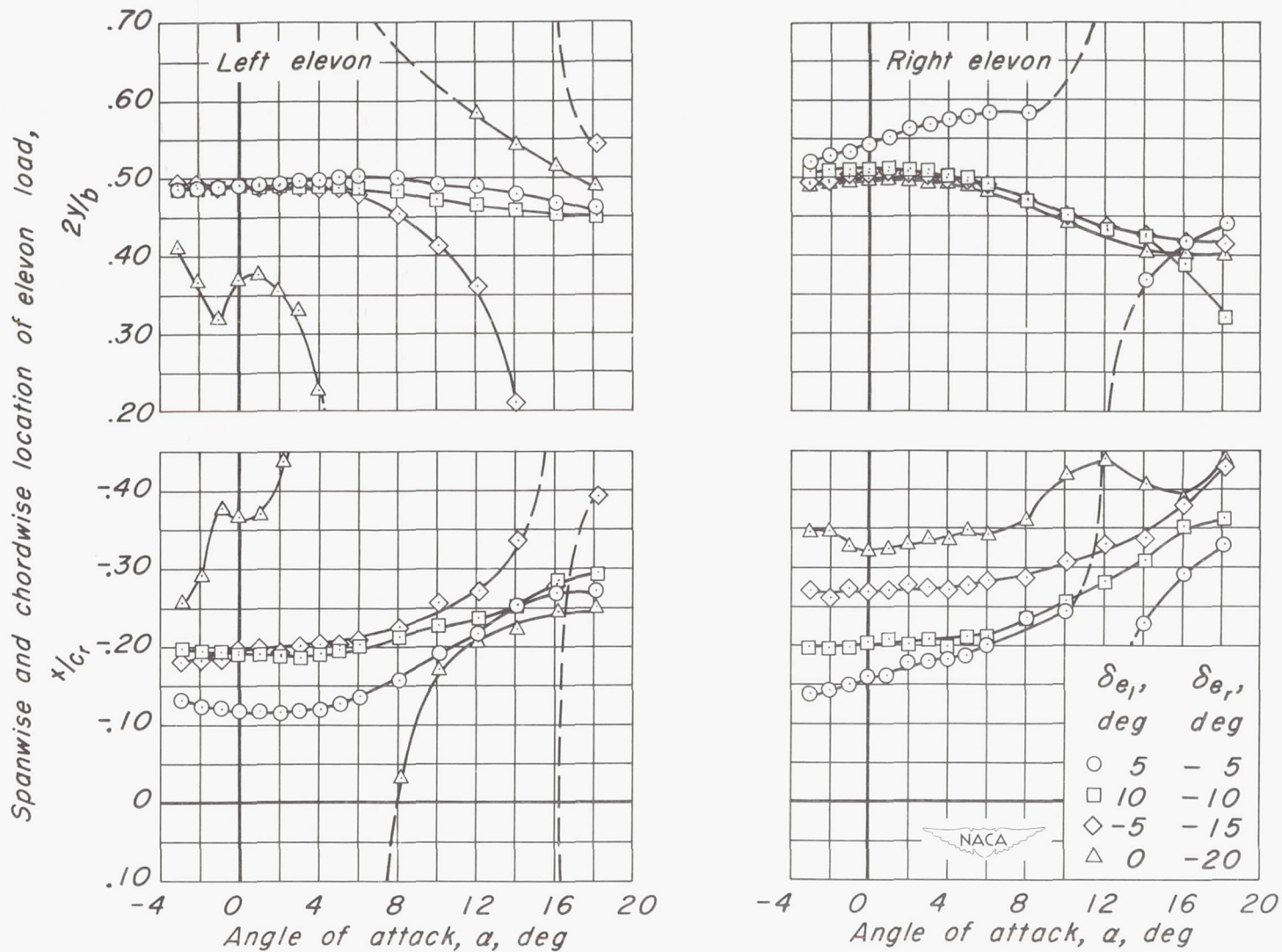
(d)  $C_{ht}$  vs  $\alpha$

Figure 8.- Continued.



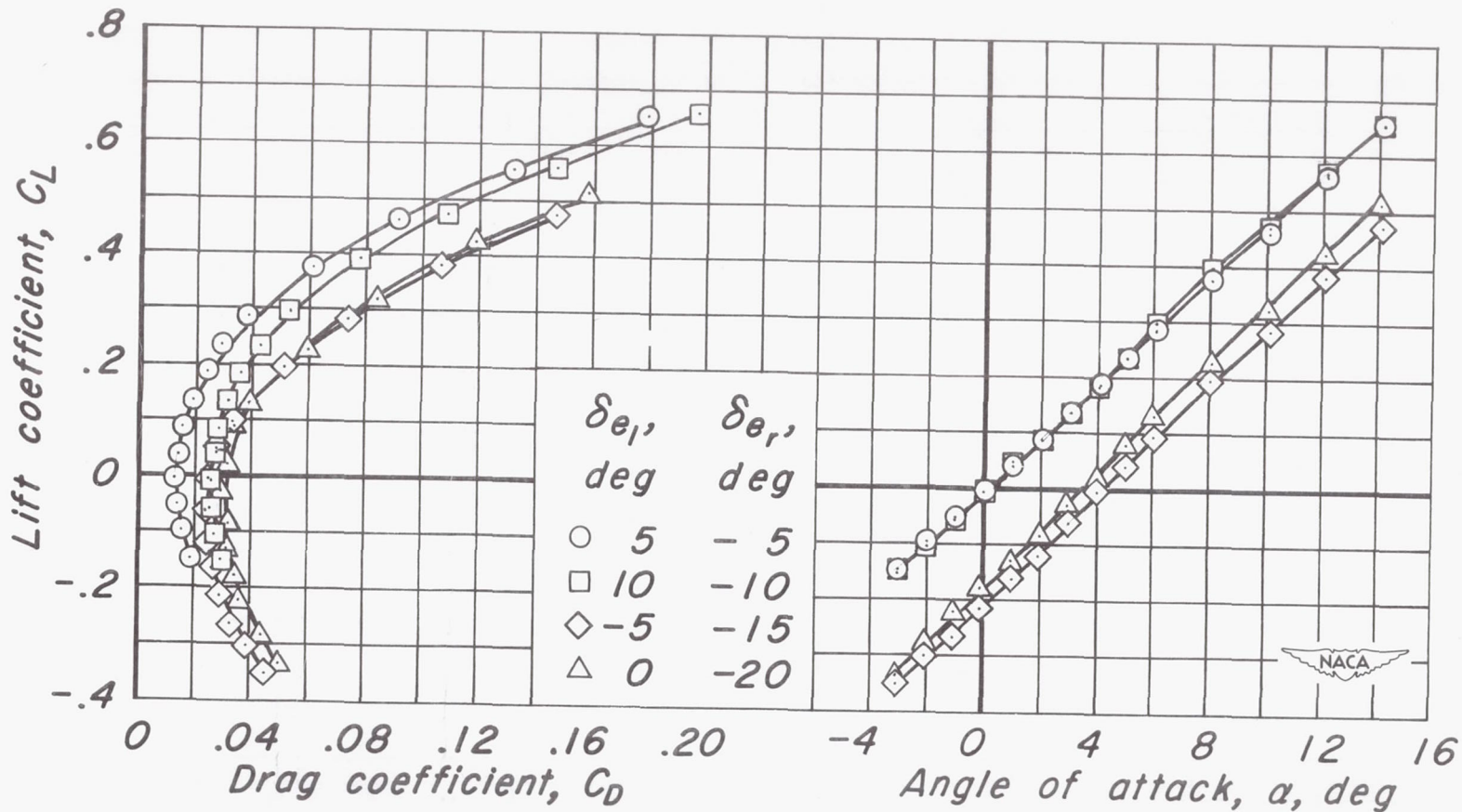
(e)  $C_F$  vs  $\alpha$

Figure 8.- Continued.



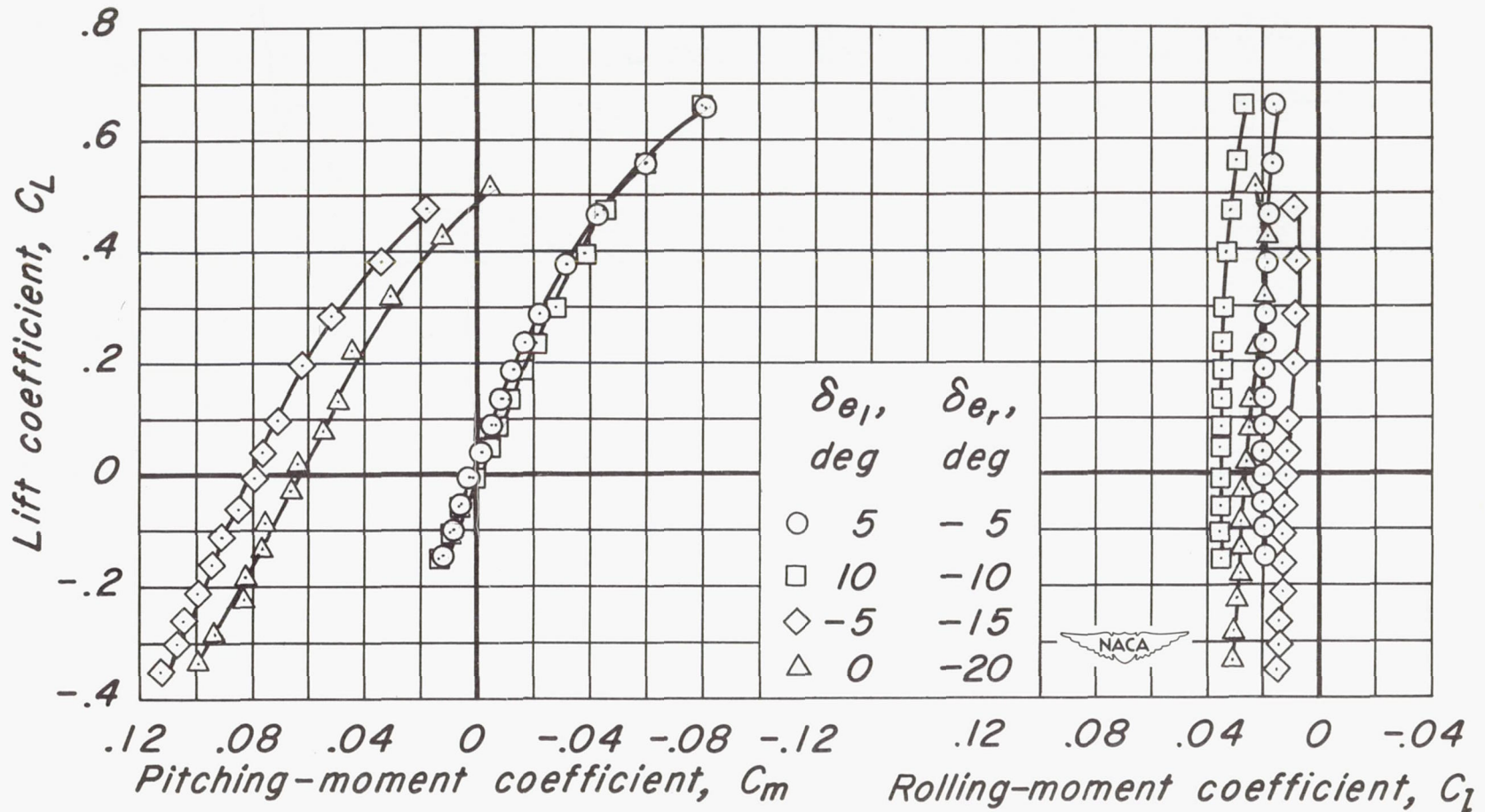
(f)  $2y/b$  vs  $\alpha$ ,  $x/c_r$  vs  $\alpha$   
 Figure 8.- Concluded.





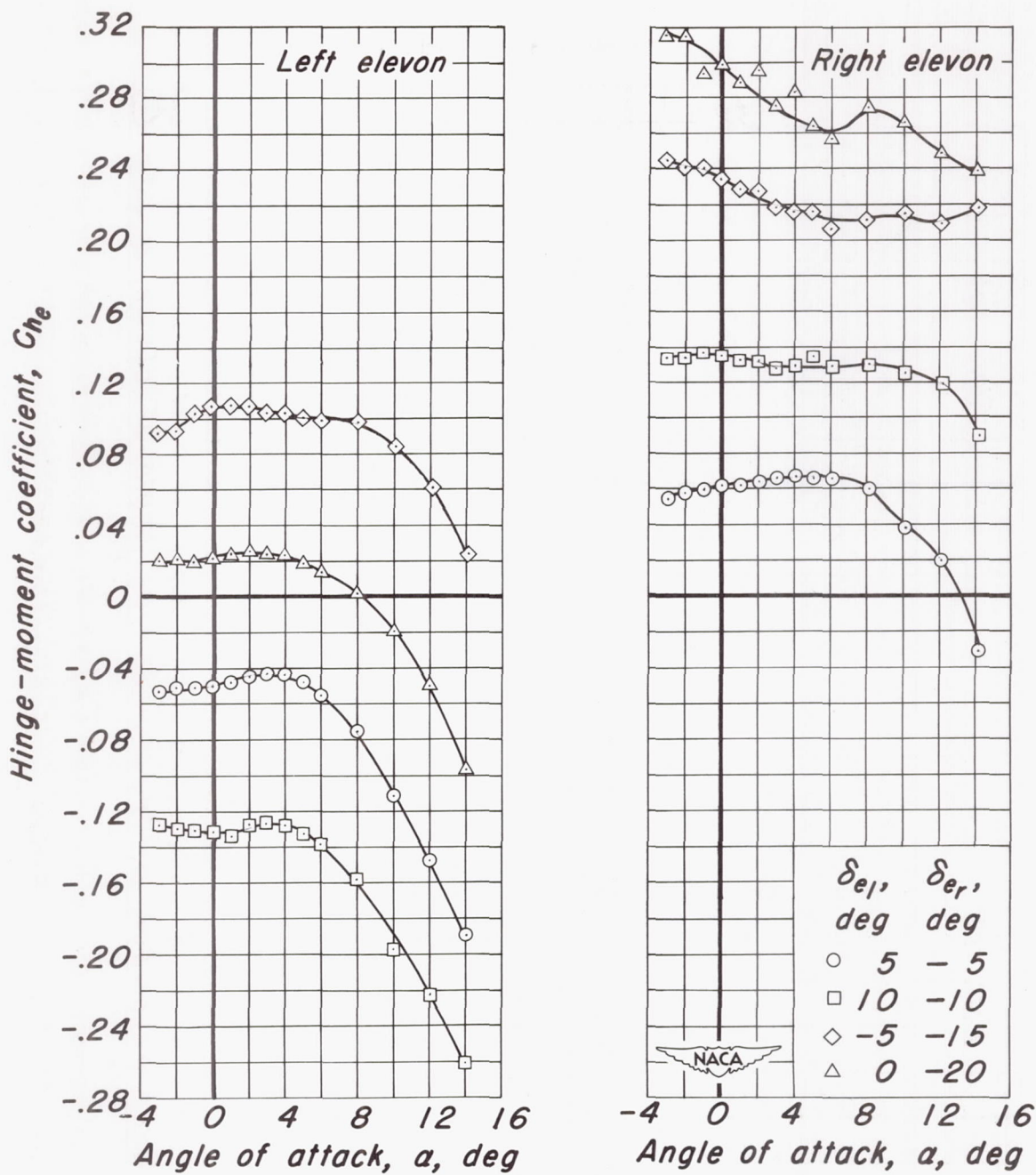
(a)  $C_L$  vs  $\alpha$ ,  $C_L$  vs  $C_D$

Figure 9.- The effect of differential elevon deflection on the aerodynamic characteristics at a Mach number of 0.92.  $R$ , 3.0 million;  $\delta_t$ ,  $0^\circ$ .



(b)  $C_L$  vs  $C_m$ ,  $C_L$  vs  $C_l$

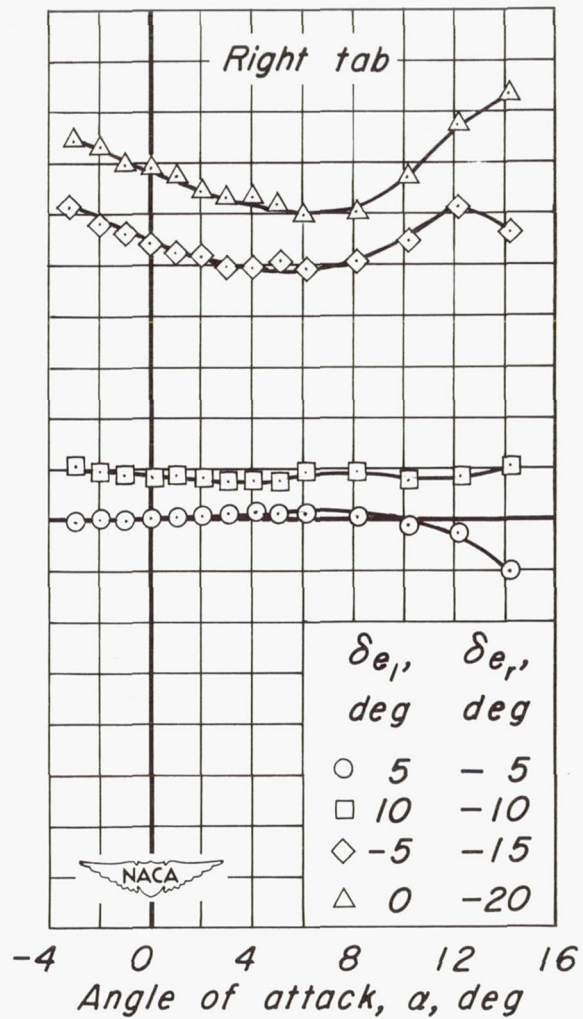
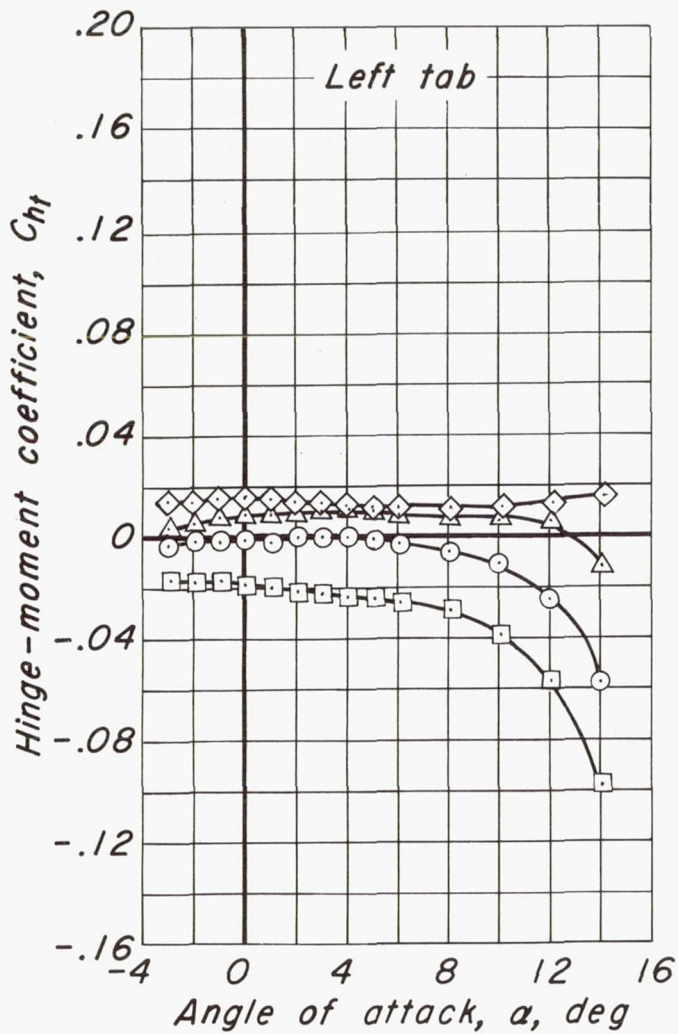
Figure 9.- Continued.



(c)  $C_{he}$  vs  $\alpha$

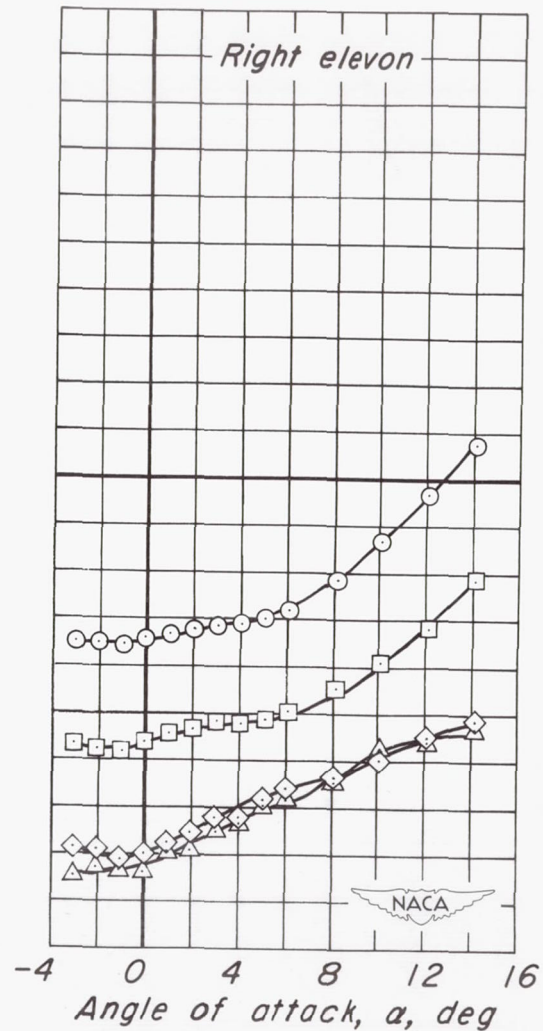
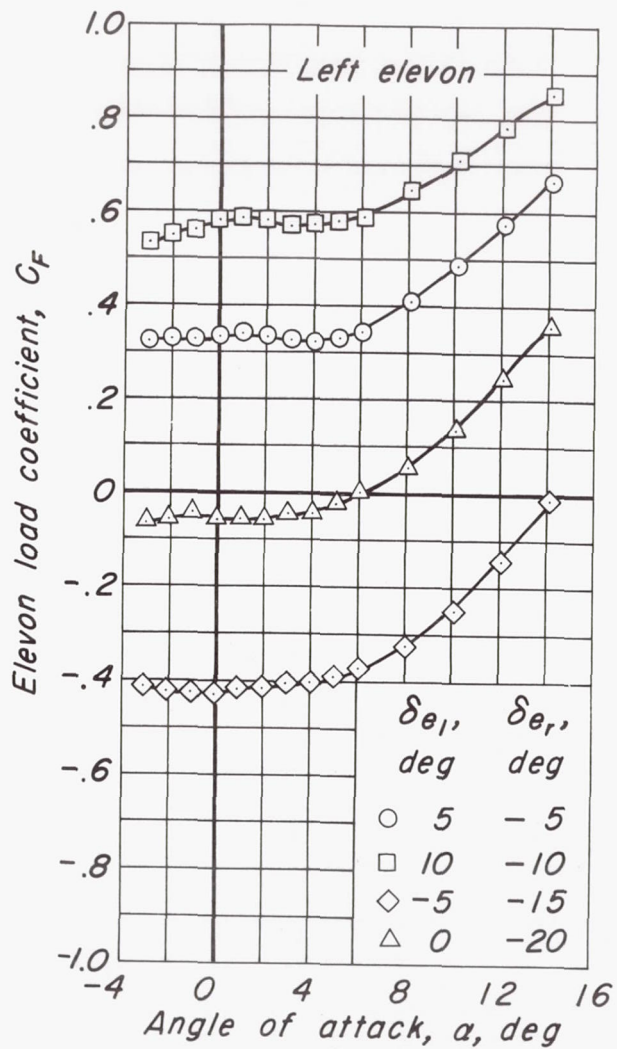
Figure 9.- Continued.





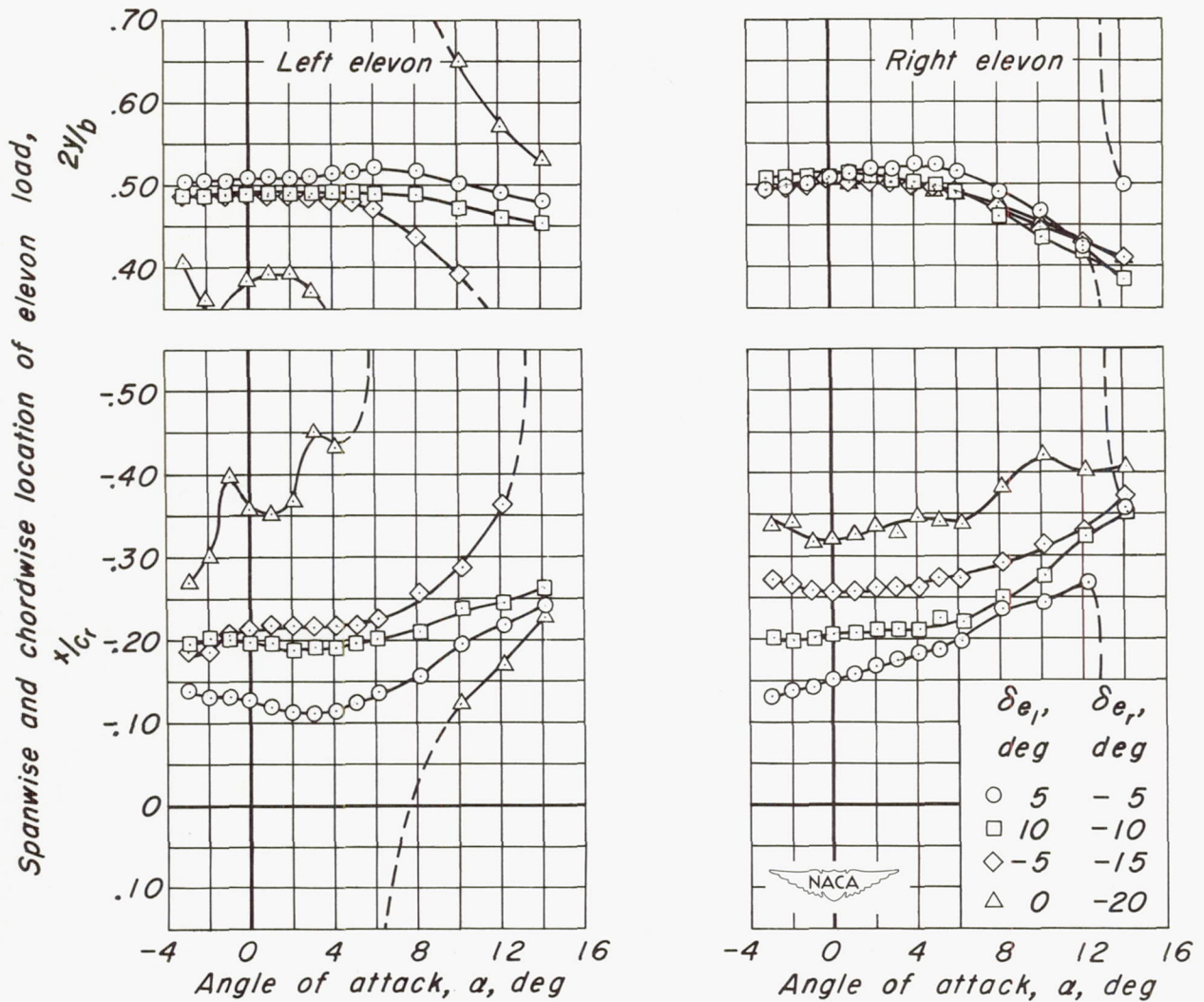
(d)  $C_{ht}$  vs  $\alpha$

Figure 9.- Continued.



(e)  $C_F$  vs  $\alpha$

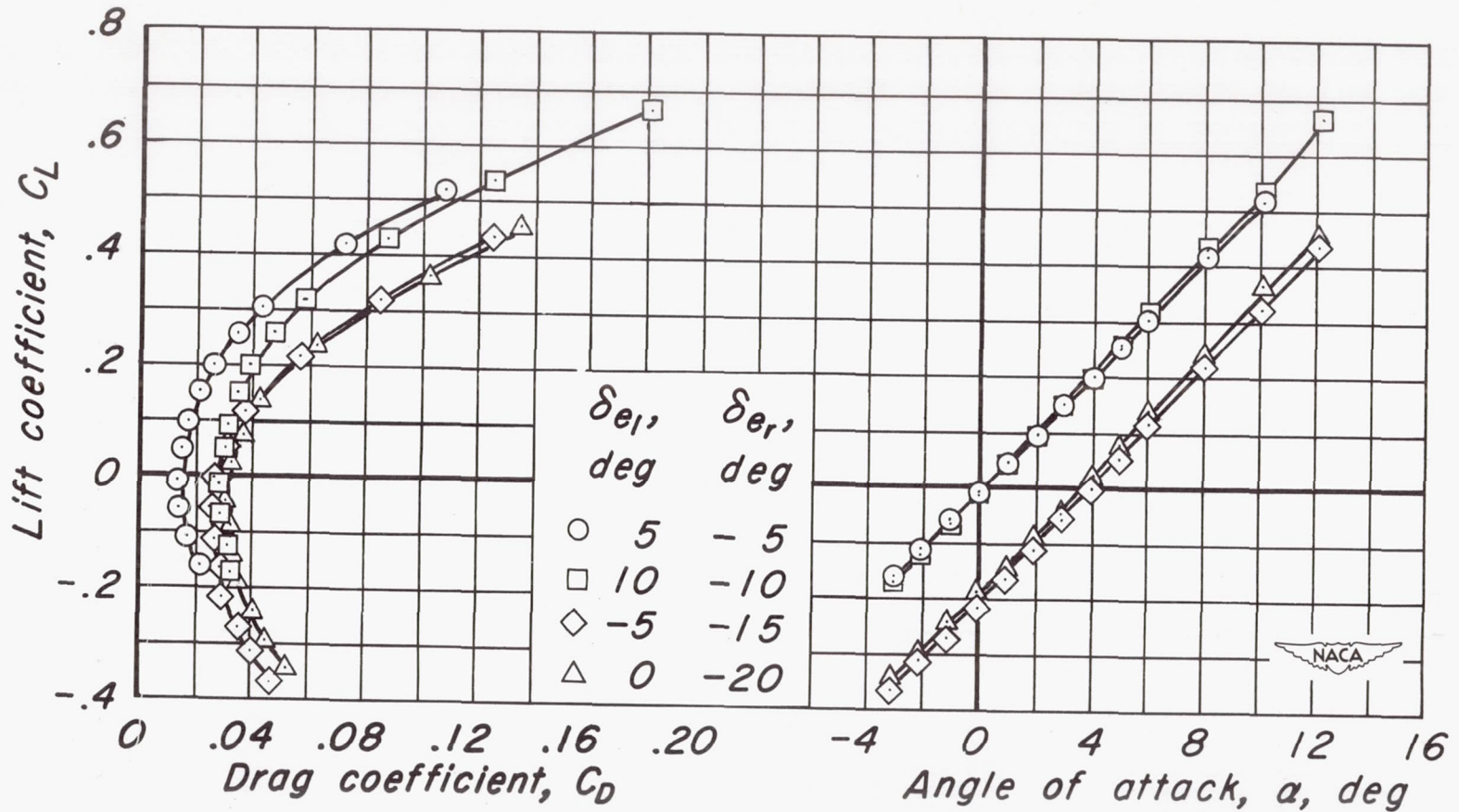
Figure 9.- Continued.



(f)  $2y/b$  vs  $\alpha$ ,  $x/c_r$  vs  $\alpha$

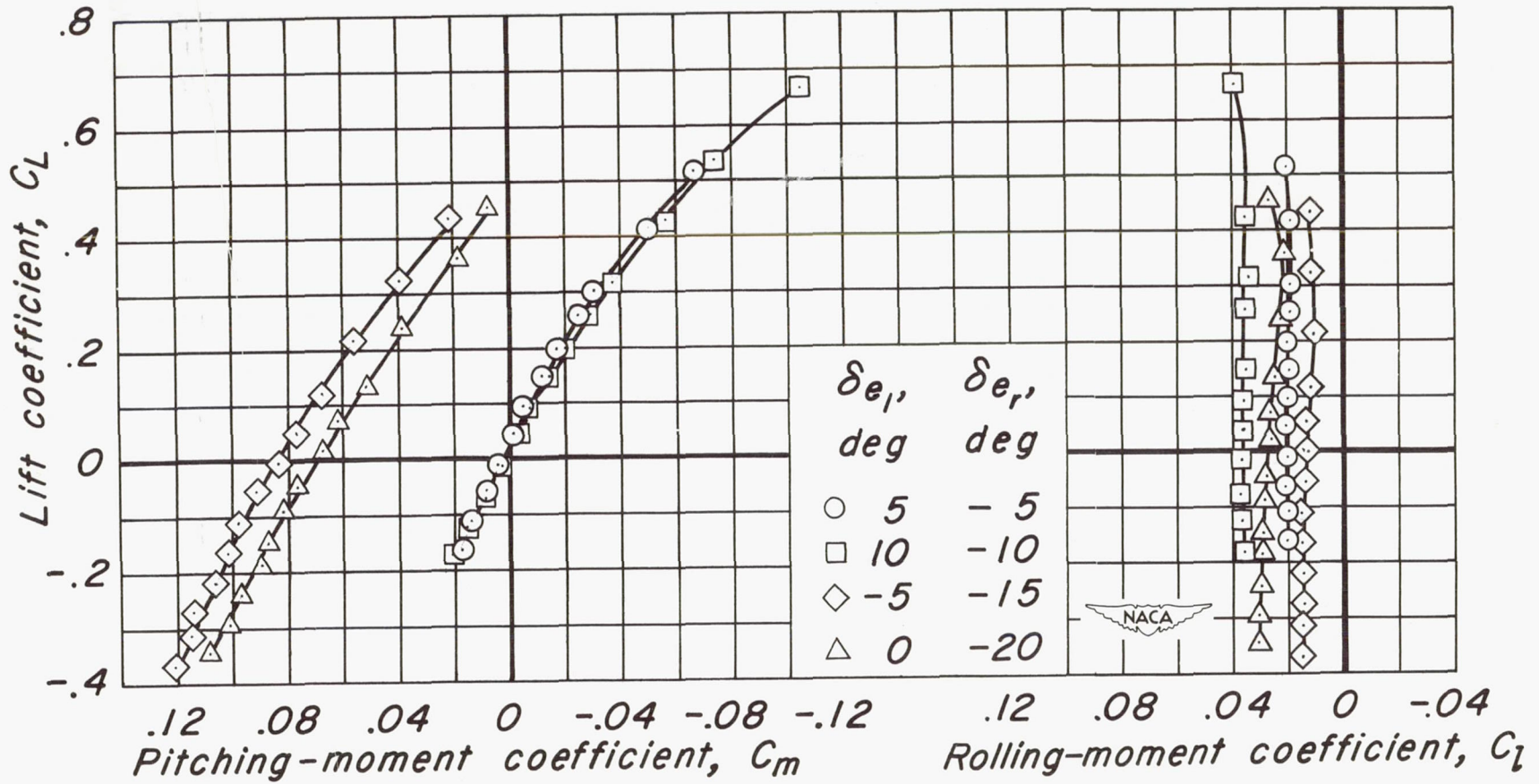
Figure 9- Concluded.



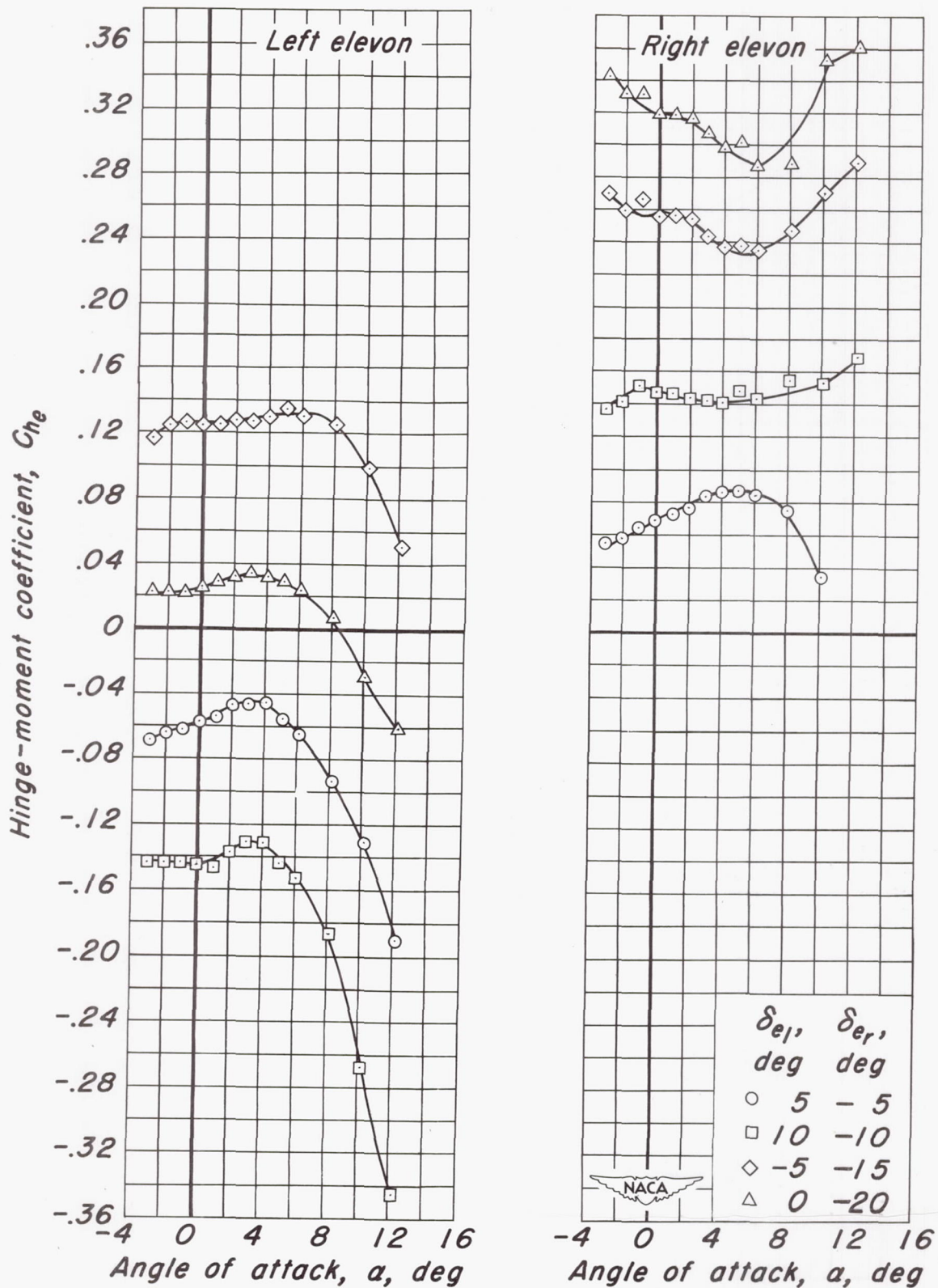


(a)  $C_L$  vs  $\alpha$ ,  $C_L$  vs  $C_D$

Figure 10.- The effect of differential elevon deflection on the aerodynamic characteristics at a Mach number of 0.95.  $R$ , 3.0 million;  $\delta_t$ ,  $0^\circ$ .



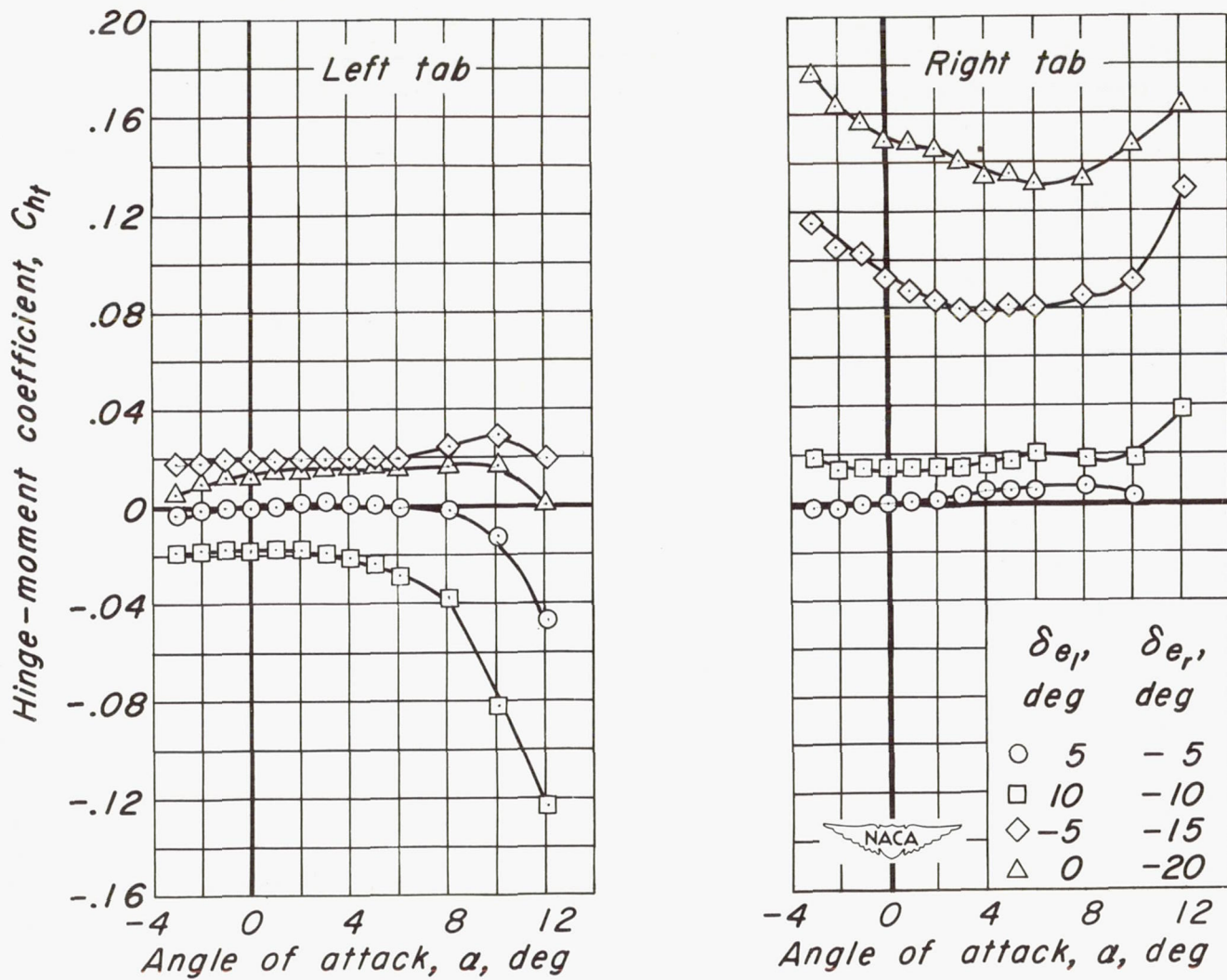
(b)  $C_L$  vs  $C_m$ ,  $C_L$  vs  $C_l$   
 Figure 10.- Continued.



(c)  $C_{he}$  vs  $\alpha$

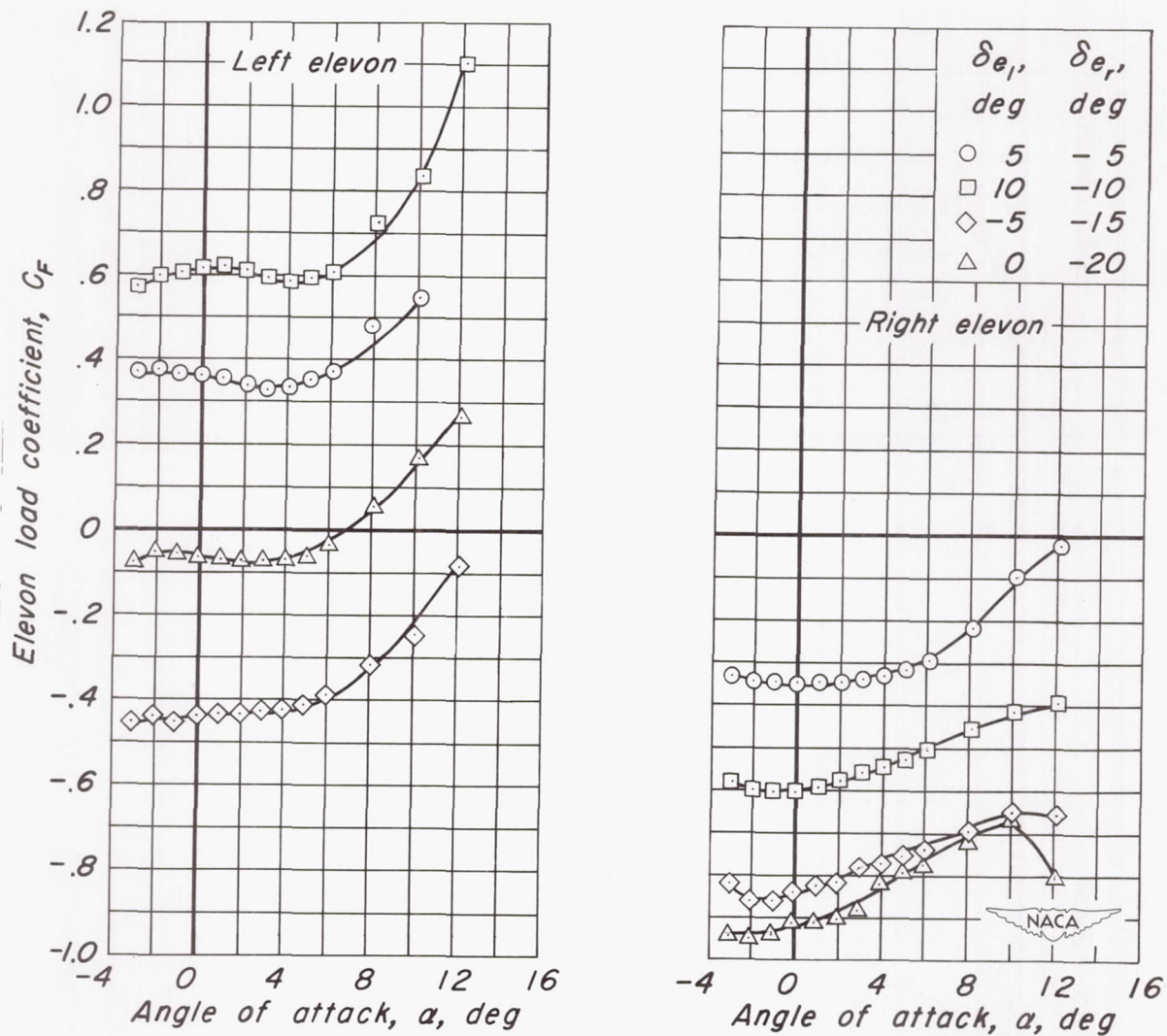
Figure 10.- Continued.





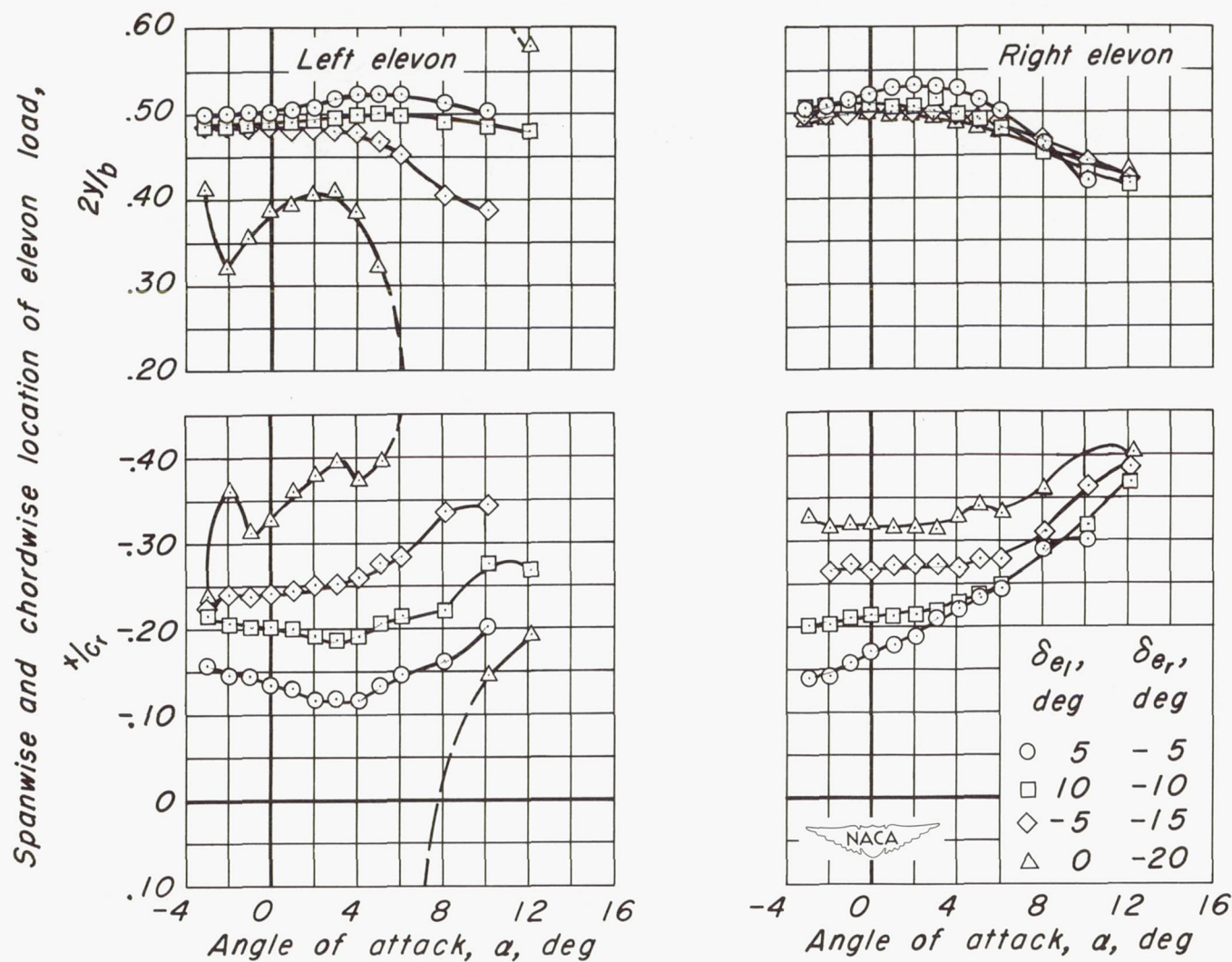
(d)  $C_{h_t}$  vs  $\alpha$

Figure 10.- Continued.



(e)  $C_F$  vs  $\alpha$

Figure 10- Continued.

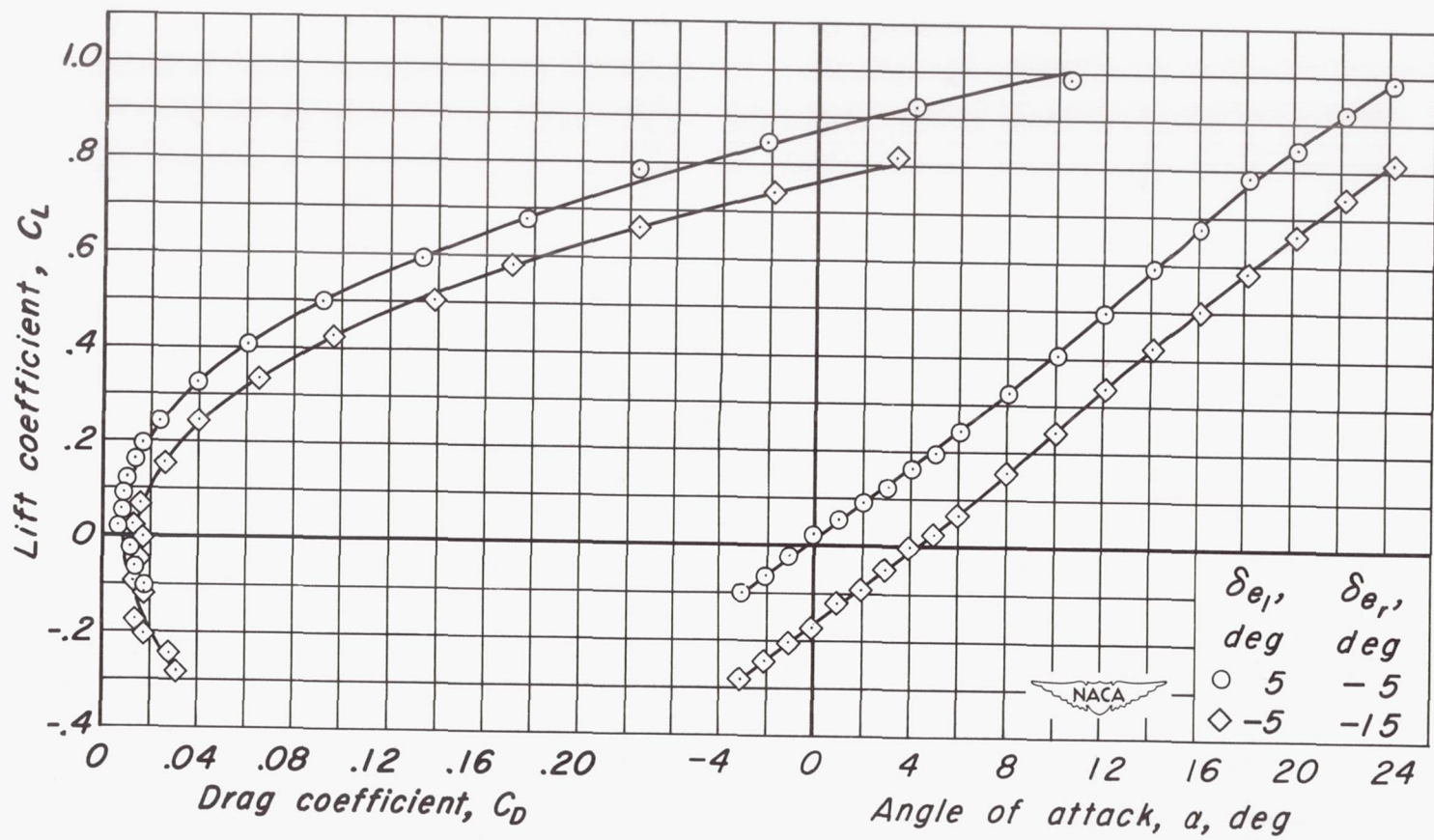


(f)  $2y/b$  vs  $\alpha$ ,  $x/c_r$  vs  $\alpha$

Figure 10.- Concluded.

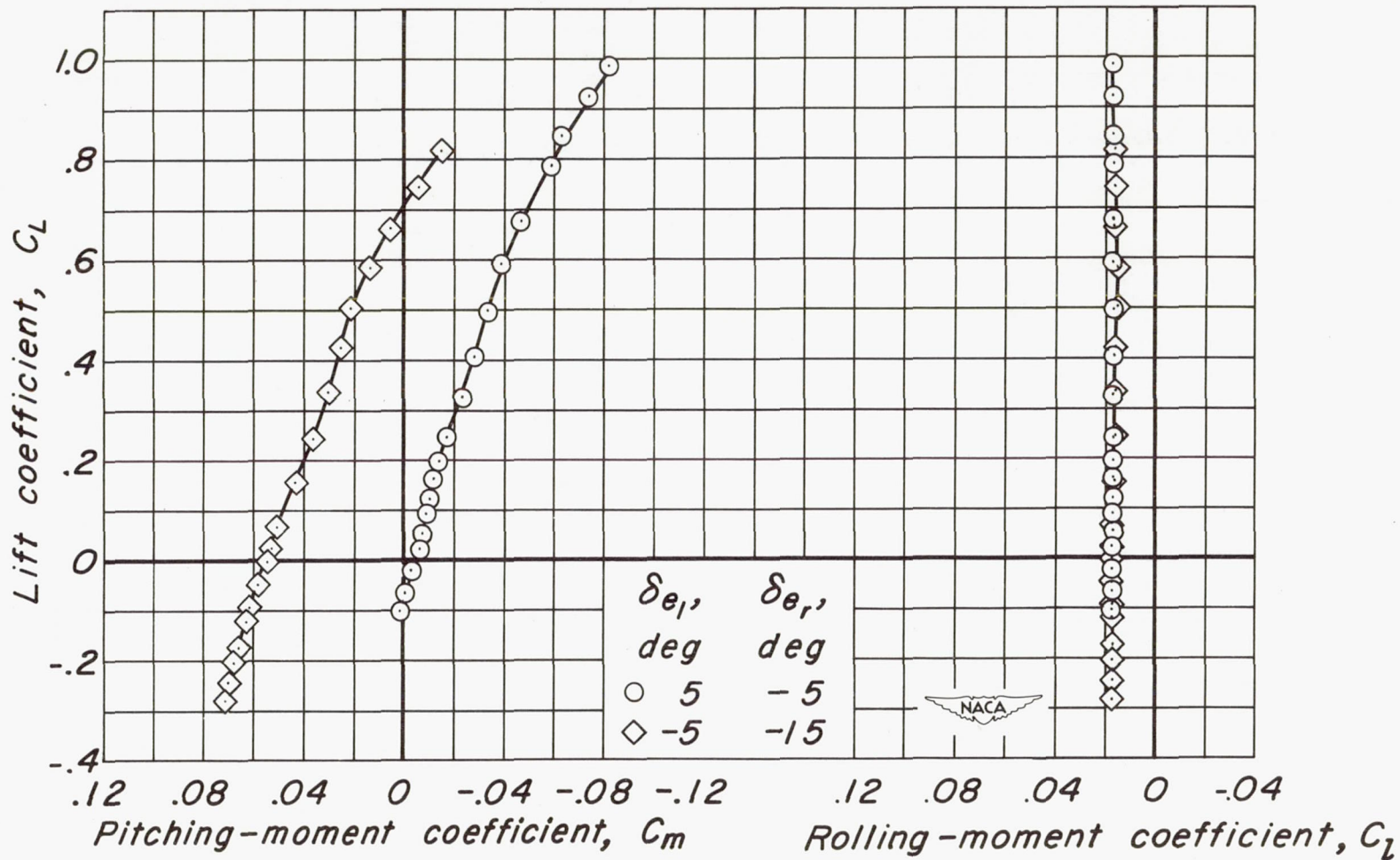


CONFIDENTIAL



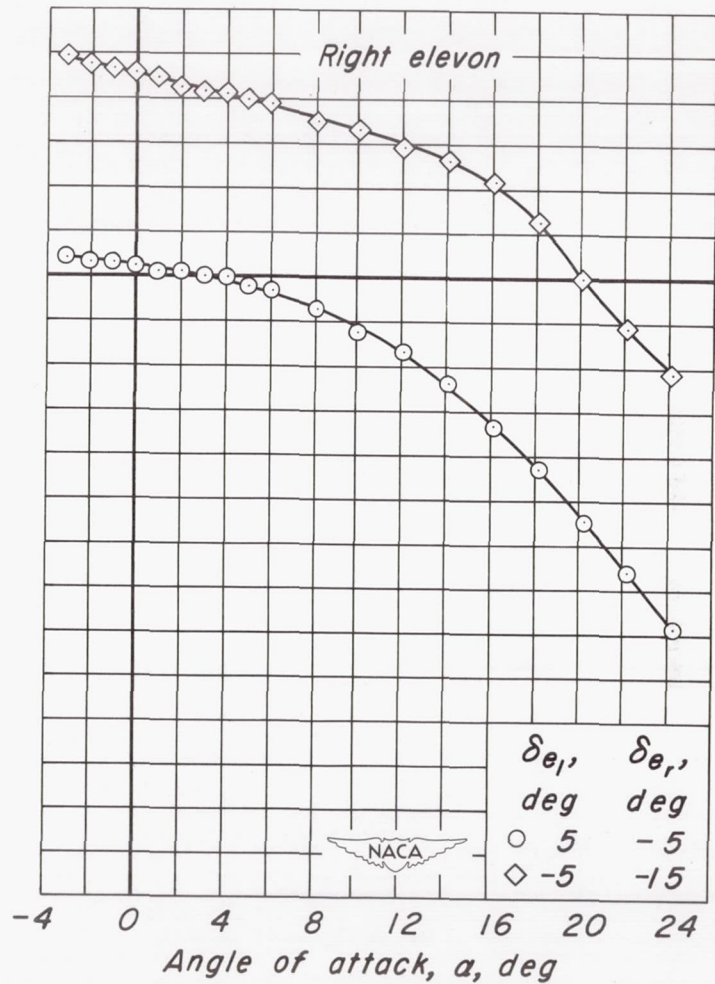
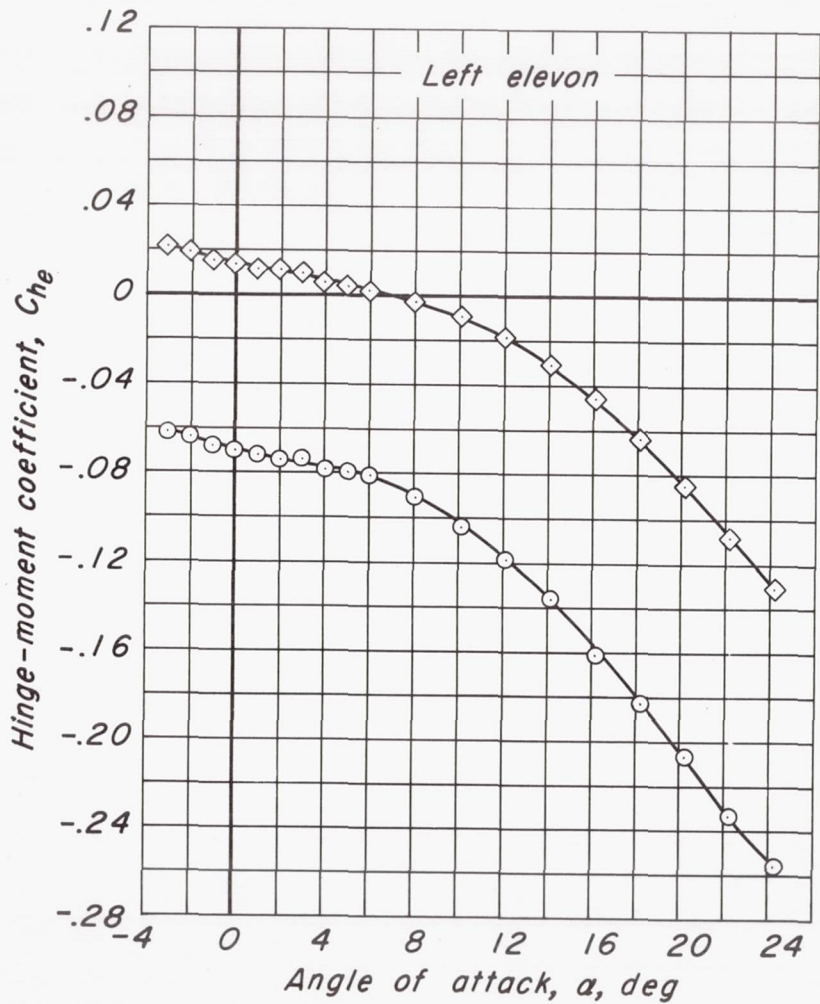
(a)  $C_L$  vs  $\alpha$  ,  $C_L$  vs  $C_D$

Figure 11 .- The effect of differential elevon deflection on the aerodynamic characteristics at a Mach number of 0.24.  $R$ , 3.0 million;  $\delta_t$ ,  $5^\circ$ .



(b)  $C_L$  vs  $C_m$ ,  $C_L$  vs  $C_l$

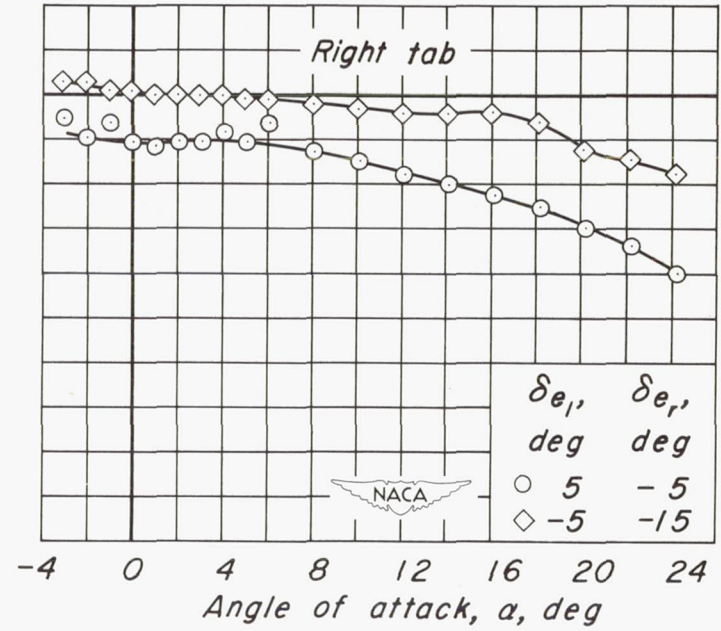
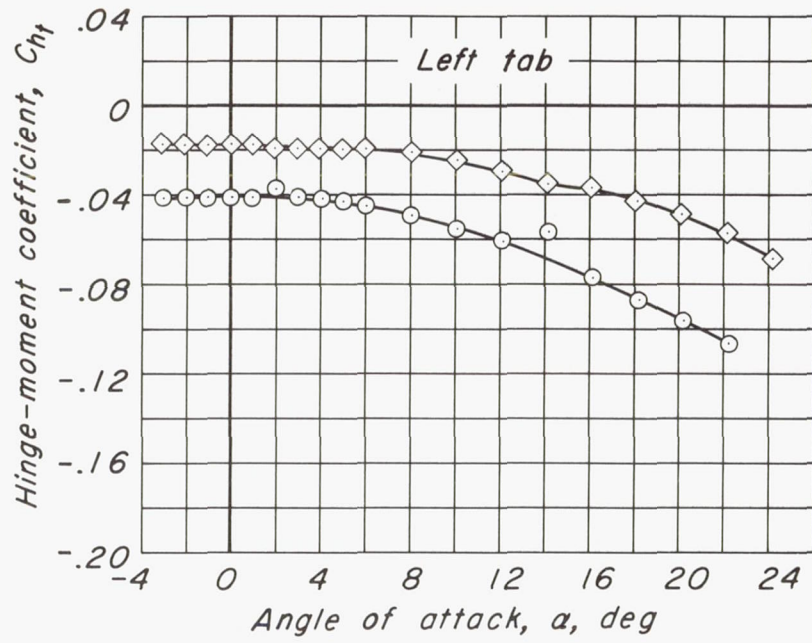
Figure 11 - Continued.



(c)  $C_{he}$  vs  $\alpha$

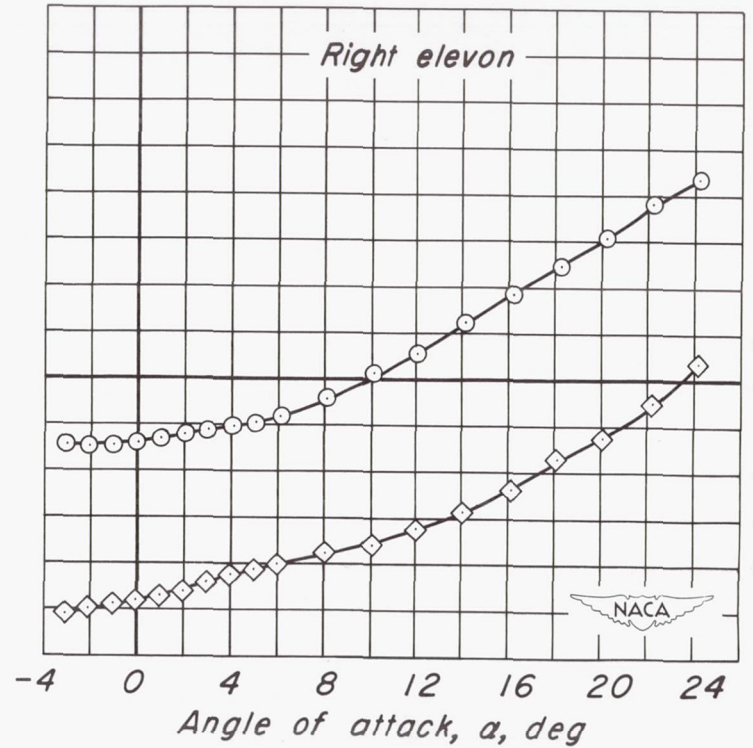
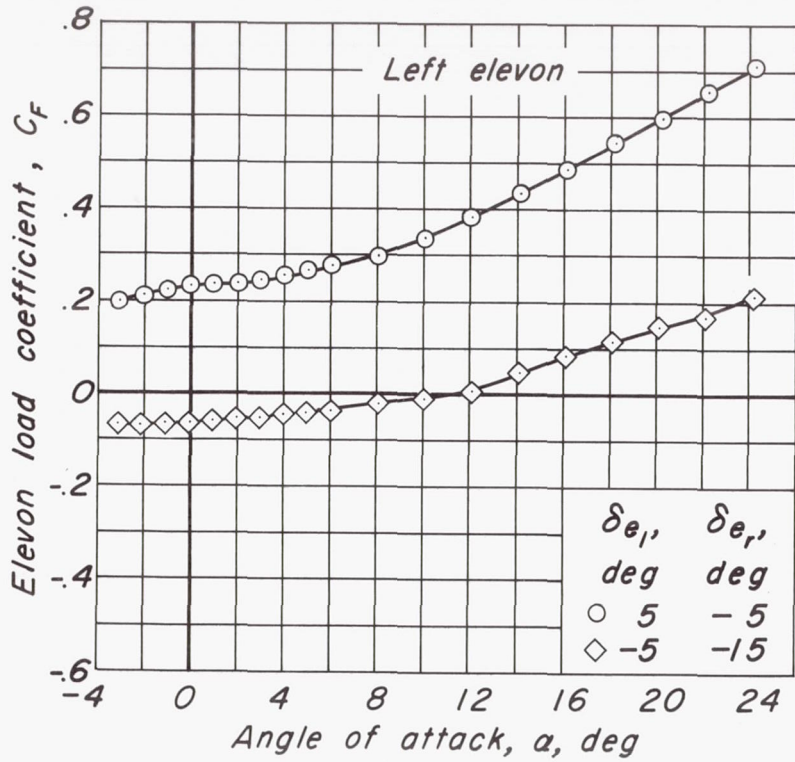
Figure 11 - Continued.





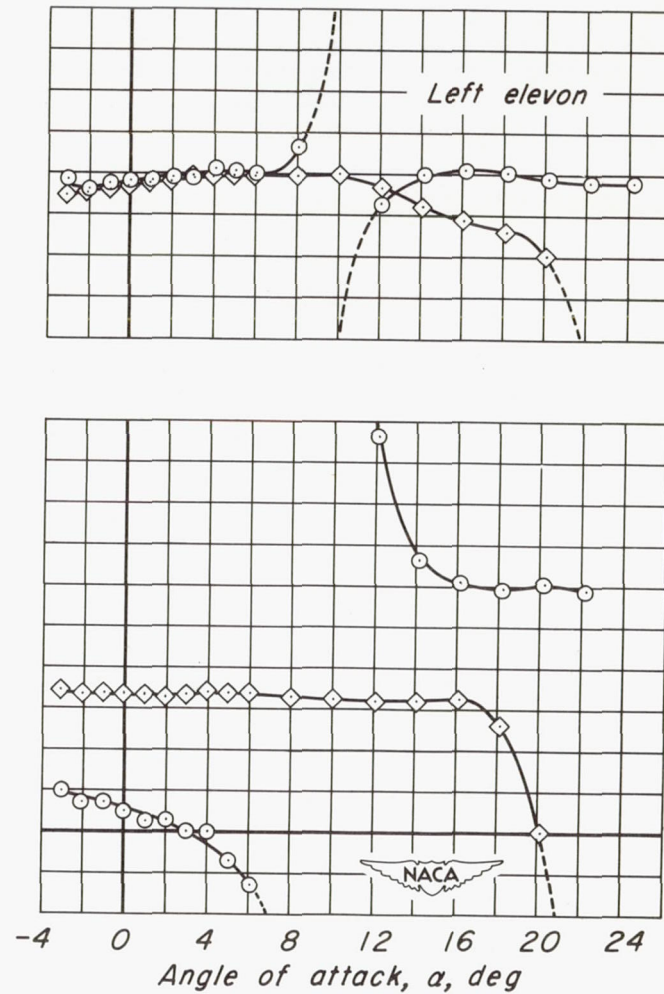
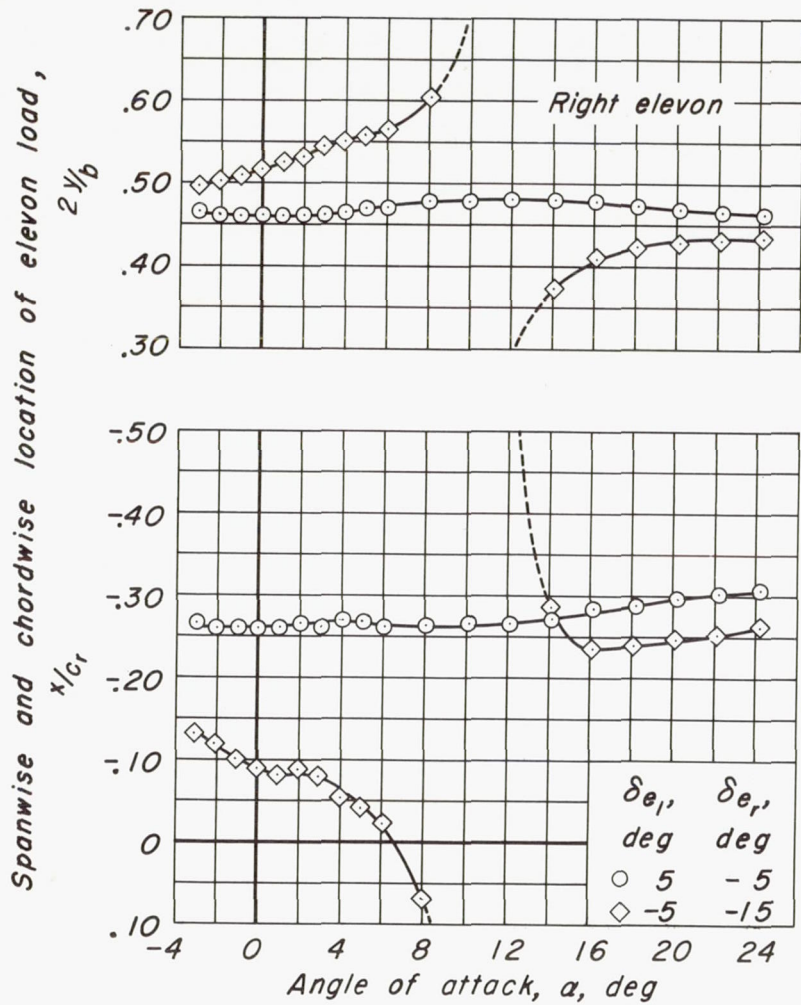
(d)  $C_{h_t}$  vs  $\alpha$

Figure 11 - Continued.



(e)  $C_F$  vs  $\alpha$

Figure 11 - Continued.

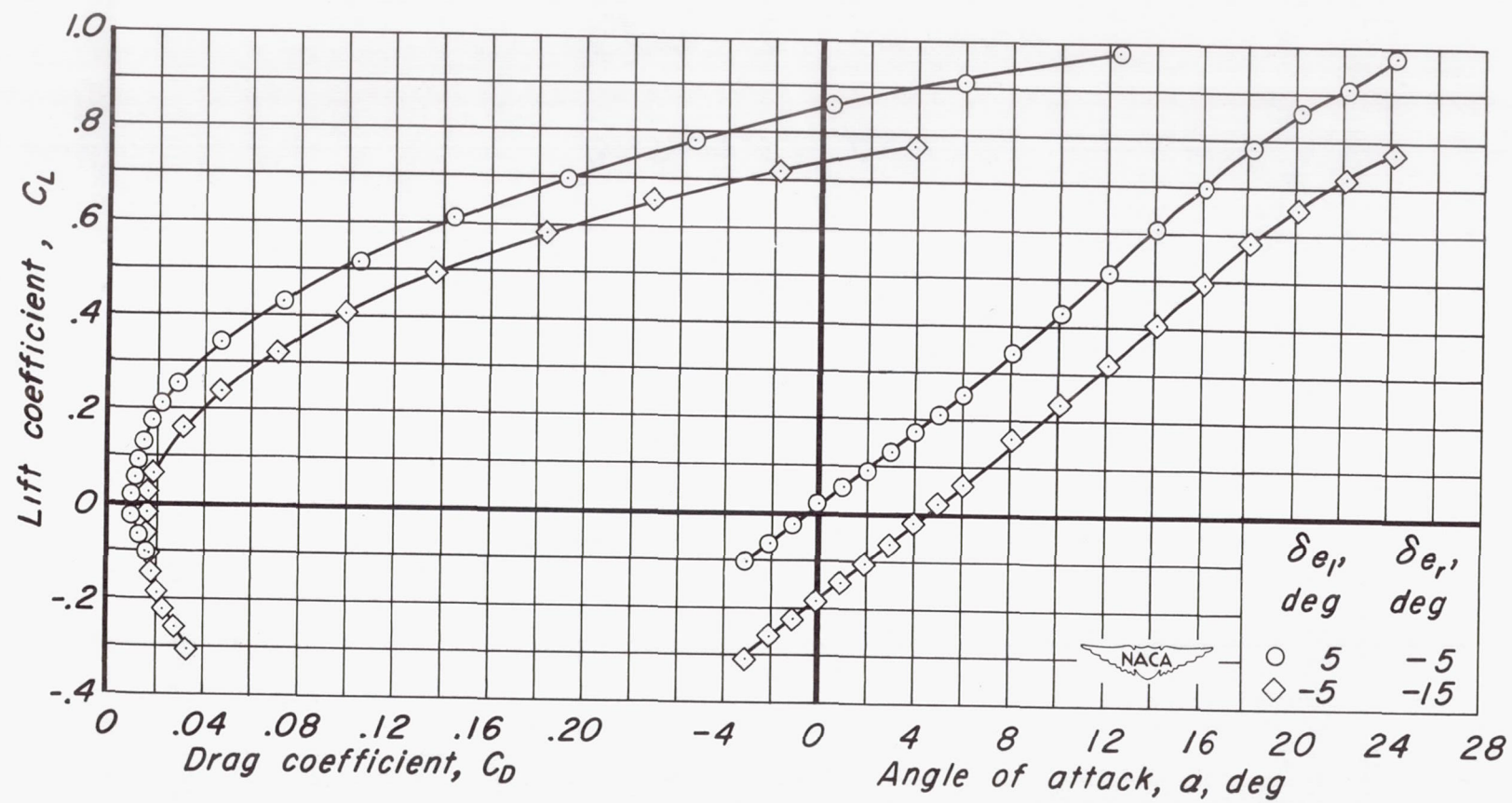


(f)  $2y/b$  vs  $\alpha$ ,  $x/c_r$  vs  $\alpha$

Figure 11. - Concluded.

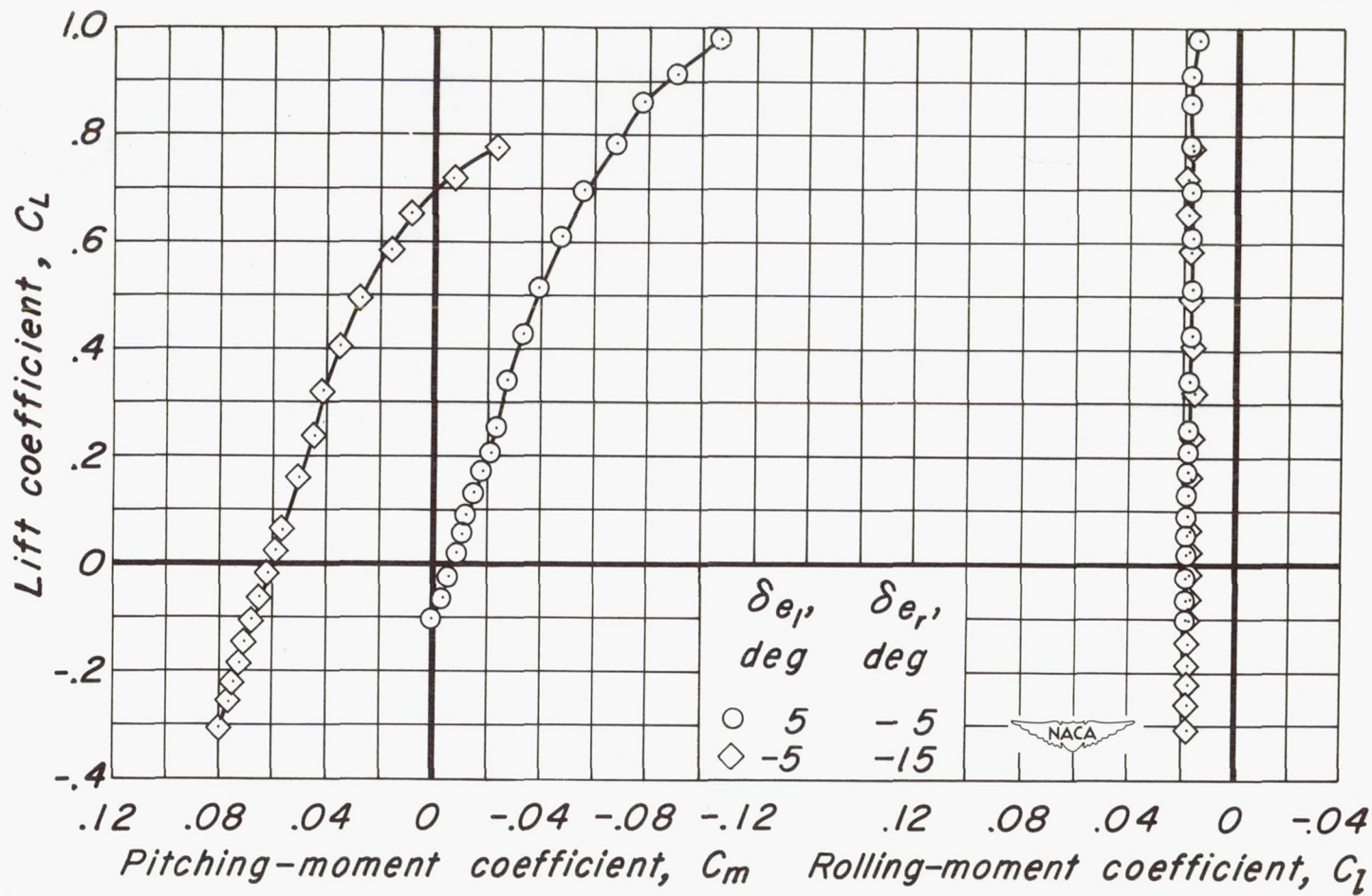


CONFIDENTIAL



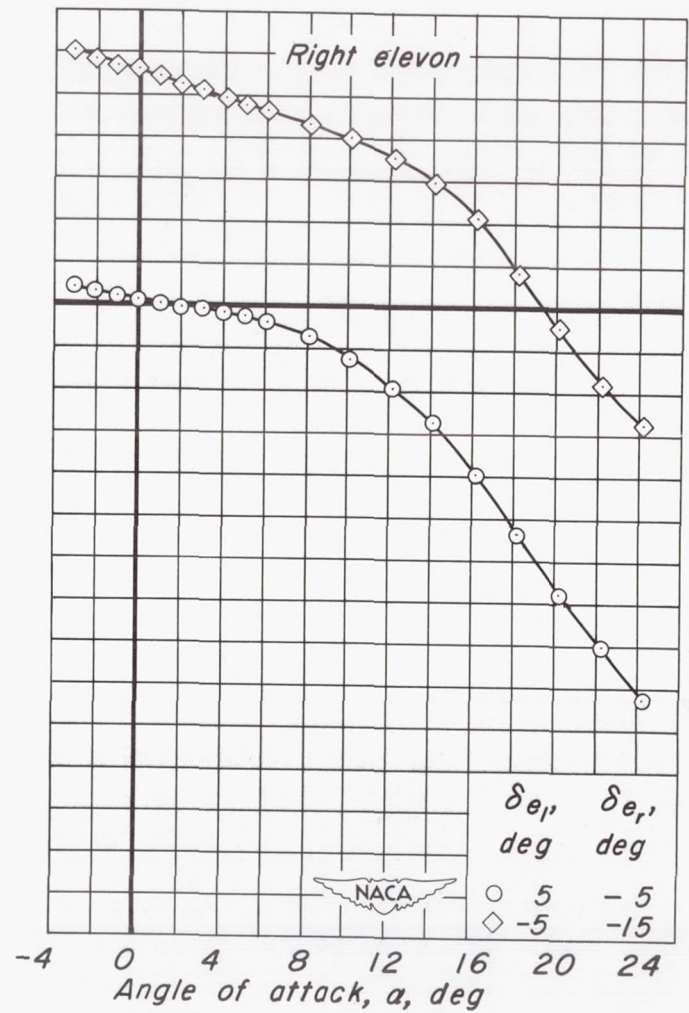
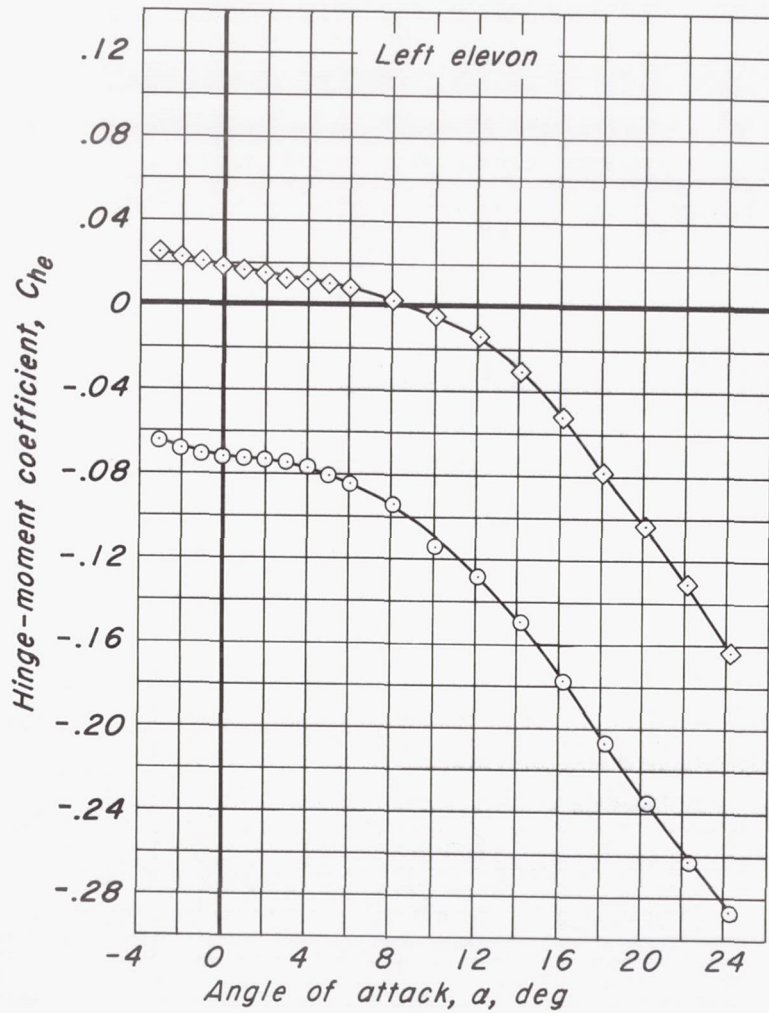
(a)  $C_L$  vs  $\alpha$  ,  $C_L$  vs  $C_D$

Figure 12.- The effect of differential elevon deflection on the aerodynamic characteristics at a Mach number of 0.60.  $R$ , 3.0 million;  $\delta_t$ ,  $5^\circ$ .



(b)  $C_L$  vs  $C_m$ ,  $C_L$  vs  $C_l$

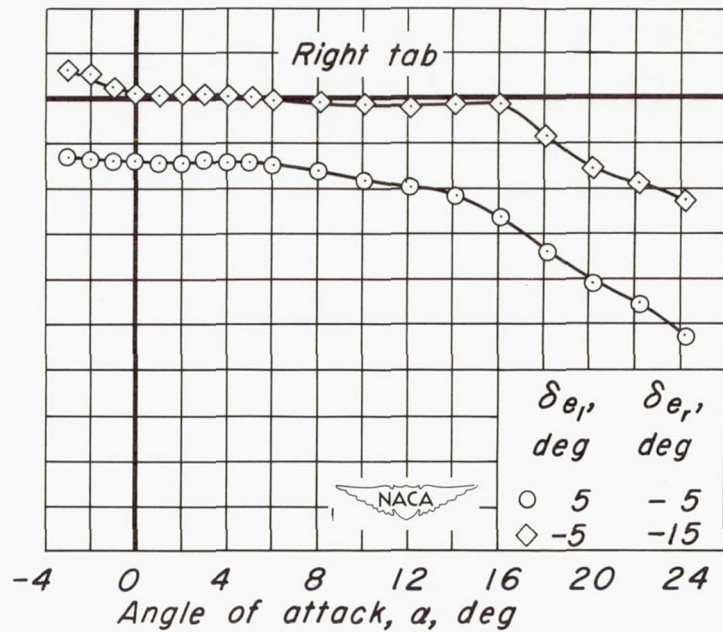
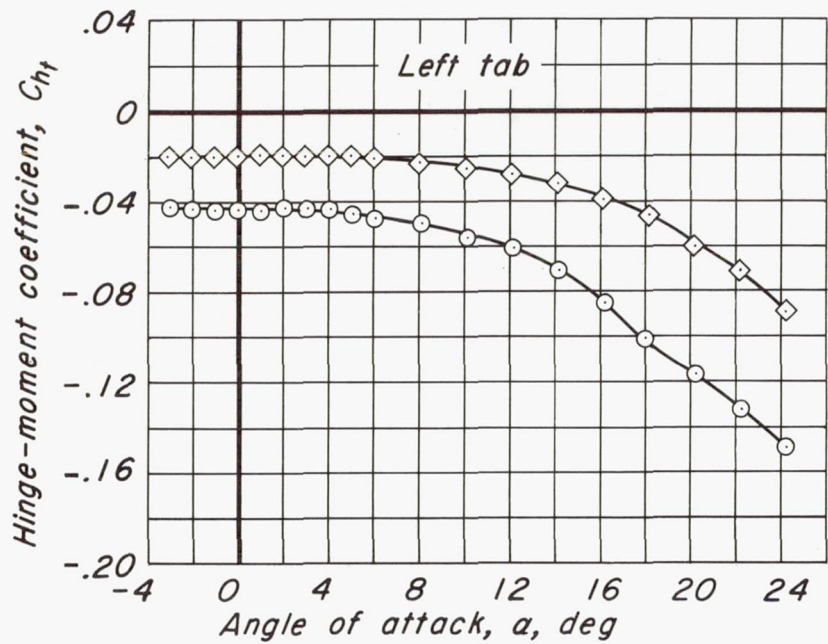
Figure 12.- Continued.



(c)  $C_{he}$  vs  $a$

Figure 12.- Continued.





(d)  $C_{h_t}$  vs  $a$

Figure 12.- Continued.

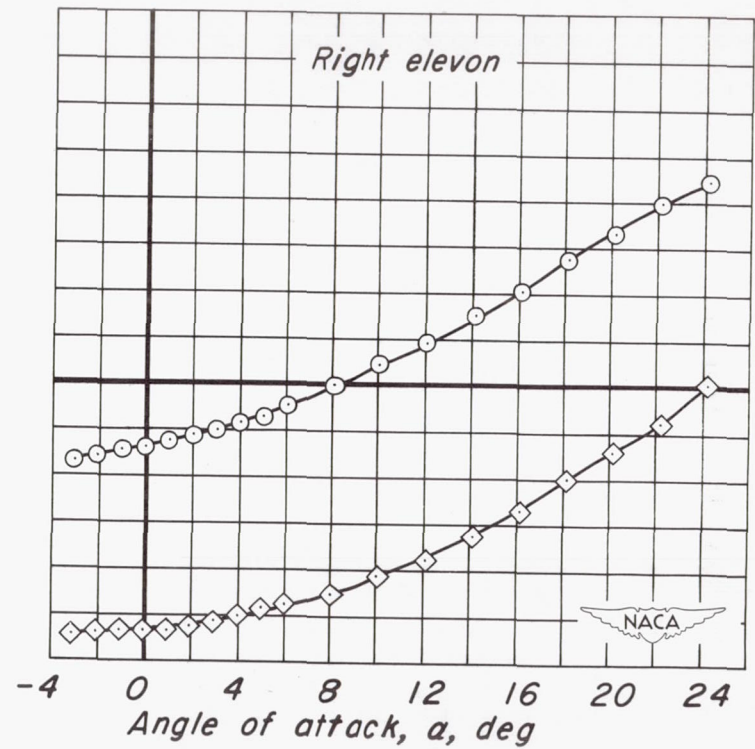
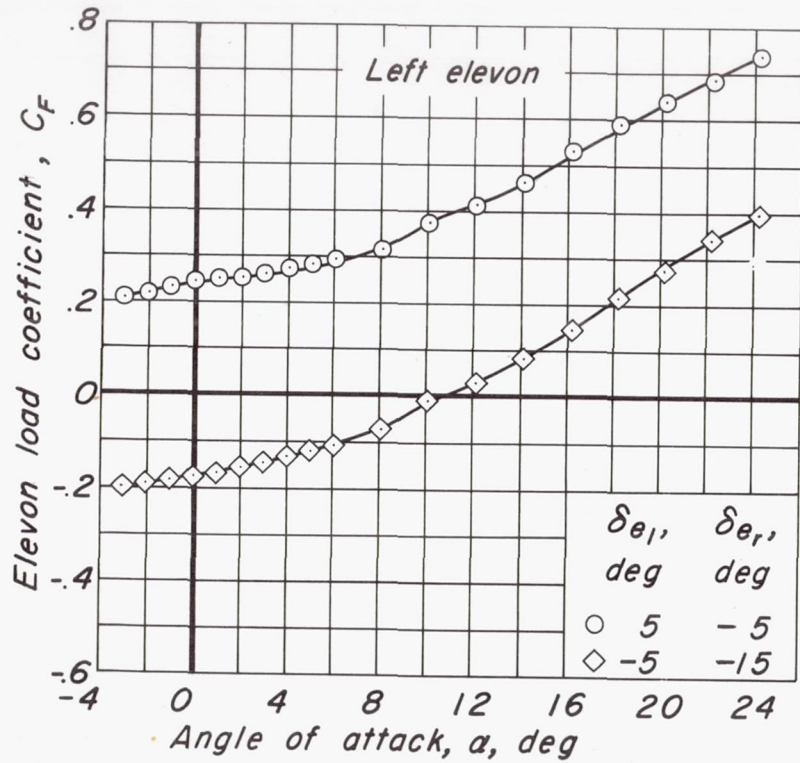
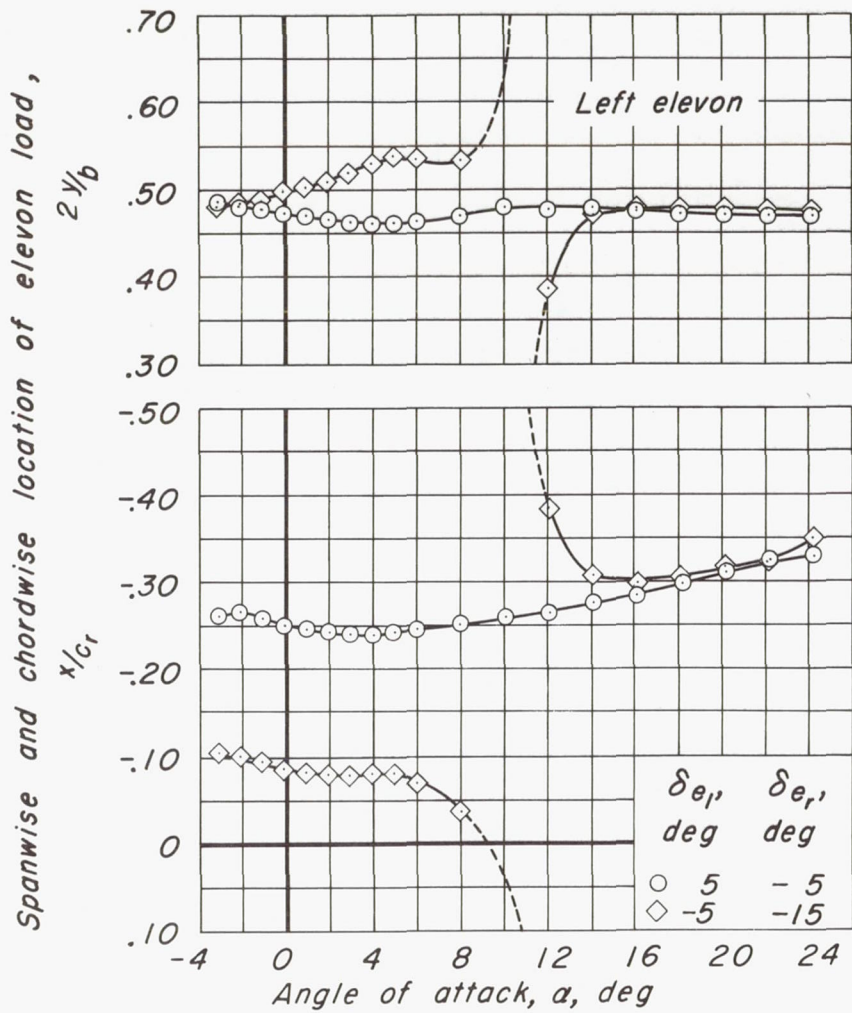
(e)  $C_F$  vs  $\alpha$ 

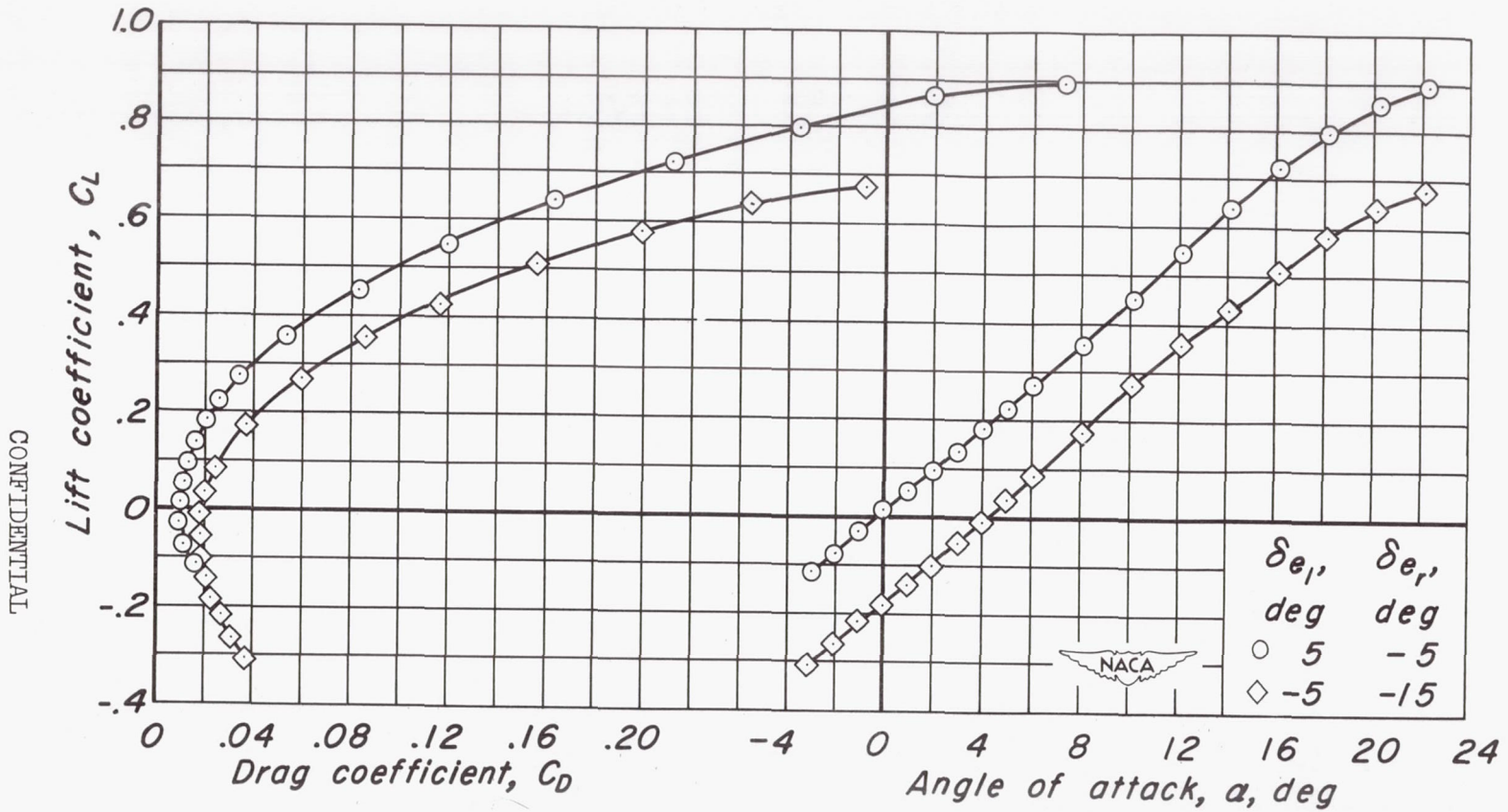
Figure 12.- Continued.



(f)  $2y/b$  vs  $\alpha$ ,  $x/c_r$  vs  $\alpha$

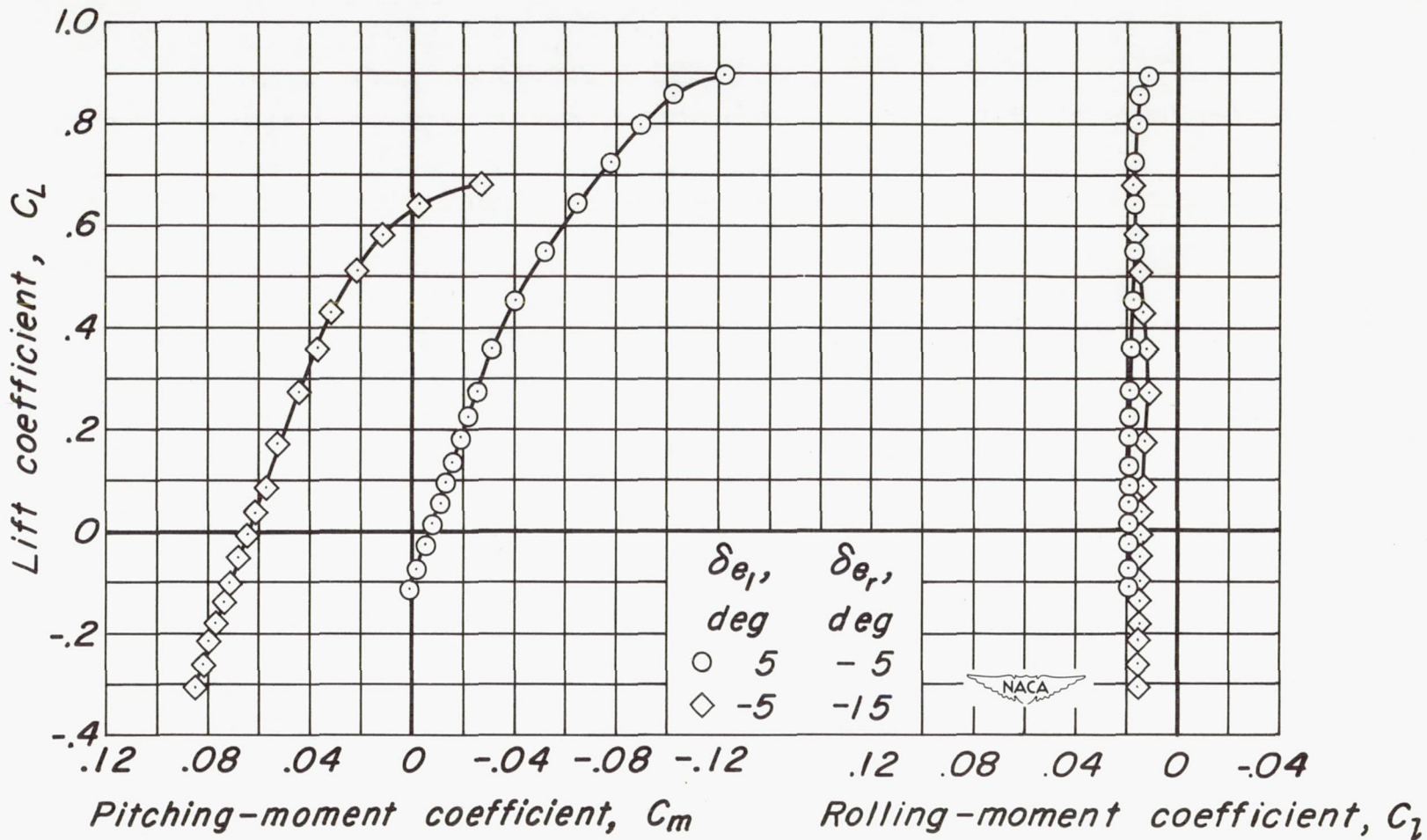
Figure 12.- Concluded.





(a)  $C_L$  vs  $\alpha$  ,  $C_L$  vs  $C_D$

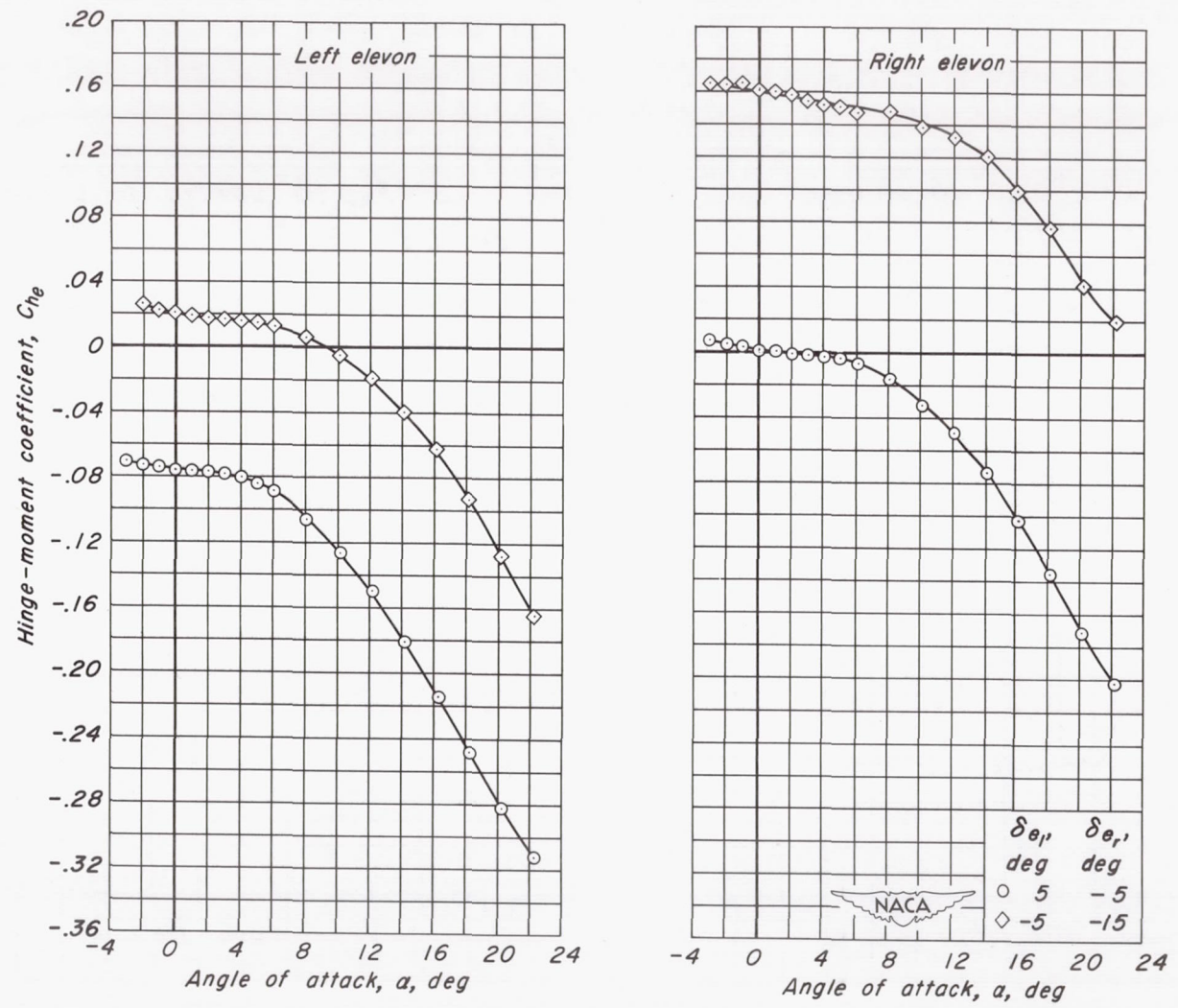
Figure 13.- The effect of differential elevon deflection on the aerodynamic characteristics at a Mach number of 0.80.  $R$ , 3.0 million;  $\delta_t$ ,  $5^\circ$ .



(b)  $C_L$  vs  $C_m$ ,  $C_L$  vs  $C_l$

Figure 13.- Continued.

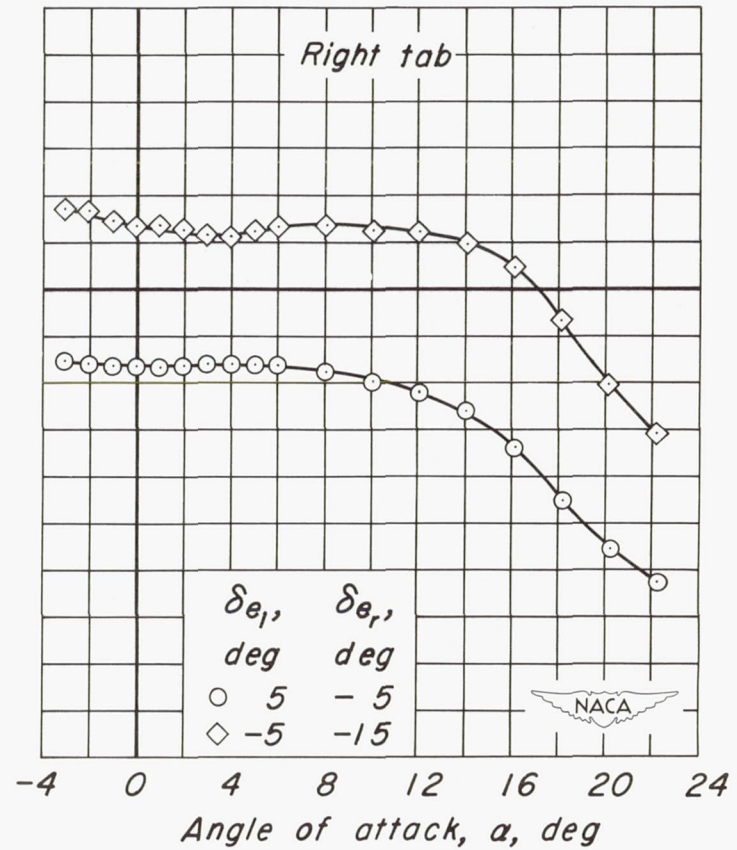
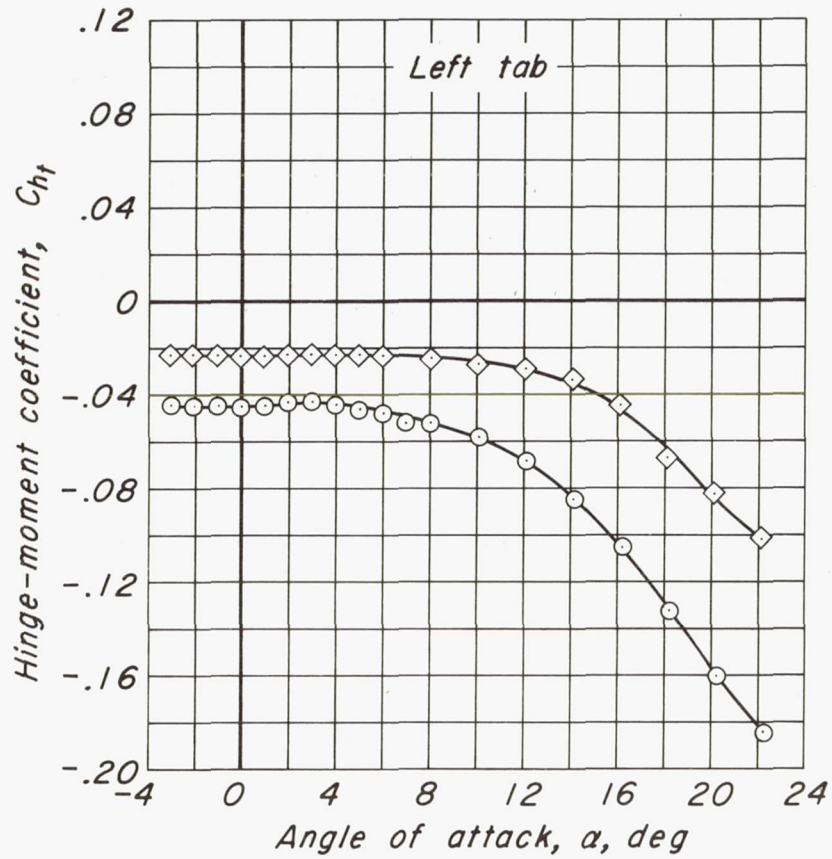
CONFIDENTIAL



(c)  $C_{he}$  vs  $\alpha$

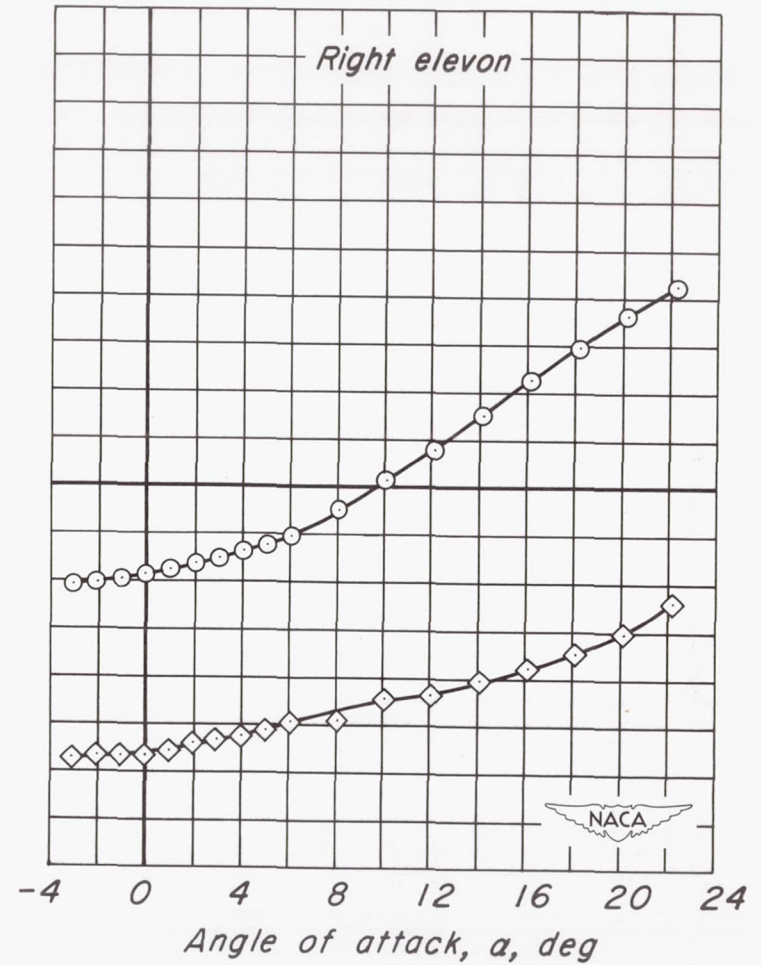
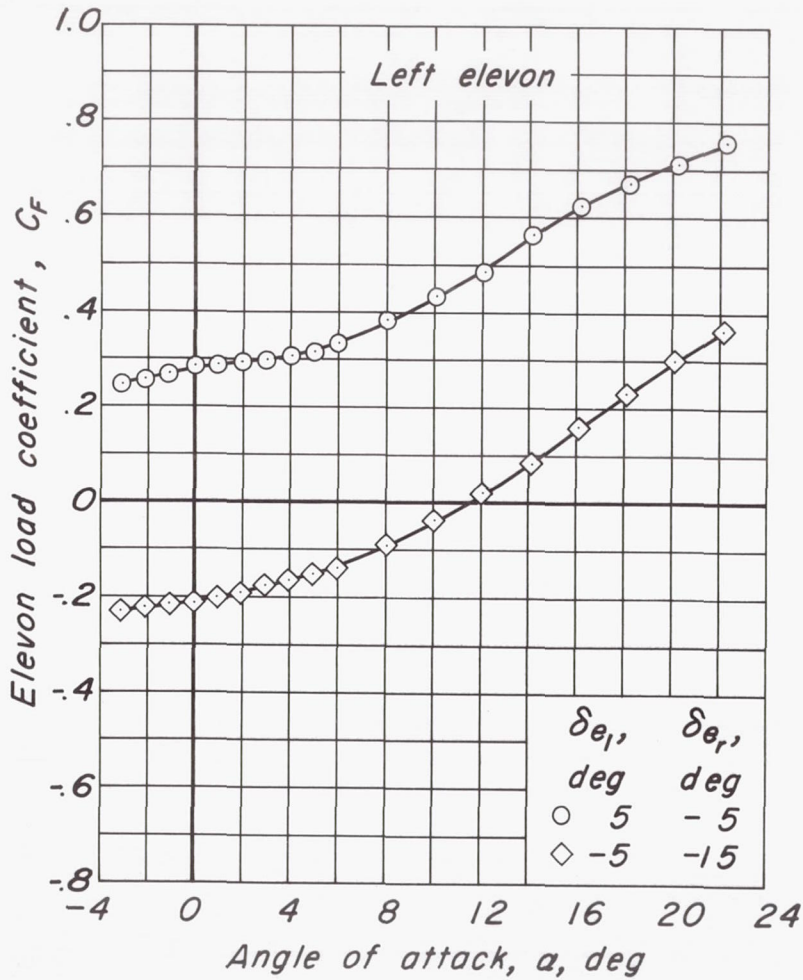
Figure 13 - Continued.





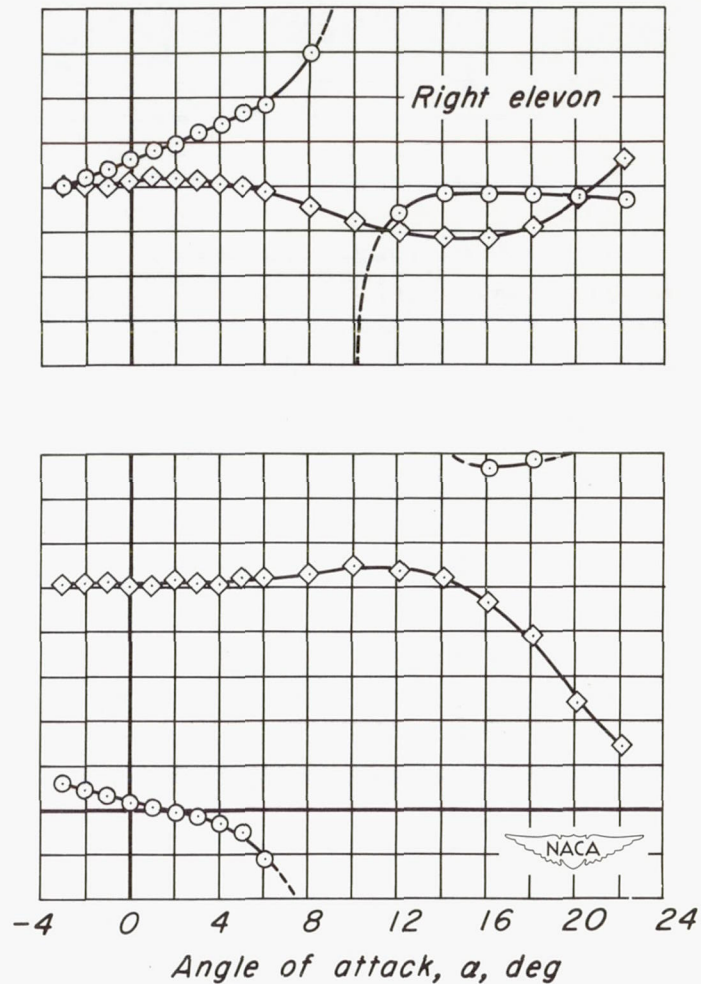
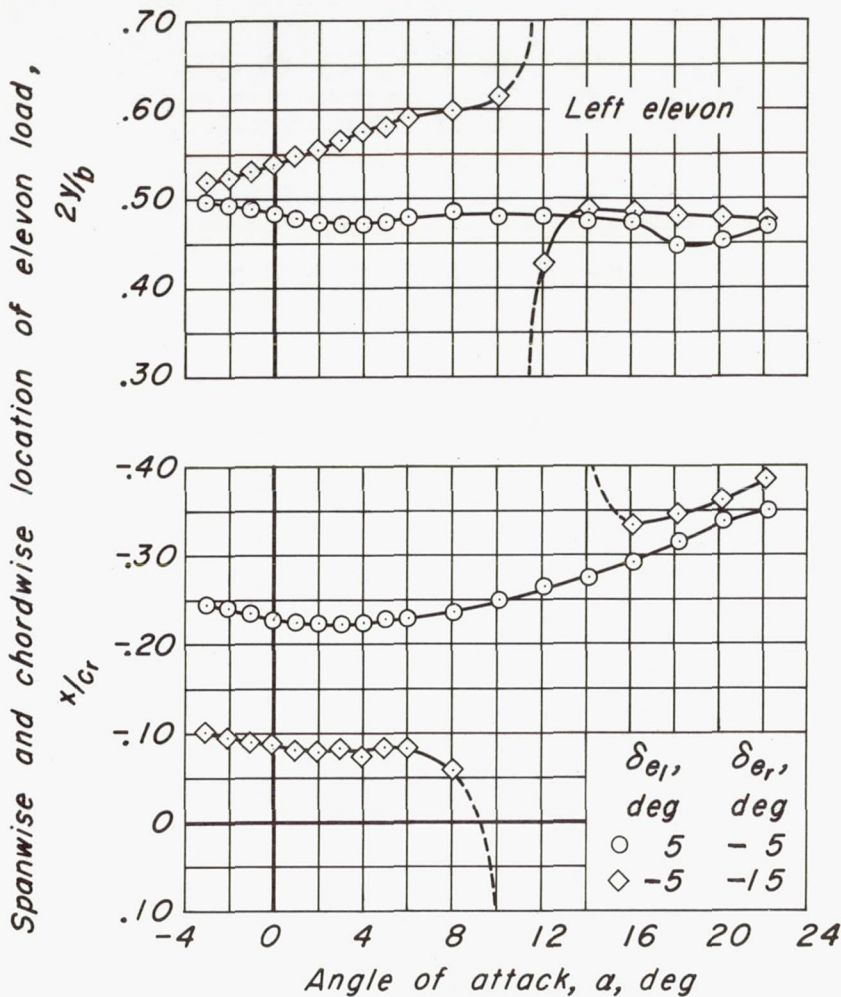
(d)  $C_{ht}$  vs  $\alpha$

Figure 13.- Continued.



(e)  $C_F$  vs  $a$

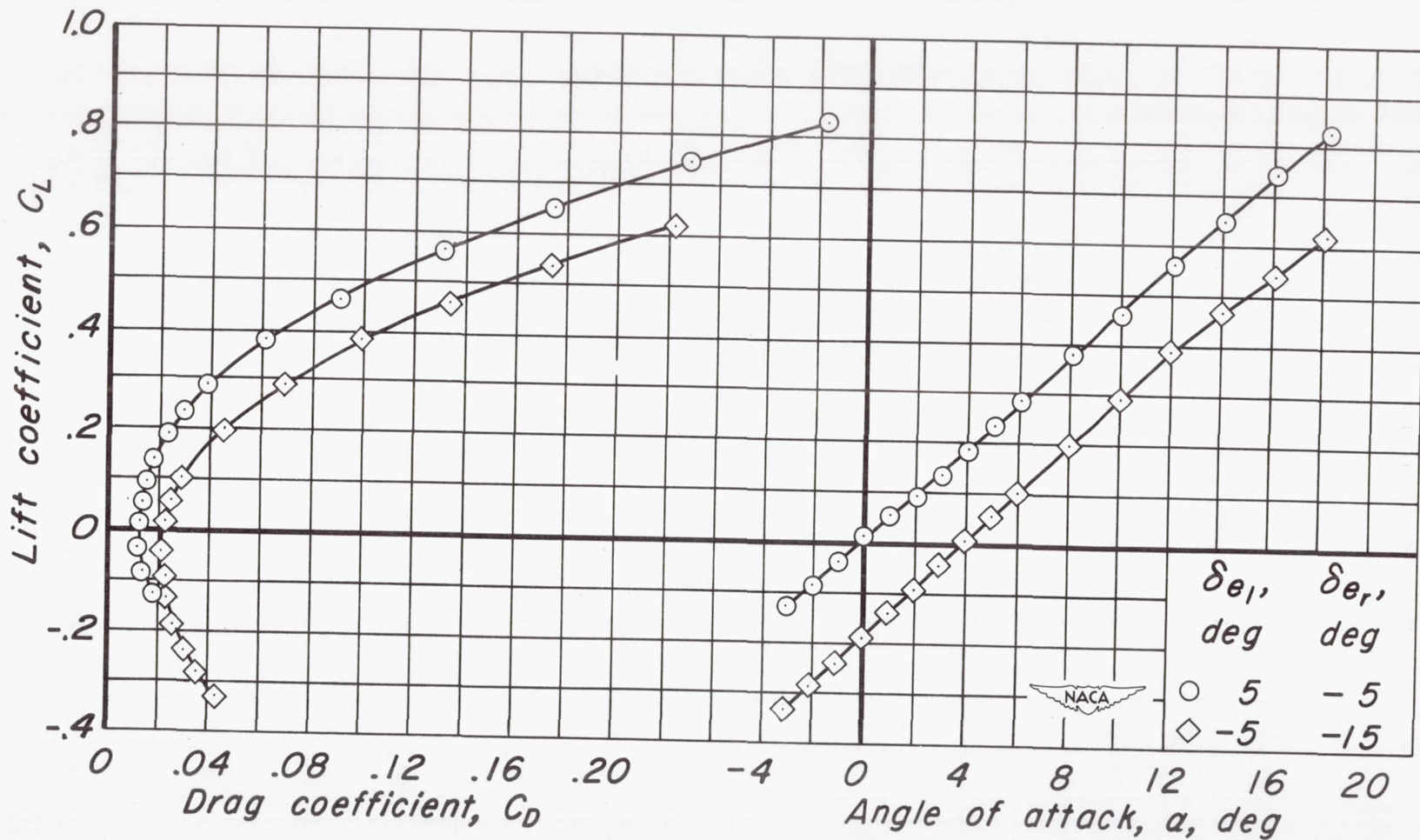
Figure 13.- Continued.



(f)  $2y/b$  vs  $\alpha$ ,  $x/c_r$  vs  $\alpha$

Figure 13.- Concluded.





(a)  $C_L$  vs  $C_D$ ,  $C_L$  vs  $\alpha$

Figure 14.- The effect of differential elevon deflection on the aerodynamic characteristics at a Mach number of 0.90.  $R$ , 3.0 million;  $\delta_t$ ,  $5^\circ$ .

CONFIDENTIAL

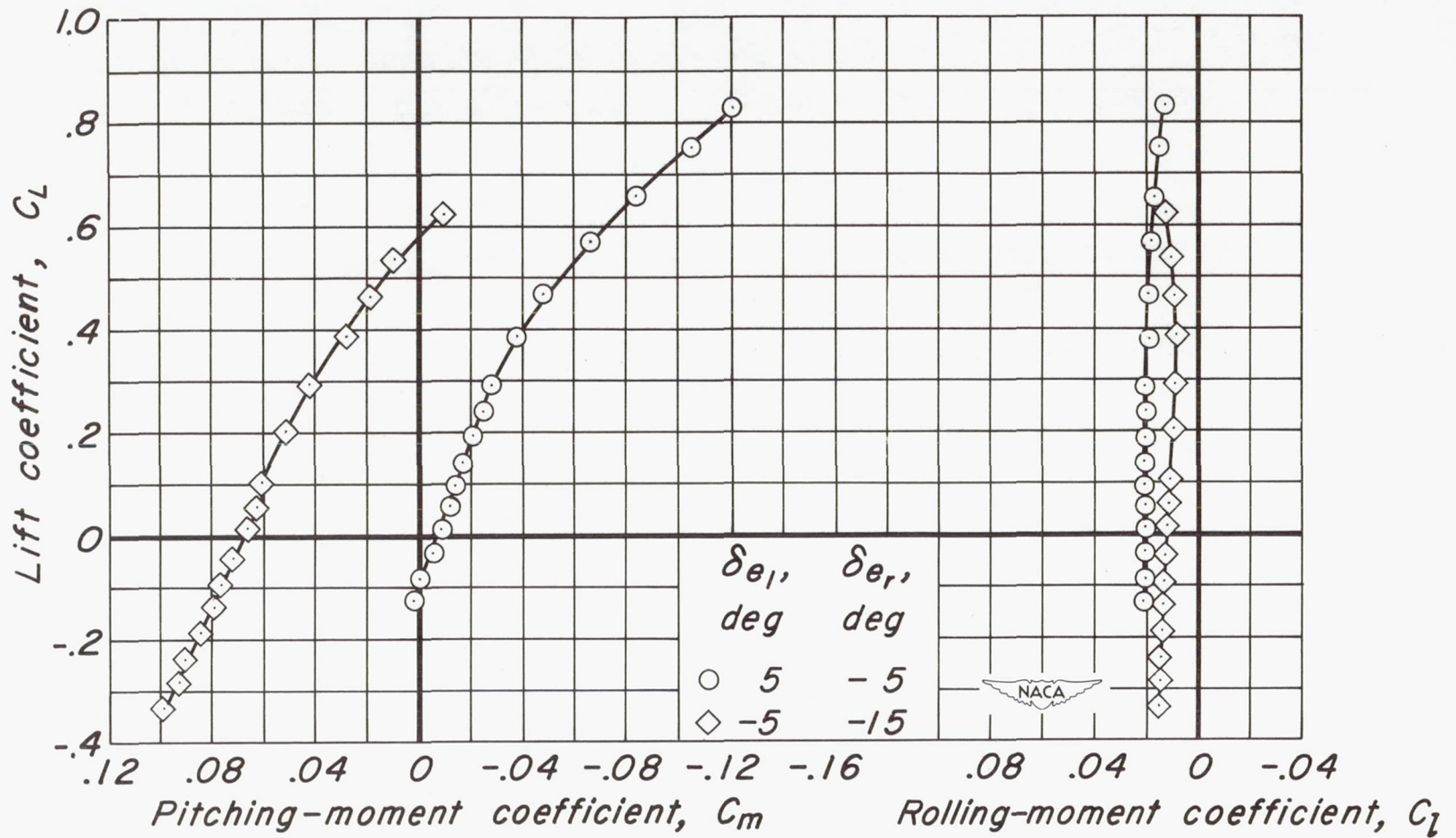
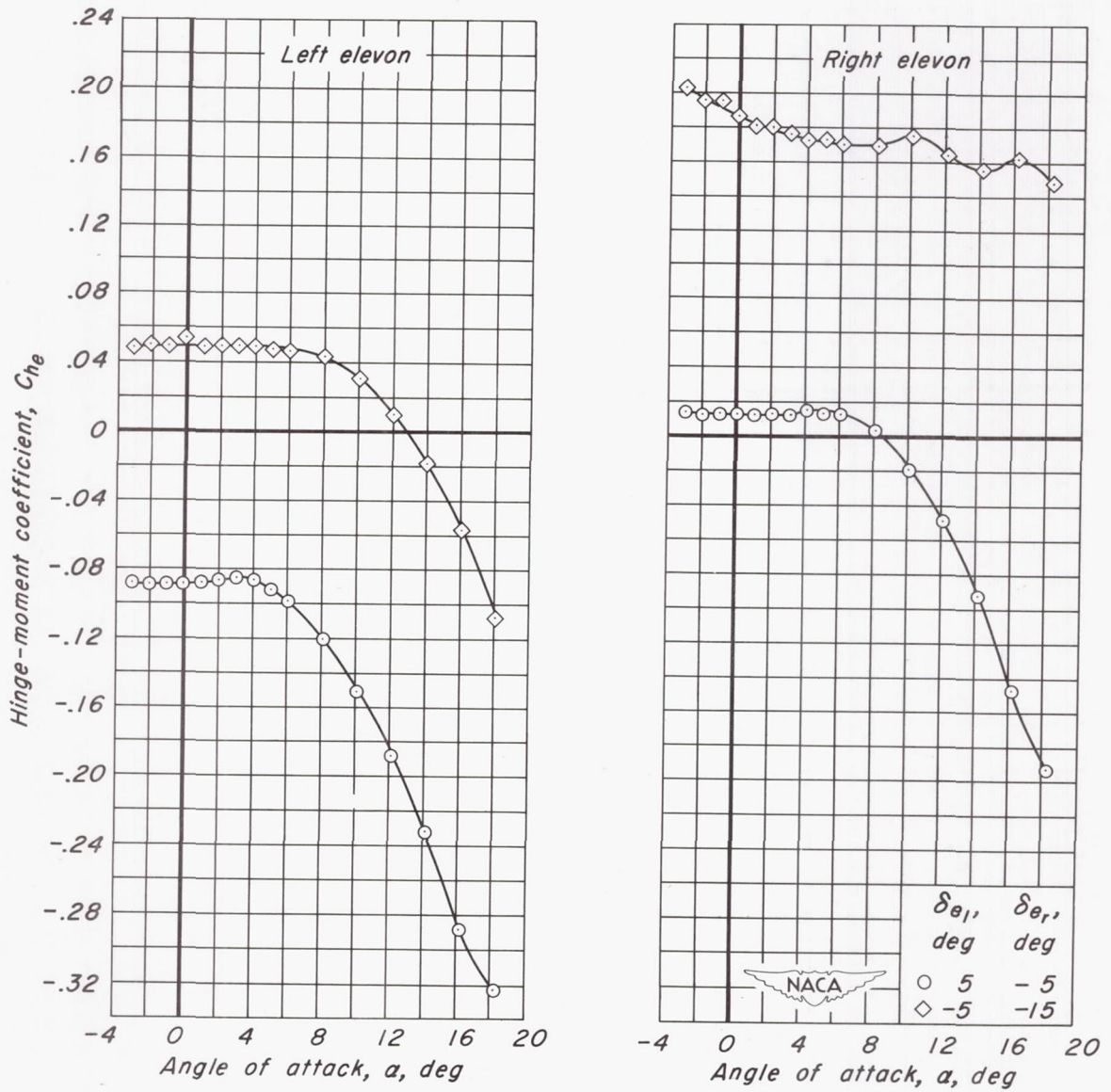
(b)  $C_L$  vs  $C_m$ ,  $C_L$  vs  $C_l$ 

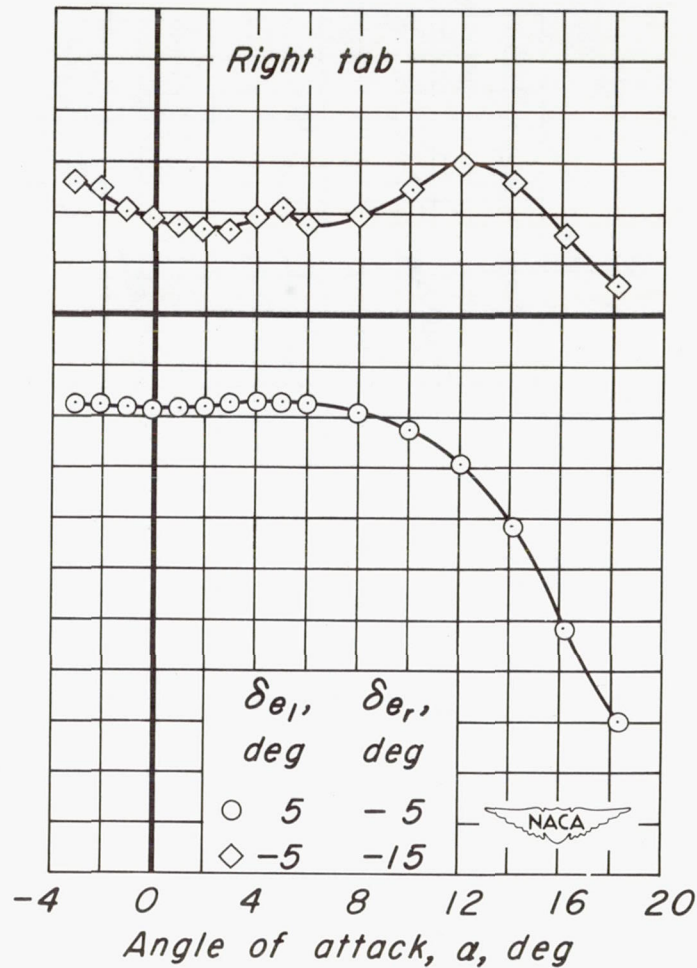
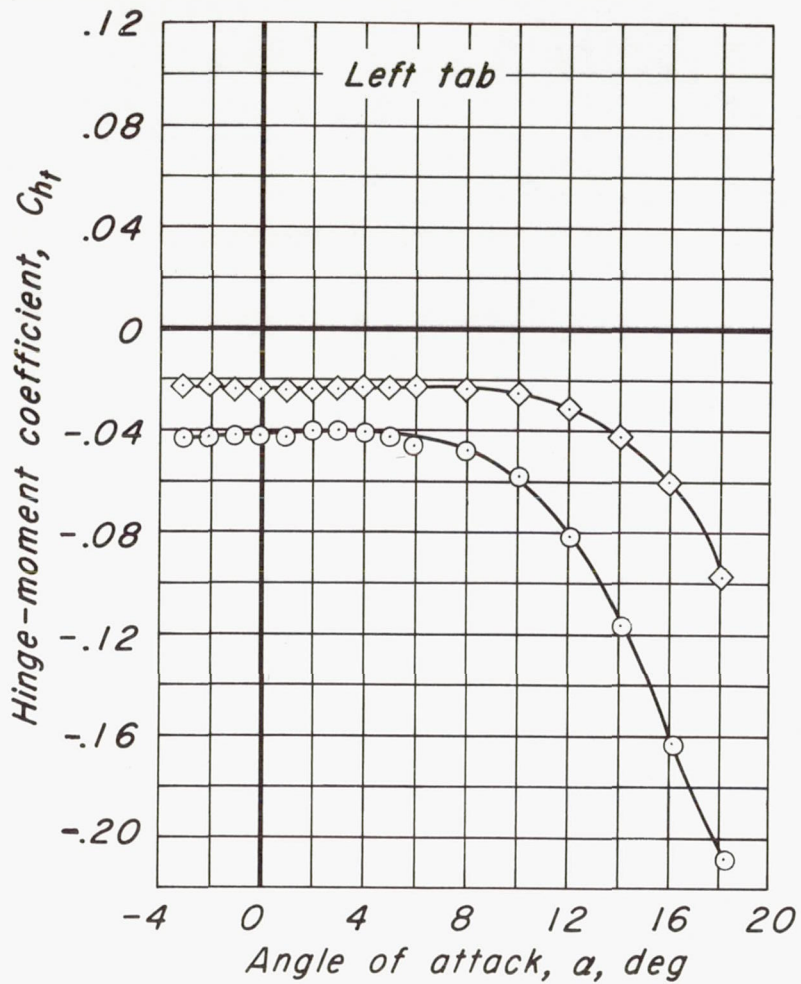
Figure 14.- Continued.



(c)  $C_{he}$  vs  $\alpha$

Figure 14.- Continued.

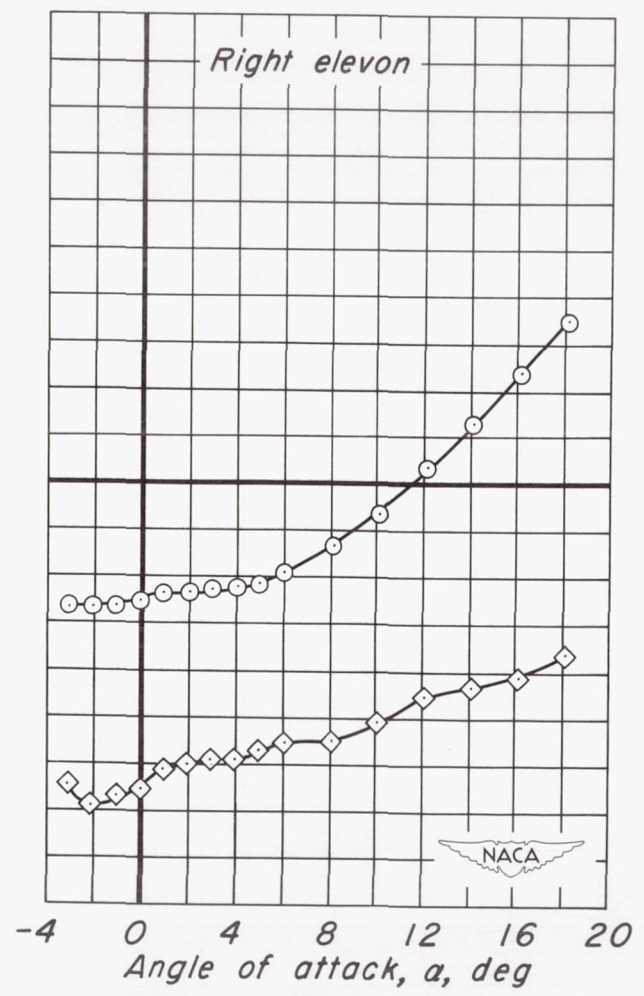
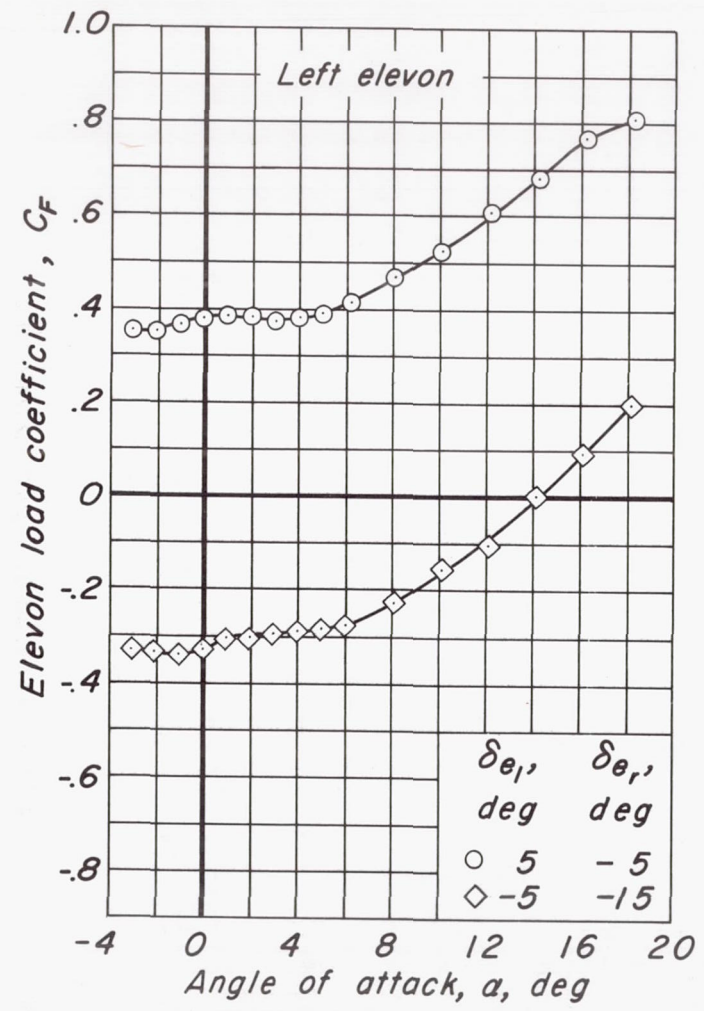




(d)  $C_{h_t}$  vs  $\alpha$

Figure 14.- Continued.

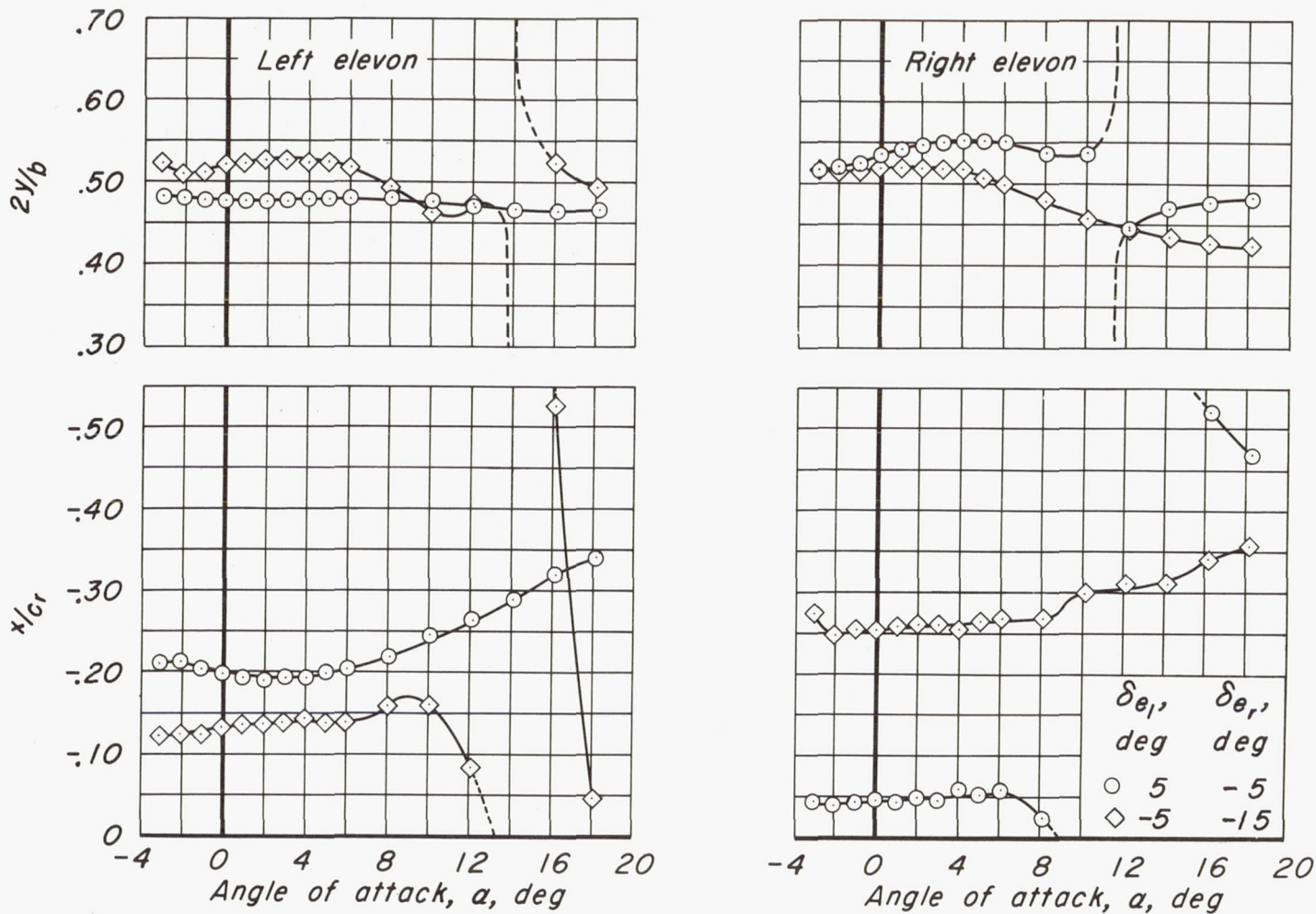
CONFIDENTIAL



(e)  $C_F$  vs  $\alpha$

Figure 14.- Continued.

Spanwise and chordwise location of elevon load,



(f)  $2Y/b$  vs  $a$ ,  $x/c_r$  vs  $a$

Figure 14.- Concluded.





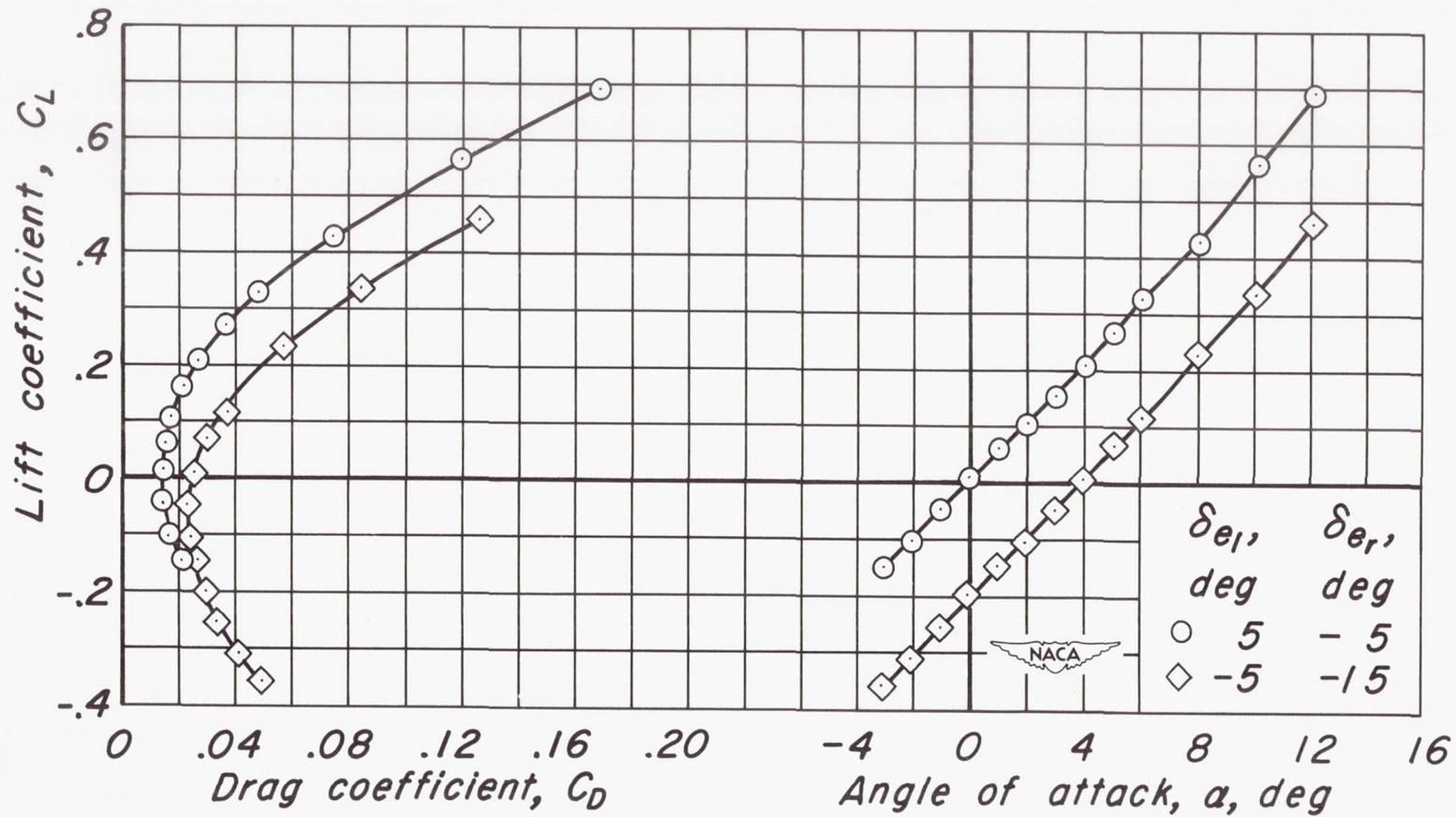
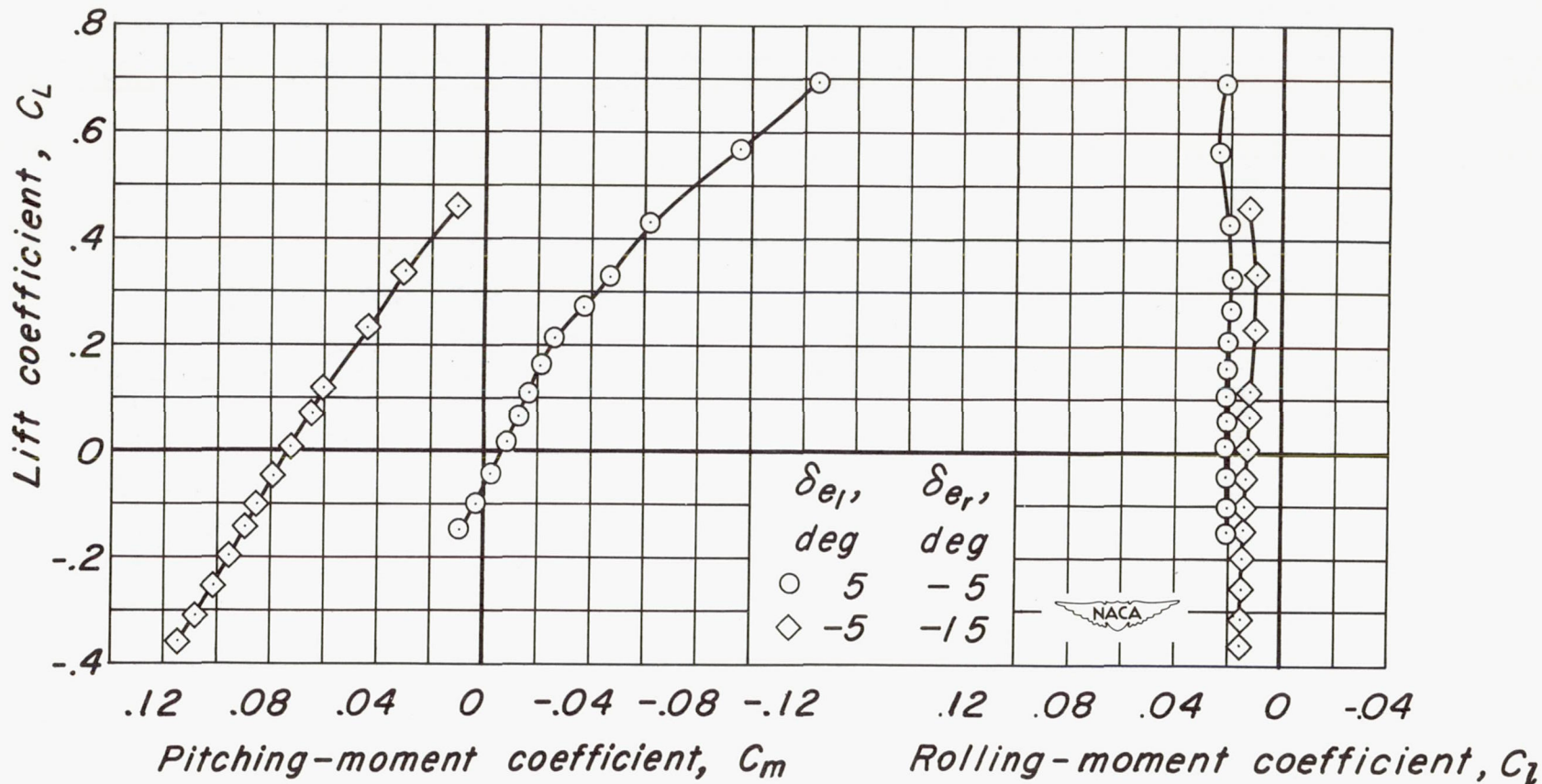
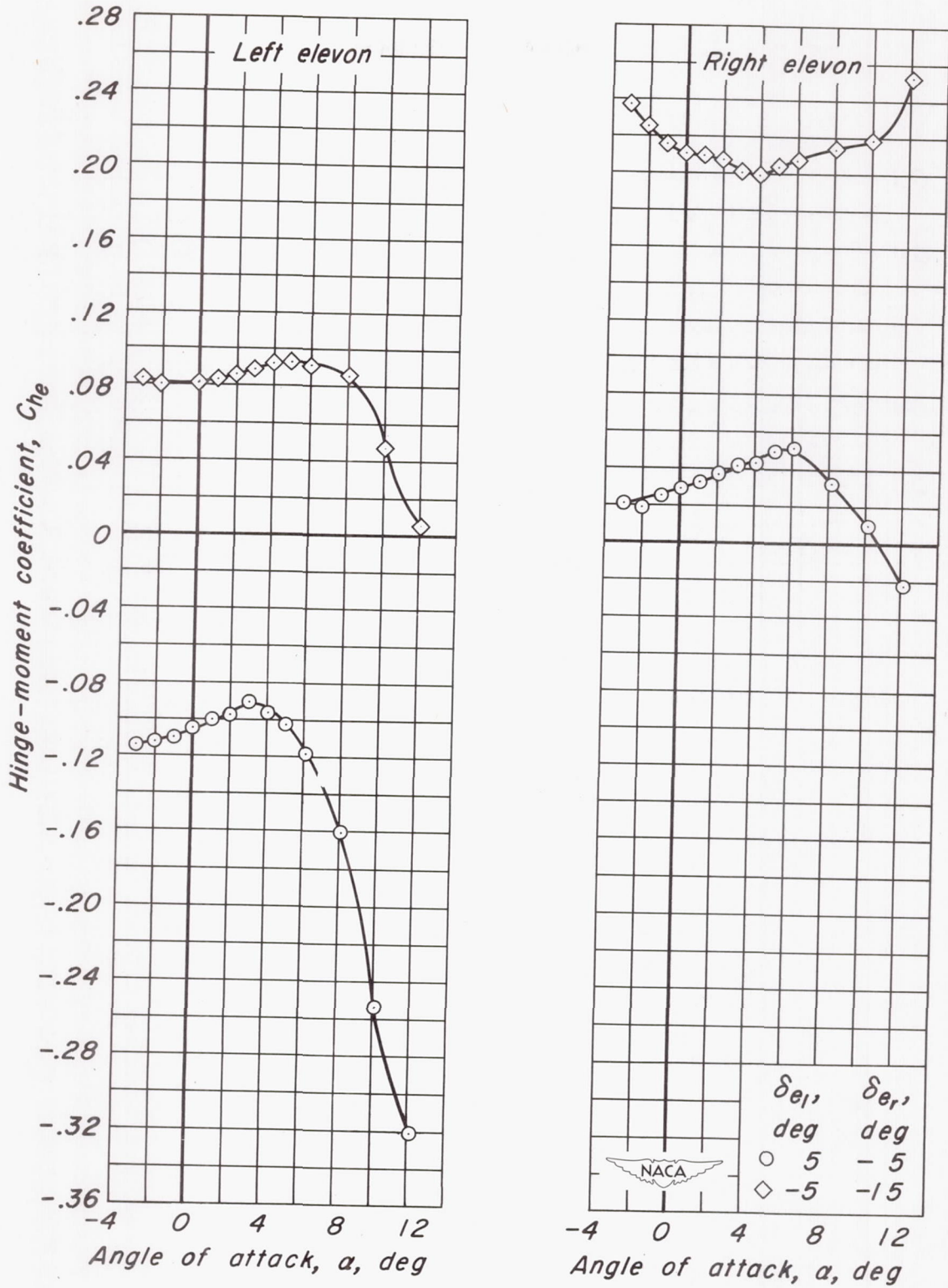
(a)  $C_L$  vs  $\alpha$  ,  $C_L$  vs  $C_D$ 

Figure 15 - The effect of differential elevon deflection on the aerodynamic characteristics at a Mach number of 0.95.  $R$ , 3.0 million;  $\delta_t$ ,  $5^\circ$ .



(b)  $C_L$  vs  $C_m$ ,  $C_L$  vs  $C_l$

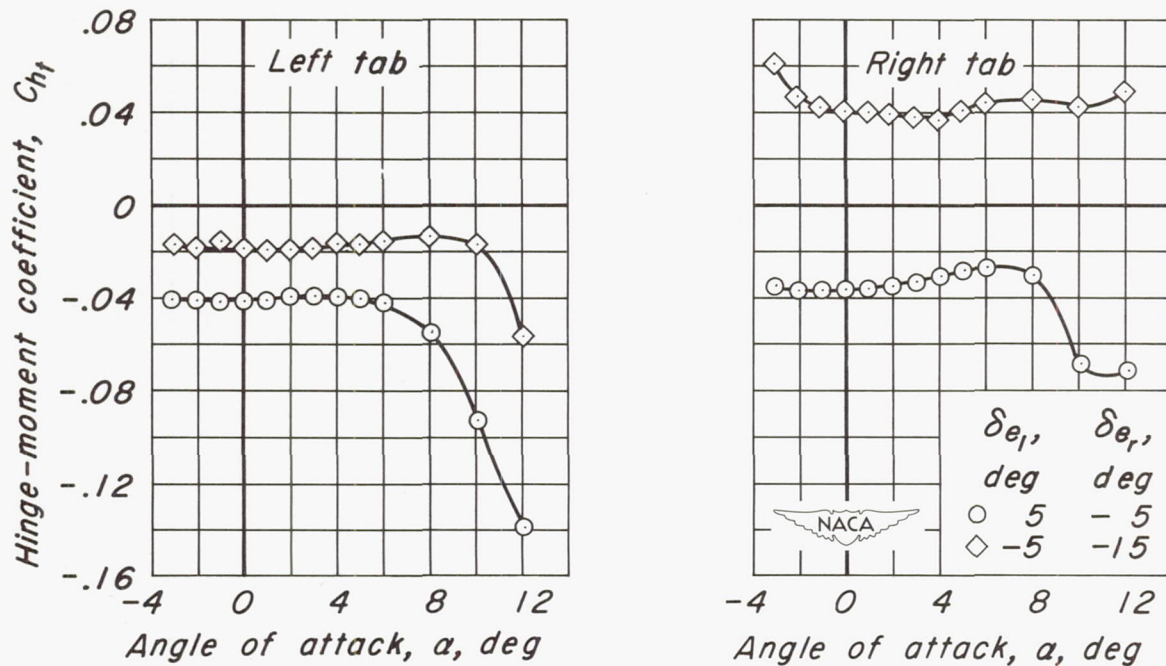
Figure 15 - Continued.



(c)  $C_{h_e}$  vs  $\alpha$

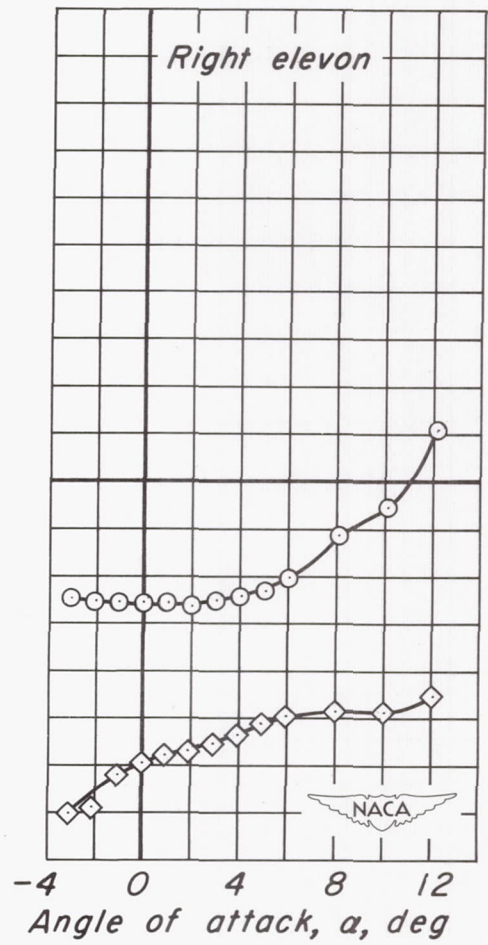
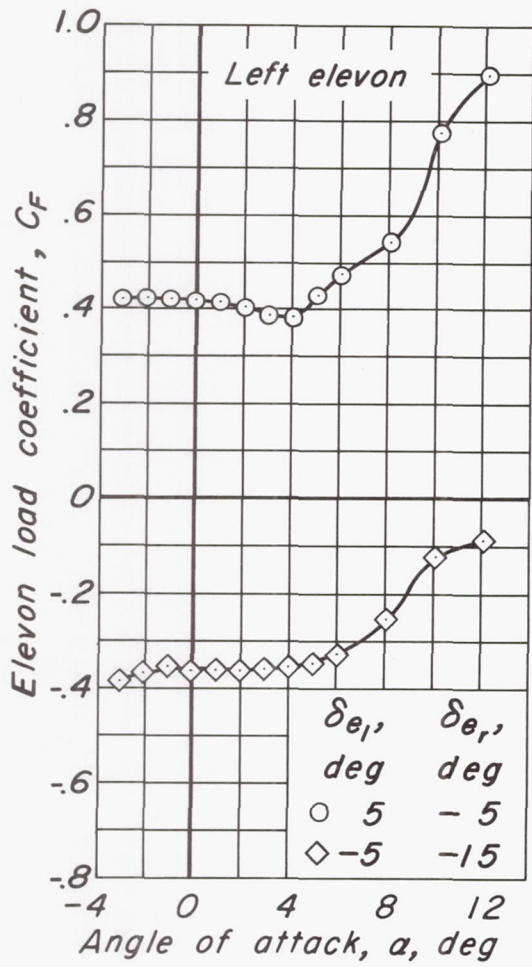
Figure 15 - Continued.





(d)  $C_{h_t}$  vs  $\alpha$

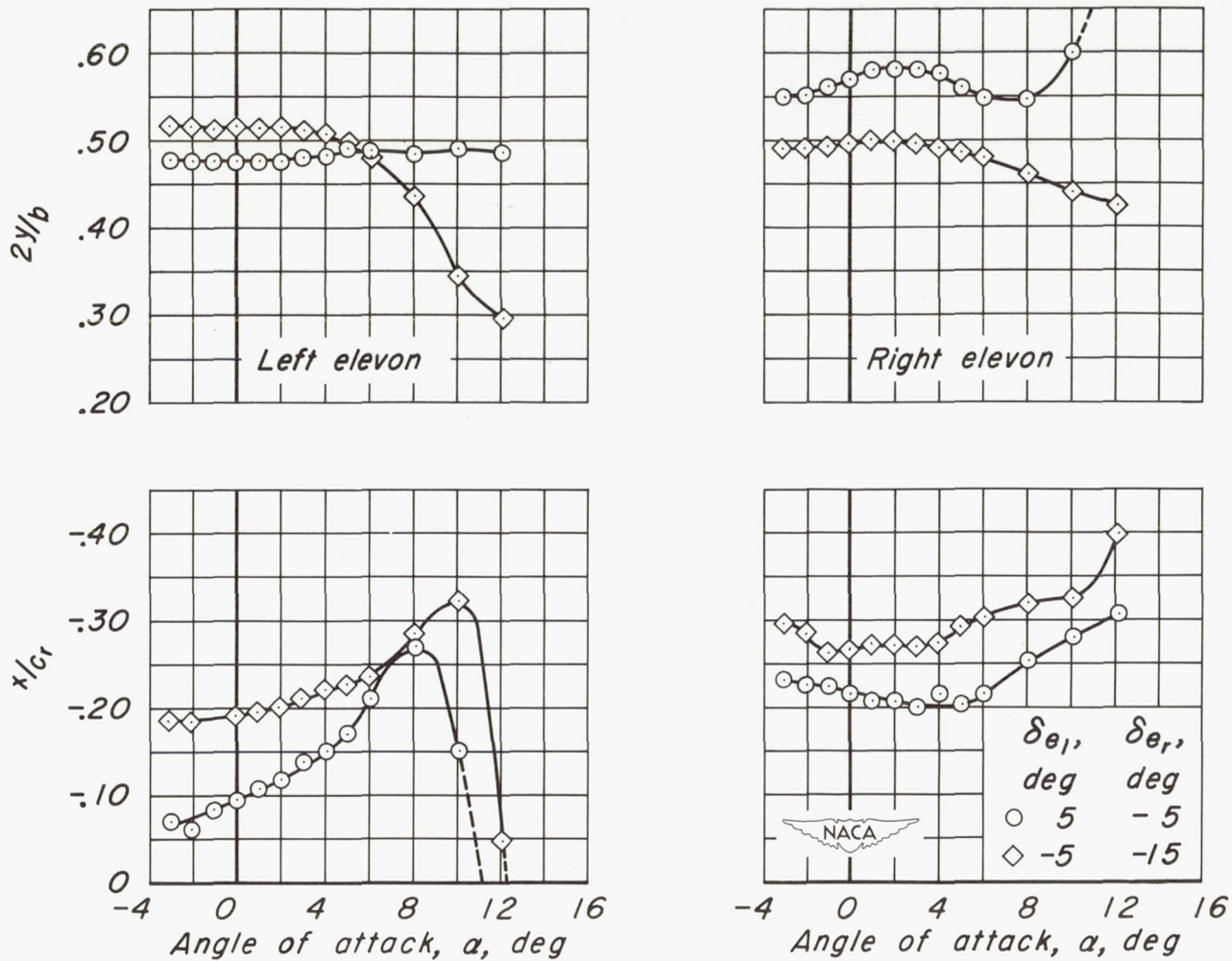
Figure 15 - Continued.



(e)  $C_F$  vs  $\alpha$

Figure 15.- Continued.

Spanwise and chordwise location of elevon load,



(f)  $2y/b$  vs  $a$ ,  $x/c_r$  vs  $a$

Figure 15.- Concluded.



CONFIDENTIAL

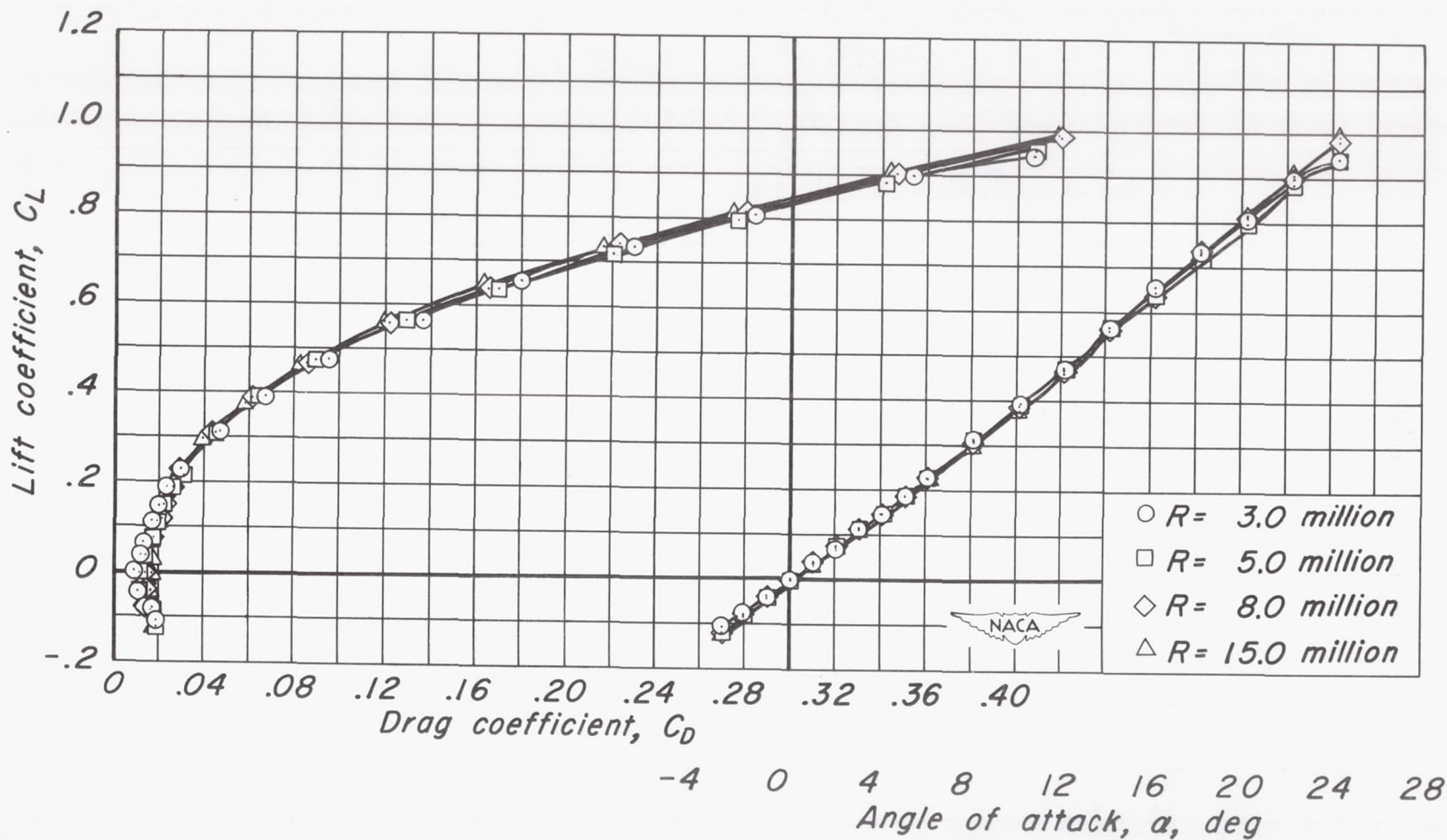
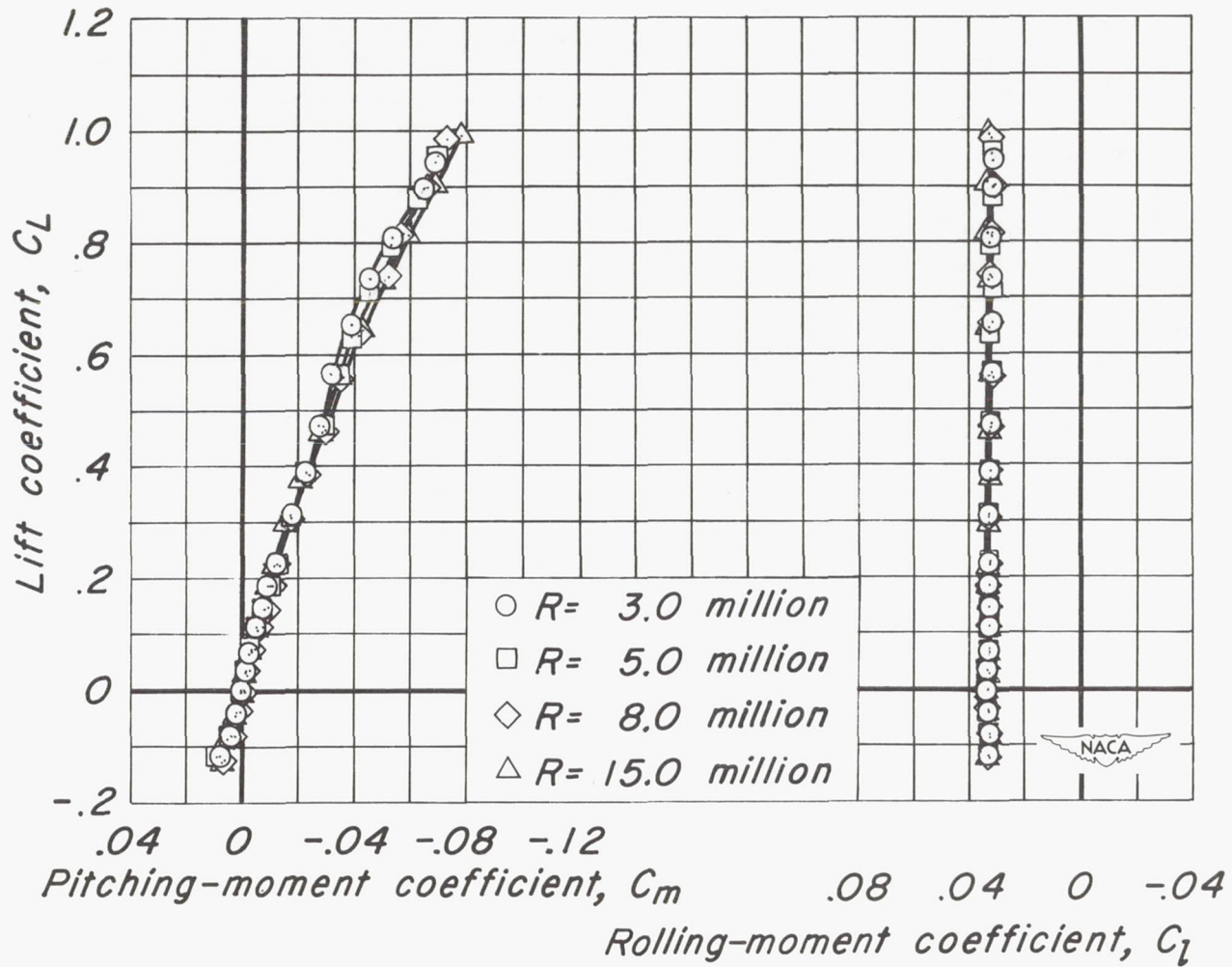
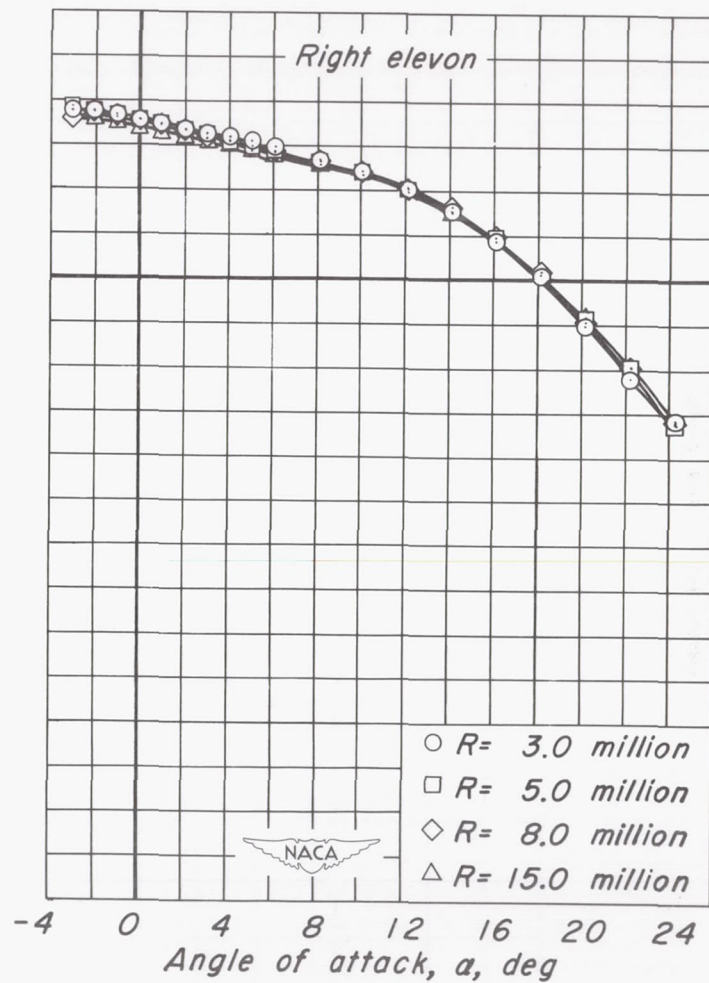
(a)  $C_L$  vs  $\alpha$ ,  $C_L$  vs  $C_D$ 

Figure 16.- The effect of Reynolds number on the aerodynamic characteristics at a Mach number of 0.24.  $\delta_{e1}$ ,  $10^\circ$ ;  $\delta_{e2}$ ,  $-10^\circ$ ;  $\delta_t$ ,  $0^\circ$ .



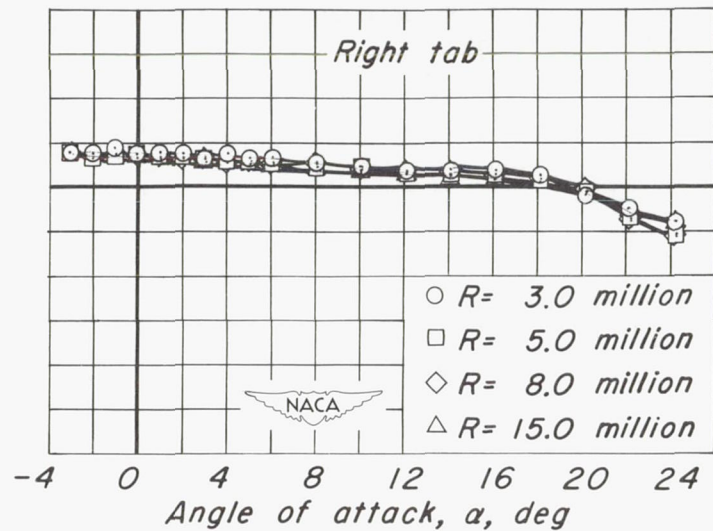
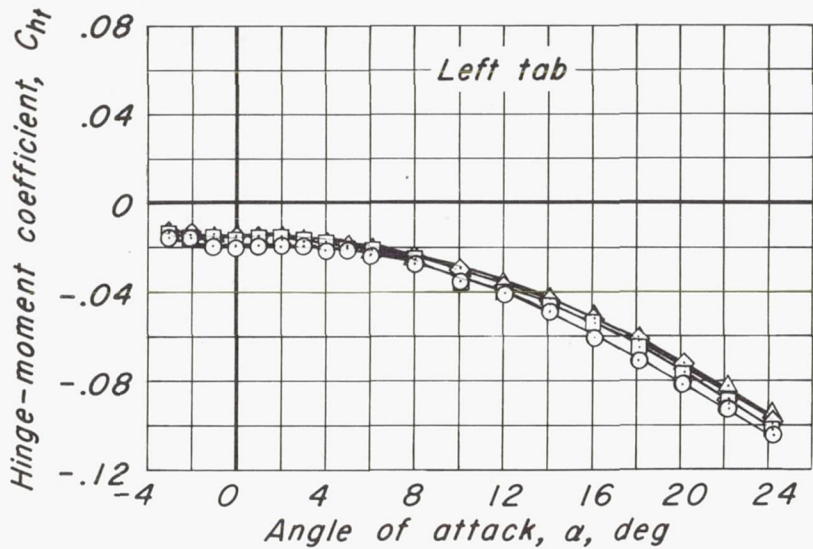
(b)  $C_L$  vs  $C_m$ ,  $C_L$  vs  $C_l$   
 Figure 16 - Continued.



(c)  $C_{he}$  vs  $\alpha$

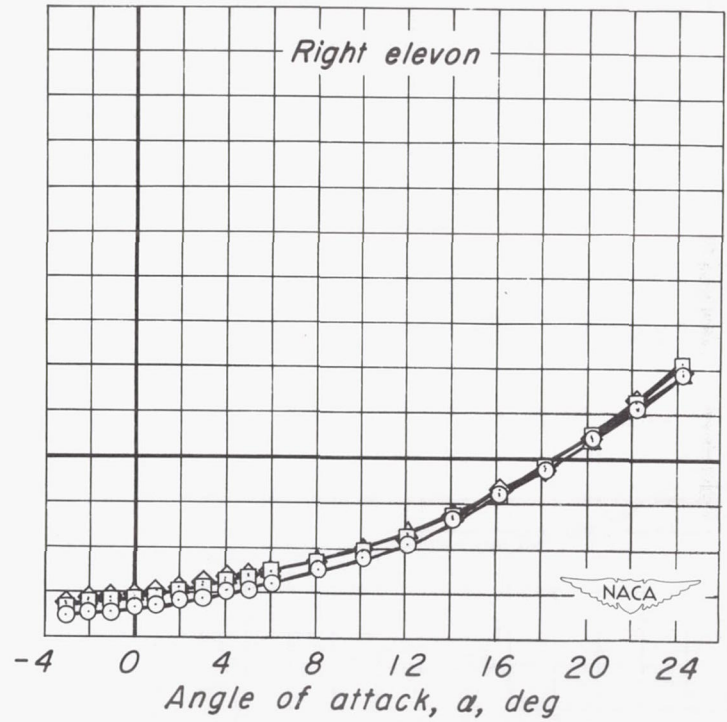
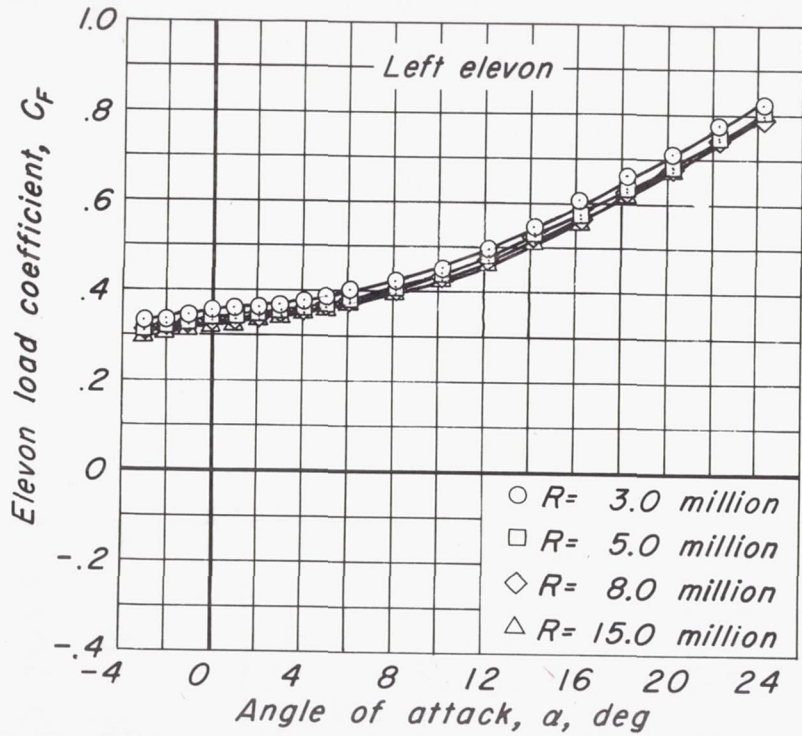
Figure 16.- Continued.



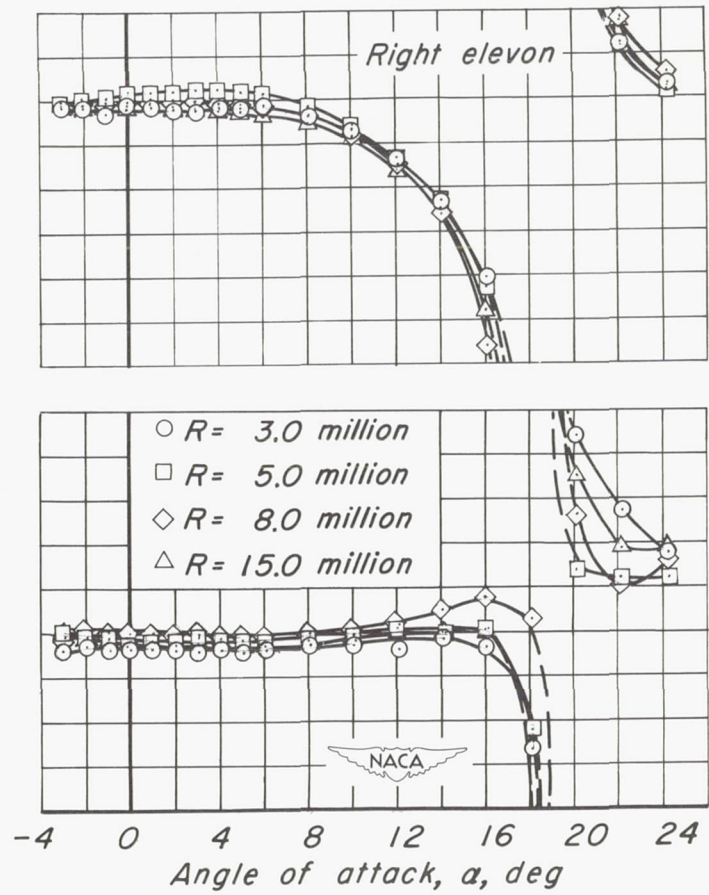
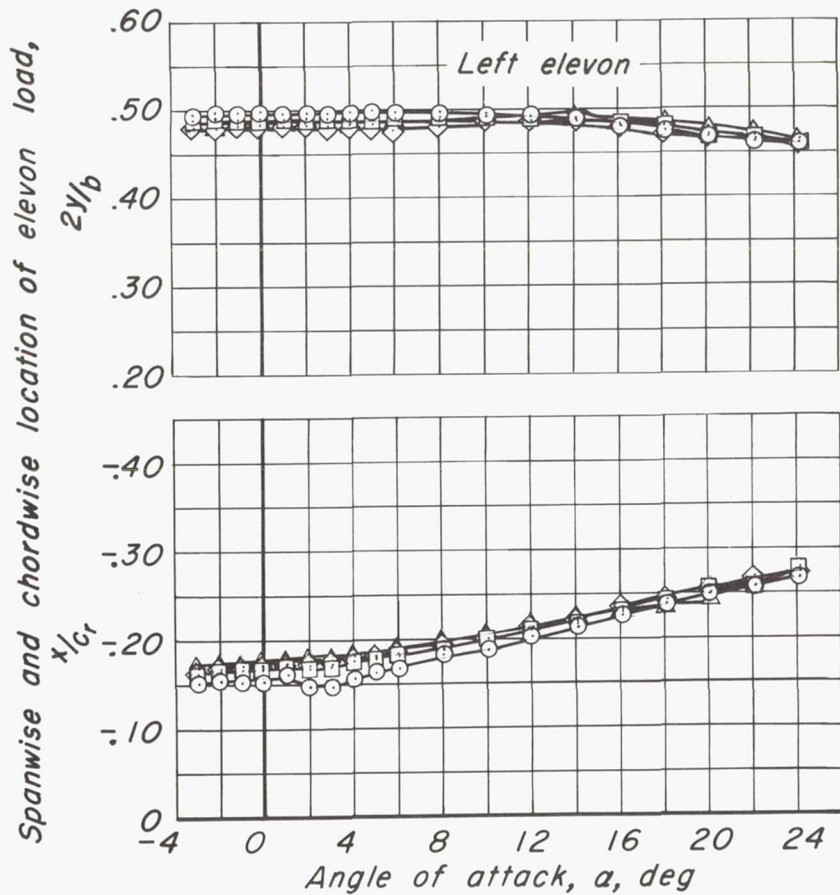


(d)  $C_{ht}$  vs  $\alpha$

Figure 16.- Continued.

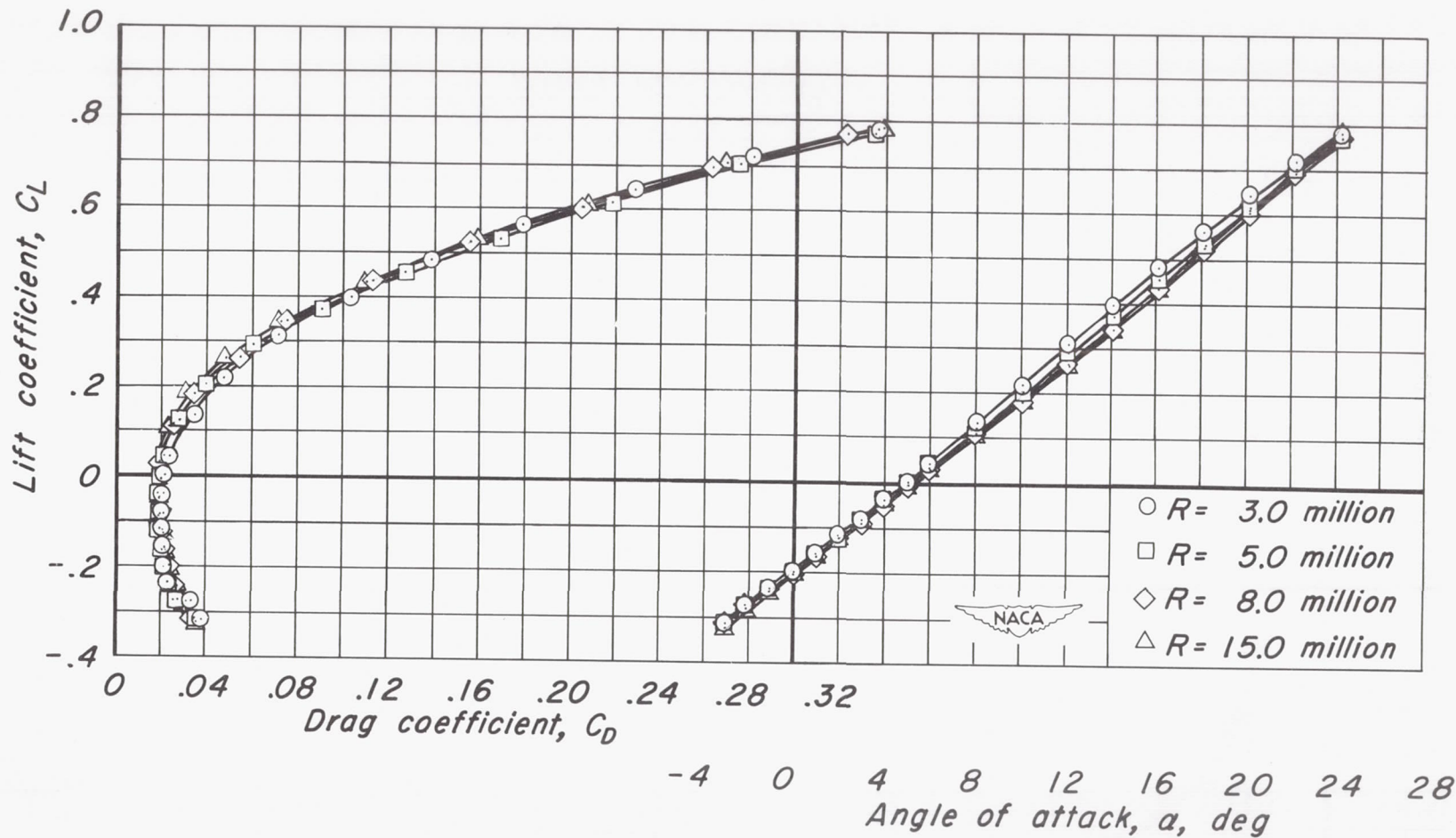


(e)  $C_F$  vs  $\alpha$   
 Figure 16.- Continued.



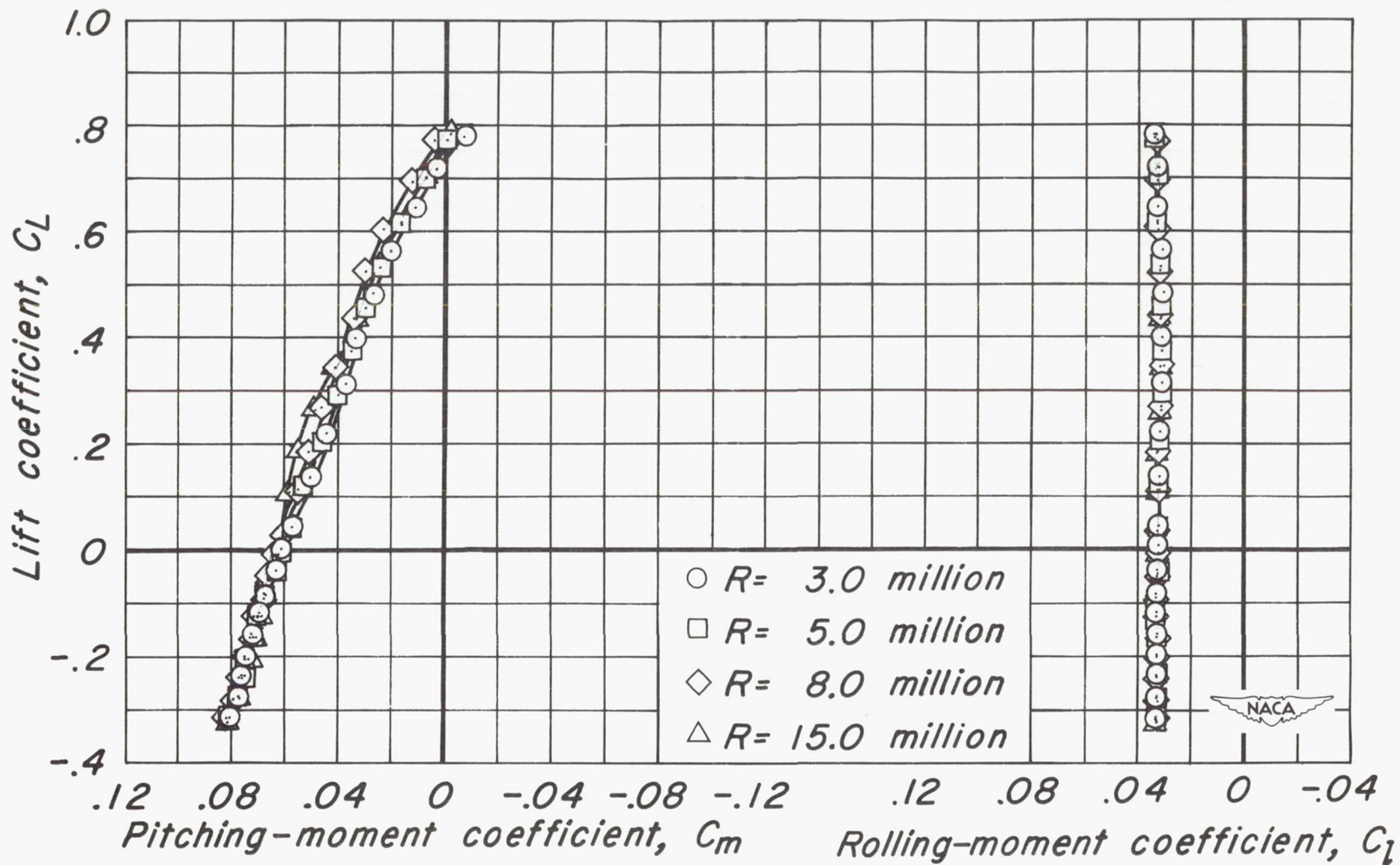
(f)  $2y/b$  vs  $\alpha$ ,  $x/c_r$  vs  $\alpha$   
 Figure 16 - Concluded.





(a)  $C_L$  vs  $\alpha$ ,  $C_L$  vs  $C_D$

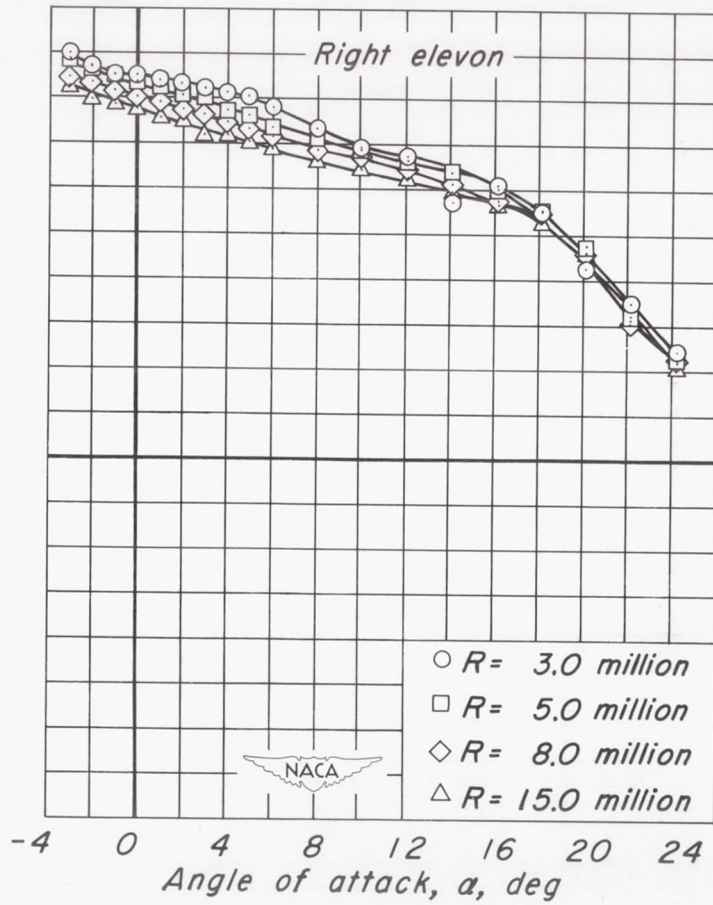
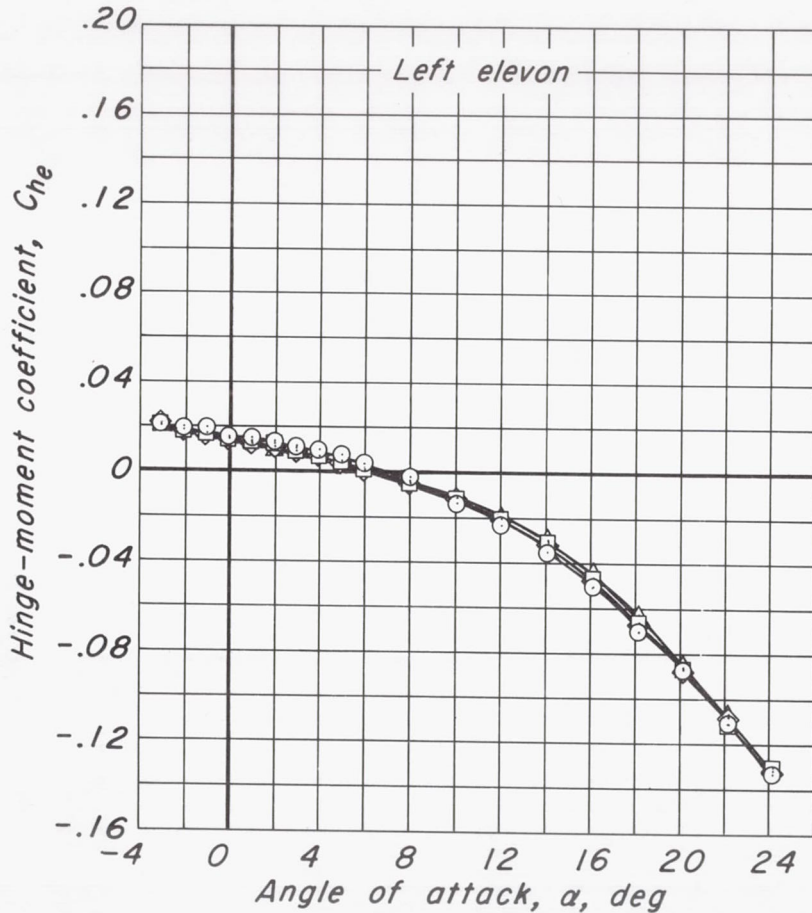
Figure 17.- The effect of Reynolds number on the aerodynamic characteristics at a Mach number of 0.24.  $\delta_{e1}$ ,  $0^\circ$ ;  $\delta_{e2}$ ,  $-20^\circ$ ;  $\delta_t$ ,  $0^\circ$ .



(b)  $C_L$  vs  $C_m$ ,  $C_L$  vs  $C_l$

Figure 17.- Continued.

CONFIDENTIAL

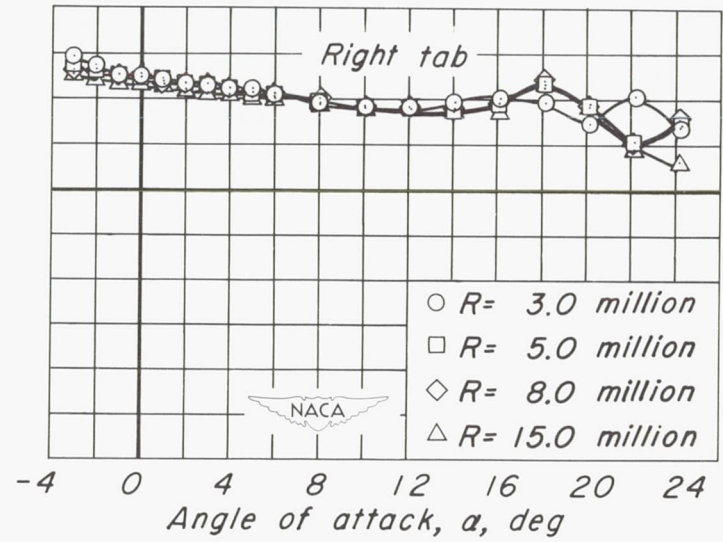
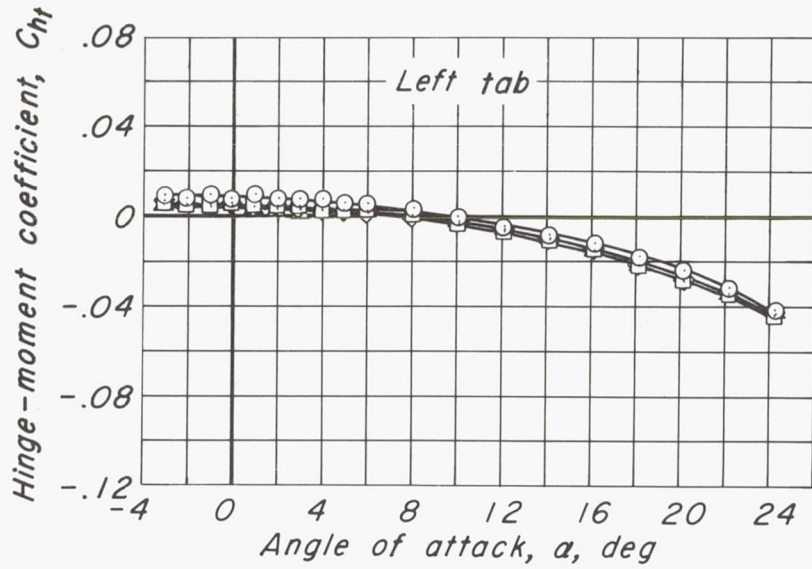


- $R = 3.0$  million
- $R = 5.0$  million
- ◇  $R = 8.0$  million
- △  $R = 15.0$  million



(c)  $C_{he}$  vs  $\alpha$   
 Figure 17.- Continued.

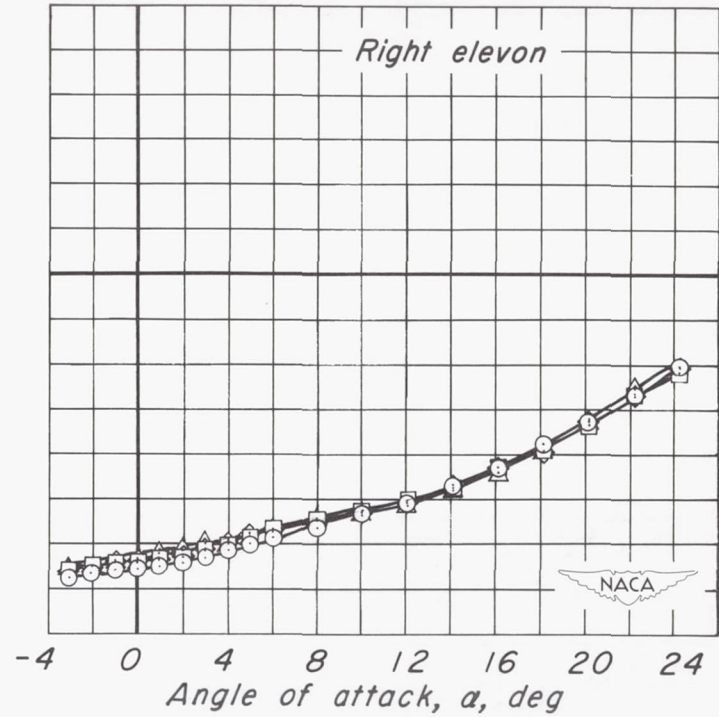
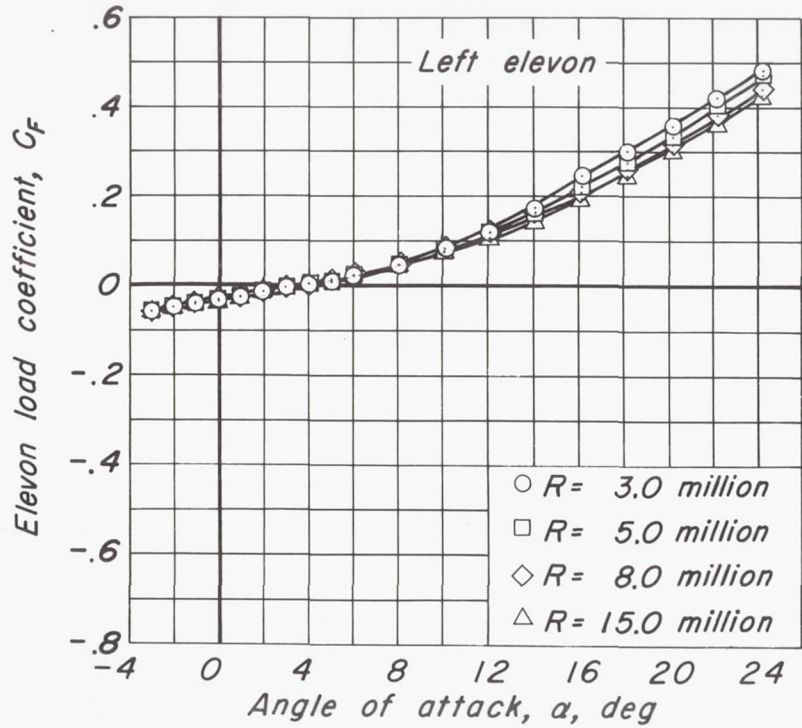




- $R= 3.0$  million
- $R= 5.0$  million
- ◇  $R= 8.0$  million
- △  $R= 15.0$  million

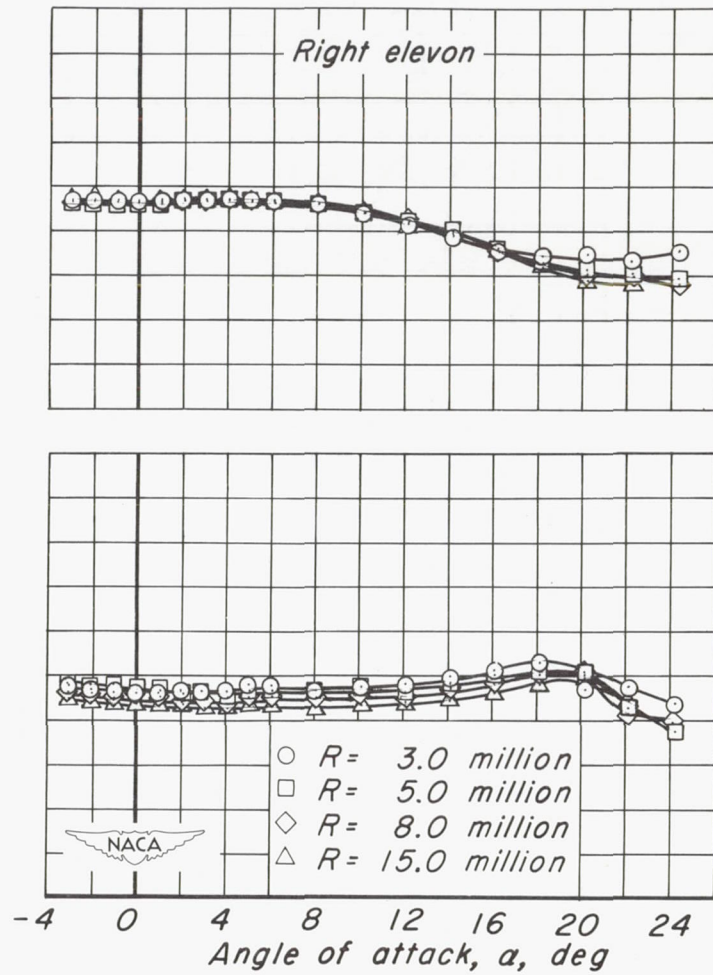
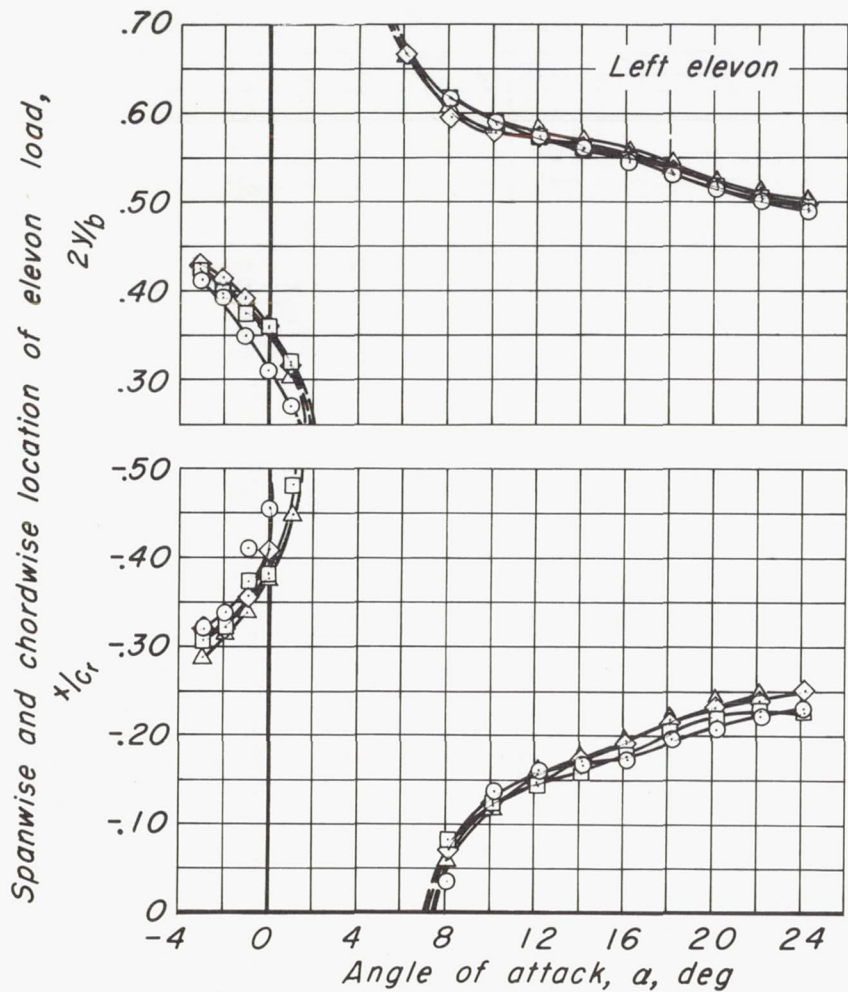


(d)  $C_{ht}$  vs  $\alpha$   
 Figure 17.- Continued.



(e)  $C_F$  vs  $\alpha$

Figure 17.- Continued.



- $R = 3.0$  million
- $R = 5.0$  million
- ◇  $R = 8.0$  million
- △  $R = 15.0$  million



(f)  $2y/b$  vs  $\alpha$ ,  $x/c_r$  vs  $\alpha$   
 Figure 17.- Concluded.



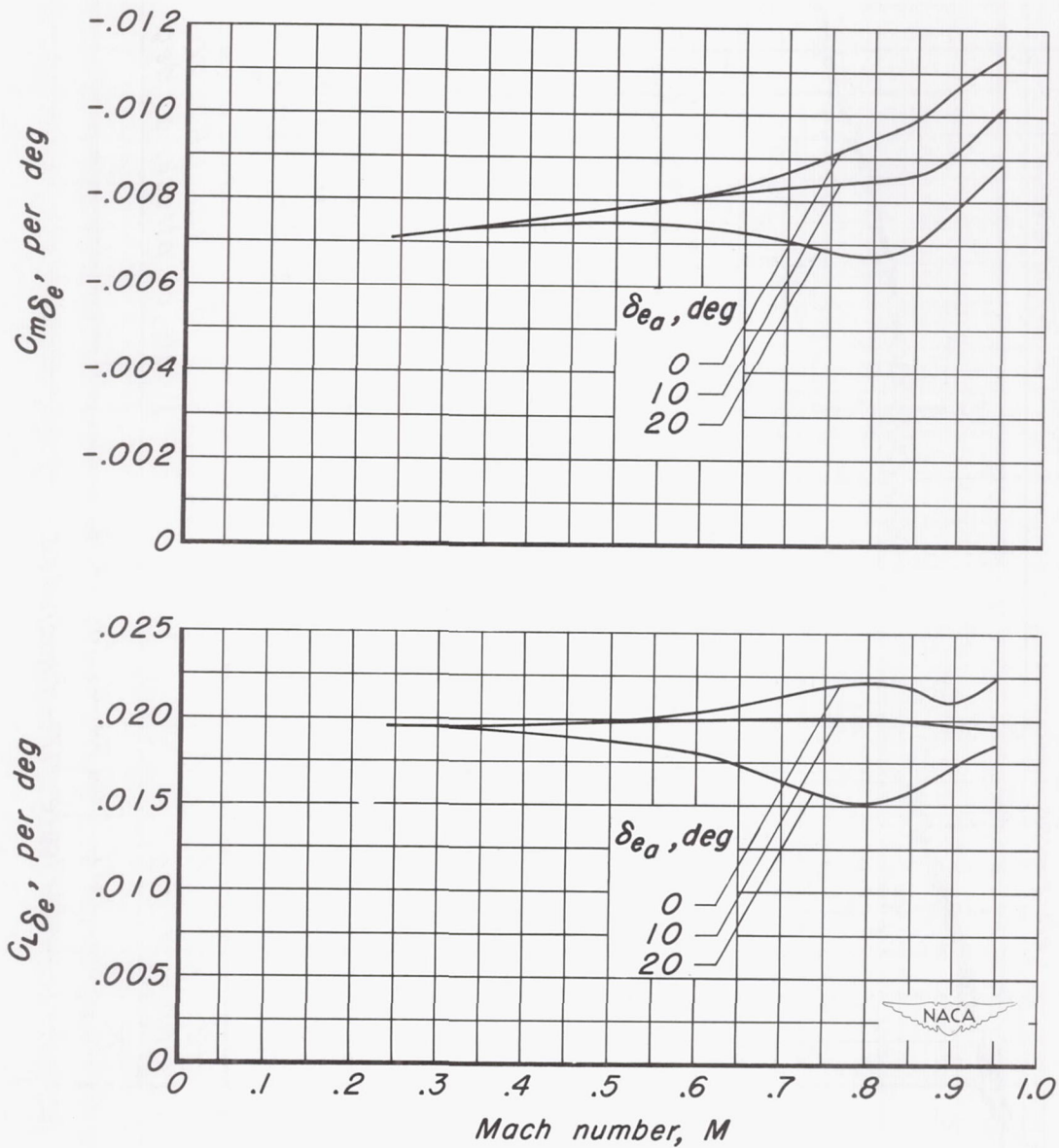


Figure 18.- The variation with Mach number of the lift and pitching-moment effectiveness parameters,  $C_{L\delta_e}$  and  $C_{m\delta_e}$ , for various differential elevon deflections,  $\delta_{e\alpha}$ .  $R$ , 3.0 million;  $\delta_t$ ,  $0^\circ$ .

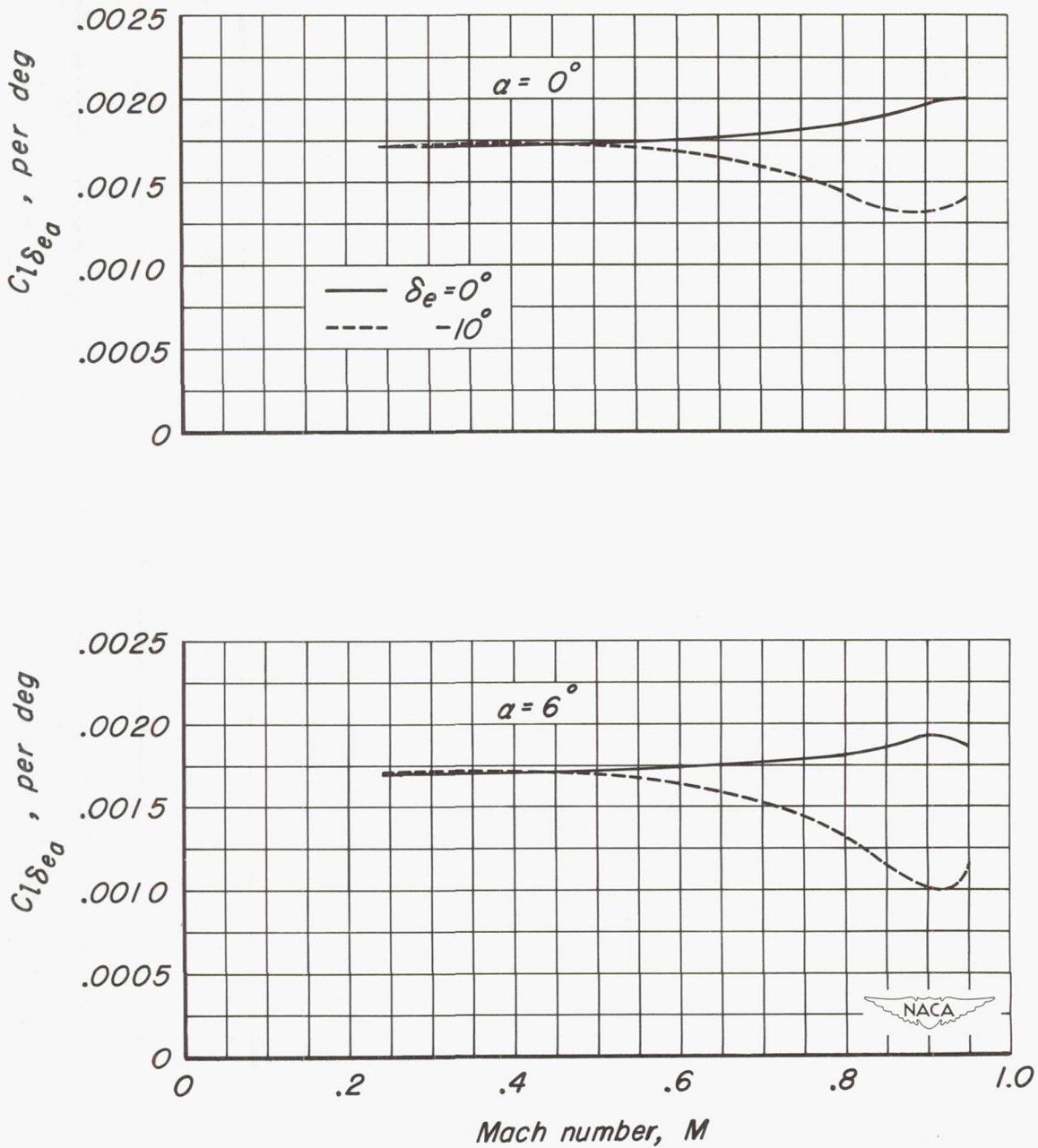


Figure 19.— The variation with Mach number of the rolling-moment effectiveness parameter,  $C_{l\delta_{e\alpha}}$ , for various values of elevon deflection and angle of attack.  $R$ , 3.0 million;  $\delta_t$ ,  $0^\circ$ .

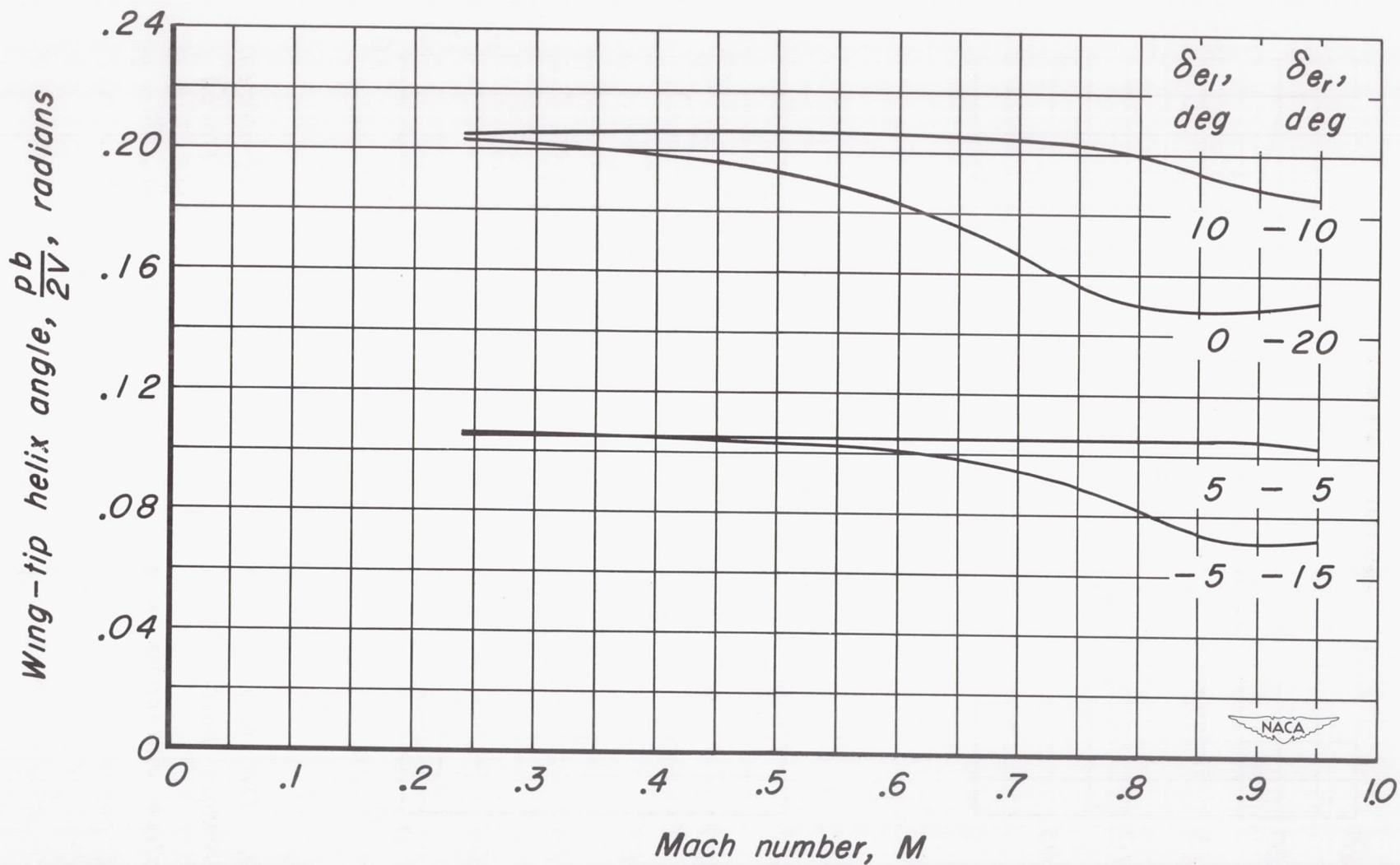
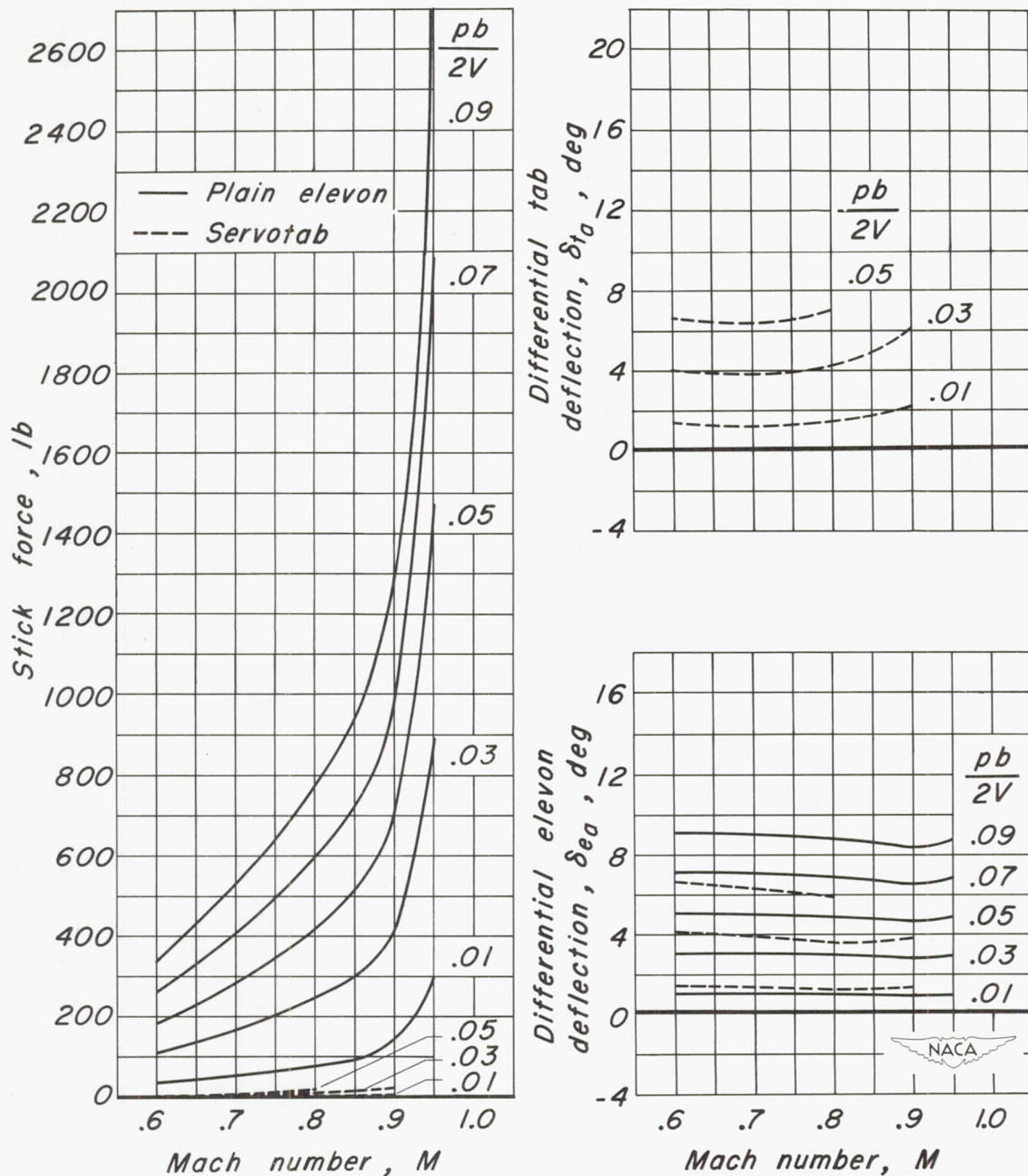


Figure 20.— The variation with Mach number of the wing-tip helix angle for various elevon deflections.  $R$ , 3.0 million;  $\delta_t$ ,  $0^\circ$ .

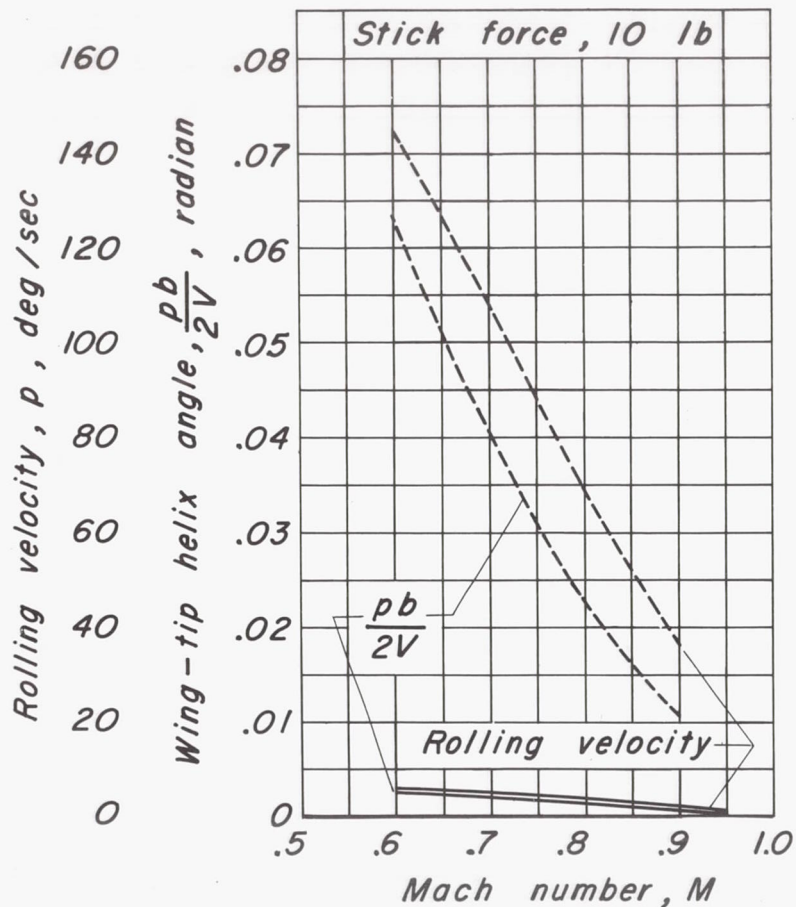




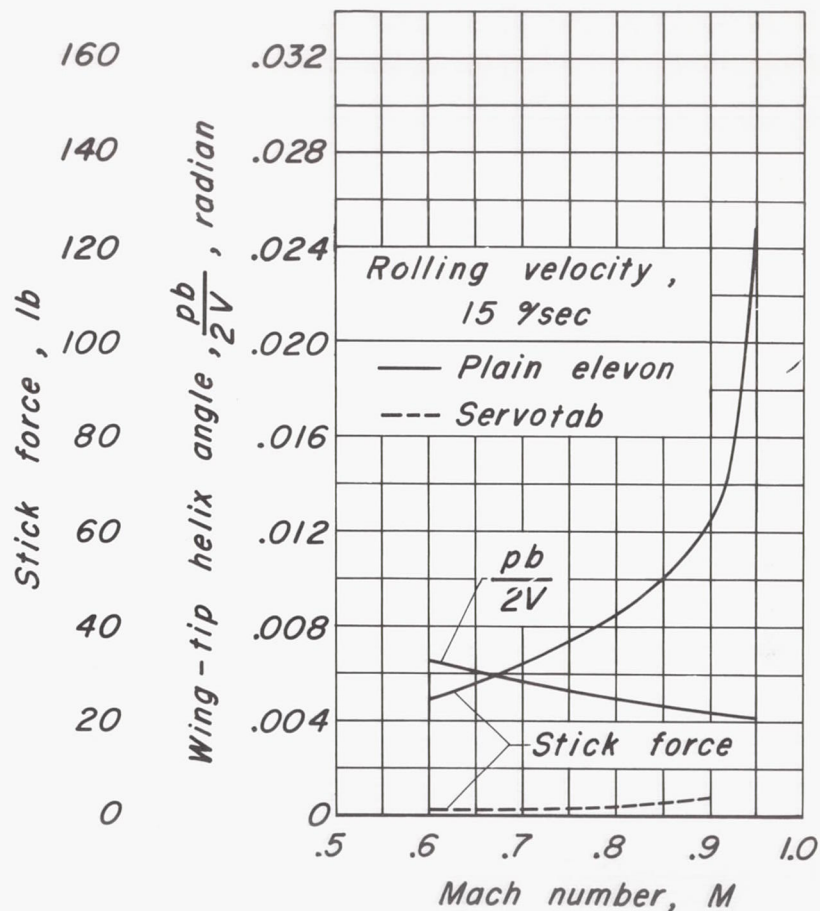
(a) Constant wing-tip helix angle.

Figure 21.- The variation with Mach number of the level flight steady rolling characteristics of the assumed airplane with two different control systems. Altitude, 30,000 feet; wing loading, 40 pounds per square foot; wing area, 450 square feet; center of gravity at  $0.25 \bar{c}$ ; control gearing,  $2.0^\circ$  per inch of stick travel.

CONFIDENTIAL



(b) Constant stick force.



(c) Constant rolling velocity.

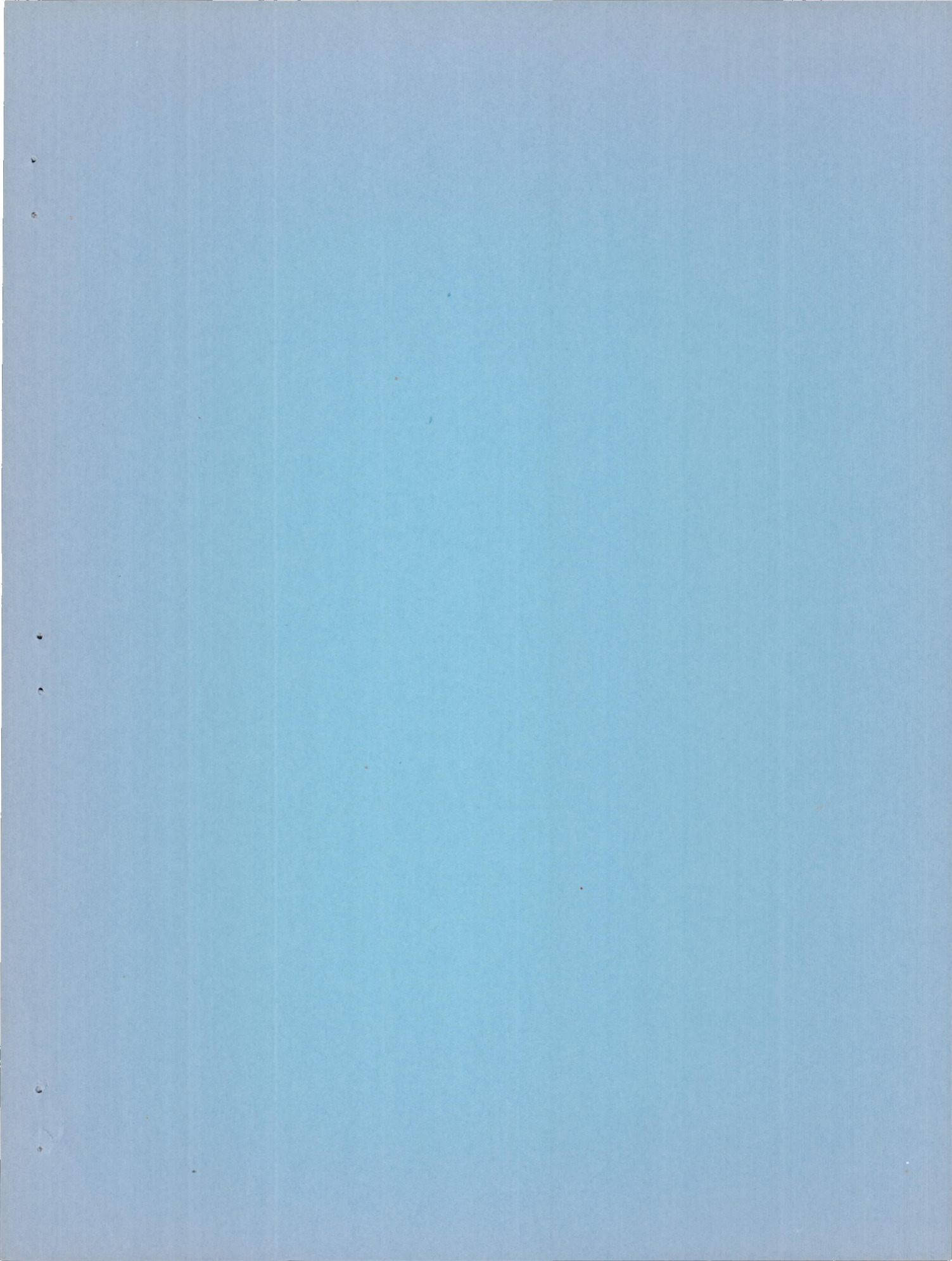
Figure 21.- Concluded.



CONFIDENTIAL









SECURITY INFORMATION

CONFIDENTIAL

*[Faint, illegible markings or bleed-through]*

CONFIDENTIAL